KU LEUVEN

FACULTEIT INGENIEURSWETENSCHAPPEN

Biomechanical Evaluation of a Personalized External Aortic Root Support applied in the Ross procedure

Julie Vastmans

Thesis submitted for the degree of
Master of Science in
Biomedical Engineering

Thesis supervisors:

Prof. dr. ir. Jos Vander Sloten
Prof. dr. Filip Rega,
Dr. ir. Nele Famaey

Assessors:

Prof. dr. ir. Harry Van Lenthe
Dr. Peter Verbrugghe

Mentor:

Ir. Heleen Fehervary

Academic year 2014 – 2015

Preface

My sincere gratitude goes to my daily supervisor Ir. Heleen Fehervary and promotor Dr. Ir. Nele Famaey, who helped me with various problems, ranging from difficulties during mechanical tests to programming issues. I would also like to express my gratitude towards my promotor Prof. Dr. Ir. Jos Vander Sloten for his professional advice. I would also like to thank my promotor Prof. Dr. Filip Rega and Dr. Peter Verbrugghe for providing the samples used in this thesis as well as their medical counsel on the content of this thesis. Furthermore, I would like to thank ir. Marija Smoljkić for her advice and help in the construction of the finite element model. Finally, I would like to thank Benedicte Vanwanseele and ir. Siegfried Jaecques for their advice on the determination of a representative set of parameters.

Julie Vastmans

Contents

Abstract

A treatment for patients suffering from aortic valve disease is the Ross procedure, where the surgeon replaces the diseased aortic root with a pulmonary root autograft. This autograft is subsequently exposed to systemic pressures possibly resulting in dilatation. [47] This study investigates the influence of adding a PEARS. A simplified version of the Ross procedure was performed on seven Lovenaar sheep: a part of the thoracic aorta descendens is replaced by part of the truncus pulmonalis and a wrapping is positioned around the pulmonary autograft. During this procedure pulmonary tissue was harvested. After six months, the sheep were sacrificed. Three types of tissue were harvested: aorta, reinforced aorta, and reinforced pulmonalis. The tissues underwent planar biaxial tests, and stress-strain curves for the four types of tissues were calculated from the obtained force-displacement curves. These curves served as input for the Gasser-Holzapfel-Ogden material model. [15] Subsequently, a finite element model (FEM) of the simplified procedure with and without reinforcement was constructed, as well as a FEM of solely the aorta or pulmonalis under physiological loading conditions. The following outputs were collected: the profile of the deformed shape after applying diastolic and systolic pressure, and the stresses in the three directions in diastolic and systolic conditions.
From the finite element analysis can be concluded that inserting a pulmonary section in the aorta position, alters the stress pattern. Adding a reinforcement changes the stress pattern compared to the unreinforced simulation and compared to the normal situation. Furthermore, the Ross procedure without reinforcement results in a larger diameter where the pulmonalis is positioned, while the wrapping appears to constrain the pulmonary section. The change in stress imposed on the pulmonalis in the aorta position with and without reinforcement, may have an influence on the long-term results of this procedure. However, improvements regarding the model can be made regarding the boundary conditions and material representation. Moreover, the influence of the circumferential and axial residual stresses needs to be investigated.

List of Figures

List of Tables

List of Abbreviations and Symbols

Abbreviations

bpm	Beats per minute
CT	Computed Tomography
FBN1	Fibrillin-1
FEM	Finite Element Model
GHO	Gasser-Holzapfel-Ogden
HR	Heart rate
MFS	Marfan's Syndrome
MRI	Magnetic Resonance Imaging
PEARS	Personalized External Aortic Root Support
PTFE	Polytetrafluorethylene
RMSE	Root Mean Square Error

Symbols

When not specified otherwise, the symbols printed in bold correspond to tensor quantities

r	subscript which refers to the radial direction
θ	subscript which refers to the circumferential direction, corresponds with the x direction of the biaxial tensile tester
z	subscript which refers to the longitudinal or axial direction, corresponds with the y direction of the biaxial tensile tester
t	Thickness of the vessel
P	Pressure in the vessel
ϵ	Stretch
m	Mass
Ψ	Strain-energy function
$\boldsymbol{B}$	Left Cauchy-Green tensor
$\boldsymbol{C}$	Right Cauchy-Green tensor
μ	Parameter of the GHO model related to the stiffness of the matrix
C_{10}	Parameter of the GHO model related to the stiffness of the matrix, equal to $\frac{\mu}{2}$
k_1	Parameter of the GHO model related to the stiffness of the fibers
k_2	Parameter of the GHO model related to the nonlinear behavior
α	Parameter of the GHO model related to angle of the fibers
κ	Parameter of the GHO model related to the dispersion of the fibers
I_i	The ith invariant of the Cauchy-stress tensor
λ_r	Principal stretch in the radial direction
λ_θ	Principal stretch in the circumferential direction
λ_z	Principal stretch in the axial direction
$\boldsymbol{F}$	Deformation gradient
$\boldsymbol{R}$	Rotation tensor
$\boldsymbol{U}$	Stretch tensor
$\boldsymbol{\sigma}$	Cauchy stress
$\boldsymbol{T}$	First Piola-Kirchoff stress
$\boldsymbol{P}$	Second Piola-Kirchoff stress
$L_{j,i}$	Load in the i^{th}-direction present at instant j
r	Radius of the blood vessel
h	Width of the sample
$\boldsymbol{a}_{01,02}$	Vector denoting the directions of the collagen fibers
l_i	Length in the ith direction
$l_{i,0}$	Original length in the ith direction
λ_{ii}	Stretch ratio in the ith direction
$\boldsymbol{E}$	Green strain tensor

Chapter 1

Introduction

A possible treatment for patients suffering from aortic valve disease is the Ross procedure, in which the surgeon replaces the diseased aortic root with a pulmonary root autograft. Consequently, this pulmonary autograft is subjected to systemic pressures, often resulting in dilatation of the autograft.[47] Complementing the Ross procedure by adding a Personalized External Aortic Root Support (PEARS) is investigated in this thesis. Initially, a PEARS is intended for patients with Marfan's syndrome whose aortic root is dilated.

1.1 Research Background

1.1.1 Marfan's syndrome

Marfan's syndrome (MFS) is an autosomal genetic disorder that affects the connective tissue throughout the body. Approximately 1 out of 10 000 to 20 000 persons are affected by this disease.[59]
In 1991, there was identified that mutations in the Fibrillin 1 gene (FBN1) caused Marfan's syndrome. The FBN1 gene encodes for the FBN1 protein, a major component of the microfibrils.[39] Microfibrils maintain the structural integrity of the extracellular matrix.[24] Pathogenic mutations in FBN1 consequently lead to elongation and fragility of the tissue. Hence, symptoms can be found in the skeletal, the ocular and the cardiovascular system. These symptoms include joint hyperflexibility, ectopia lentis, malformations of the digits, limbs, spine and anterior chest wall.[11]
An important consequence of the weakening of the connective tissue, is situated at the ascending aorta. Due to the weakening of the aortic tissue, the aortic wall is no longer capable of withstanding the intraluminal pressure, which may result in aneurysm formation.[3]
MFS can be managed by medical treatment and surgery. The medical treatment consists of the prescription of β-blockers. Since β-blockers reduce the heart rate and blood pressure and thus reduce the aortic stress which will delay the progression of the aortic aneurysm formation. When the aortic root diameter reaches a value of 50 mm, surgical intervention is recommended. Two different surgical procedures are

commonly used for the dilated aortic root. The Bentall procedure uses a composite graft, which comprises a mechanical valve connected to an aortic prosthesis, to replace the dilated aortic root. After this procedure, the patient needs lifelong anticoagulation therapy. The second procedure is the David's procedure in which the aortic valve remains and the root is replaced by a prosthesis.[39] In this procedure, the need for lifelong anticoagulant therapy is avoided.[10]
Both type of procedures are major surgical approaches and require cardiopulmonary bypass with full heparisation with all the accompanying risks.[34] To bypass the need for these approaches, a procedure which uses a personalized external aortic root support has been developed.

1.1.2 Ross procedure

The Ross procedure consists of the replacement of the diseased aortic valve with the autologous pulmonary graft. The procedure was initially described by Donald Ross as a subcoronary implant of the pulmonary valve, however the full root replacement has become the most used procedure.[47]
Figure 1.1 gives a schematic representation of the Ross procedure. The first step consists of excising the aortic valve with part of the adjacent aorta. Also, the pulmonary valve with part of the adjacent pulmonary artery is removed. Subsequently, this pulmonary graft is attached to the aortic annulus and to the distal aorta. A pulmonary allograft is inserted in the pulmonary artery.[27]

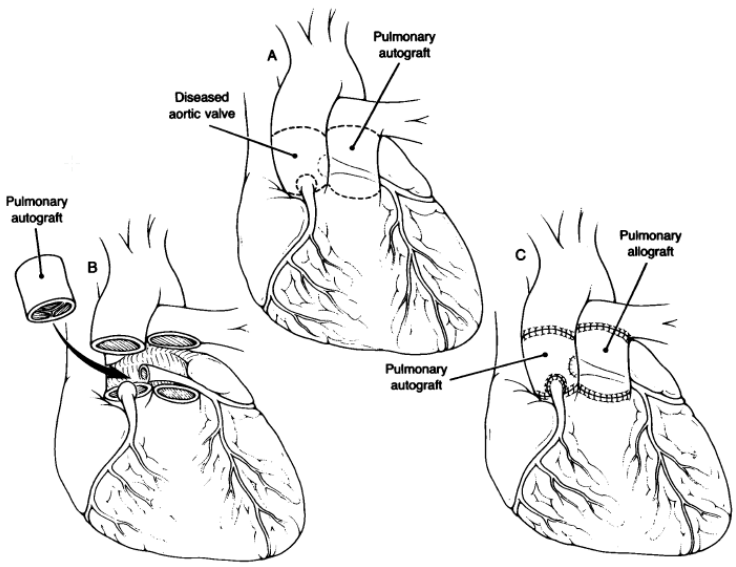

Figure 1.1: Schematic representation of the Ross procedure [27]

The Ross procedure has several advantages. The use of the living autograft ensures certain hemodynamic and biological properties which can not be reproduced by any other replacement valve. The hemodynamic performance of the Ross procedure

has been investigated by several researchers, and good exercise performance can be found in Ross patients, which is markedly better than the exercise performance in patients with mechanical valves. Moreover, no anticoagulation therapy, as is necessary with mechanical valves, is required after the Ross procedure. However, some objectives can be made regarding the Ross procedure. An important disadvantage of the Ross procedure comprises the dilation of the pulmonary autograft in the aortic position.[47] This aortic root dilation can be observed in almost 20% of the Ross patients at late follow-up.[5] The fact that two valves are at risk is another important disadvantage of the Ross procedure.[45]
To overcome the disadvantage of the dilation of the pulmonary autograft, some modifications to the Ross procedure have been suggested. Brown *et al.* modified the Ross procedure by performing an autograft root replacement using the pulmonary autograft, and placing a Dacron graft at the distal aortic anastomosis.[5]
Reinforcing the pulmonary autograft by sewing it into a prosthetic graft with artificial root design is another modification that has been experimented with. Both Ungerleider *et al.*[52], and Carrel *et al.*[7] have reported this modified Ross procedure.

1.2 Problem outline

This thesis investigates the influence of adding a PEARS to the pulmonary autograft of the Ross procedure by mechanically characterizing the PEARS when used in this procedure. Therefore, a simplified Ross procedure was performed on seven Lovenaar sheep: a part of the thoracic aorta descendens is replaced by part of the truncus pulmonalis and a wrapping is positioned around the pulmonary autograft. During this procedure a section of the pulmonalis is excised. Moreover, one sheep underwent the simplified Ross procedure without the addition of the wrapping. After six months, the sheep are sacrificed and the following tissues are harvested: aorta, reinforced aorta, and reinforced pulmonalis. In the control sheep, only aorta and pulmonary tissue in aorta position are obtained. Uniaxial and biaxial tests on samples of these different tissues have been performed. The Gasser-Holzapfel-Ogden model is used to characterize the different tissues using the stress-strain curves calculated from the force-displacement curves of the biaxial tests. After determining the parameters, the possibility of using a representative set of parameters for each tissue type is investigated. The final part of this thesis entails a finite element analysis in which a model is created of the simplified Ross procedure with and without reinforcement, as well as a model of solely the aorta or pulmonalis.
Thus, two distinct objectives are defined:

1. Perform mechanical tests and use the outcome of these experiments to mechanically characterize the behavior of the four types of tissues by means of the GHO model.

2. Develop a FEM to examine the influence of the wrapping on the Ross procedure.

In the introduction a short description of the Ross procedure and Marfan's syndrome is given.
The literature study in Chapter 2 starts by describing the cardiovascular system, both the heart and the arteries are handled. Subsequently, the different existing vascular grafts are discussed, including the PEARS. The main interest of this section lies on the mechanical behavior of the possible materials for these grafts. The third section of the literature study discusses the use of mechanical testing, both biaxial and uniaxial tests, in different studies.
The mechanical testing that have been performed in the context of this study are elaborated on the third chapter. This chapter starts with an elaboration on the specific materials and methods for the tests. Subsequently, the results of these tests are given.
The main results of the biaxial tests are force-displacement curves. These curves are used to calculate stress-strain curves which serve as input for determining the parameters of the GHO model. The determination of the parameters is the main subject of the fourth chapter. Firstly, this chapter elaborates on the GHO model. Secondly, the different steps undertaken to find the parameter sets are discussed. Parameter fitting as well as determining a representative set of parameters for the different tissue types are important subjects of this section. The results of the parameter fitting step are given in the second section. The results of the different steps undertaken in an attempt to find a representative set of parameters for each tissue type are also given in the second section. The third section interprets the results of the parameter fitting step and the steps to determine a representative set.
The fifth chapter handles on the finite element analysis. The construction of the FEM is discoursed in the first section, followed by an enumeration of the results of the simulations done by means of the FEM. The last section of this chapter discusses the obtained results of the finite element analysis.
A conclusion in which the main findings are repeated completes this thesis.

Chapter 2

Literature Study

This chapter describes the cardiovascular system, which includes the heart and the vascular system. There is focused on the structure of the arteries and their mechanical behavior. Moreover, the mechanical behavior of different vascular grafts that can be used to support blood vessels, is reviewed. A dedicated section on the PEARS describes the studies that have been conducted for this arterial support. Furthermore, since the mechanical behavior of arterial tissues will be investigated, an overview of studies using different types of mechanical testing is reported. The focus of this overview lies with the biaxial and uniaxial test methods, and their protocols. The literature review ends with a conclusion where the most important findings of the literature review are repeated.

2.1 Cardiovascular system

The cardiovascular system is composed of the heart and the circulatory system and performs many important functions. Nutrients are carried to the tissue and waste products are removed from the tissues by the circulatory system. The circulation of blood is necessary for maintaining homeostasis, the maintenance of an internal stable physiological environment.[40]

2.1.1 The heart

The heart is comprised of four chambers: the right atrium, the right ventricle, the left atrium and the left ventricle. In Figure 2.1 the heart and its main arteries are depicted. Deoxygenated blood enters the heart in the right atrium, after which it is delivered to the right ventricle and it is pumped to the lungs through the pulmonary artery. After passage through the lungs, the blood is oxygenated and it enters the heart via the left atrium, flows into the left ventricle and is transported out of the heart via the aorta, after which it will deliver oxygen to the rest of the body.[38]
The atrioventricular valves can be found between the atria and the ventricles. The right atria and right ventricle are separated by the tricuspid valve, while the bicuspid valve separates the left atrium and the left ventricle. The atrioventricular valves

ensure that the blood flows from the atria into the ventricles.[38] Two other valves that can be distinguished in the heart, are the aortic valve and the pulmonary valve. The aortic valve is located between the left ventricle and the aorta. The pulmonary valve is located between the right ventricle and the pulmonary artery. Both valves are responsible for maintaining a blood flow from the ventricles into the vessels. The aortic valve is composed of three quasi semilunar cusps, secured to a fibrous ring. The pulmonary valve consists, like the aortic valve, out of three semilunar cusps.[48] The left and right atria contract simultaneously as well as the two ventricles. During the contraction of both ventricles, blood is pumped into the pulmonary and systemic circulations. After contraction of the ventricles, the ventricles relax and are filled with blood from the atria. The period in which the right and left ventricle contract is called the systole. The diastole is the period in which the ventricles are relaxing.[38]

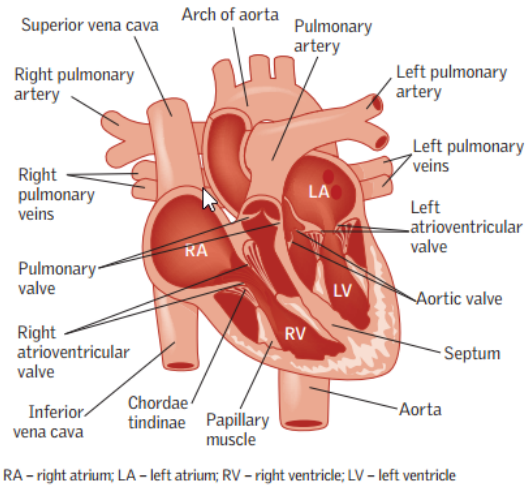

Figure 2.1: The heart with its main structures and arteries[13]

The muscle wall of the heart, called myocardium, contains connective tissue, neurons, blood vessels, and cardiomyocytes. The cardiomyocytes are electrically coupled by gap junctions. Cardiomyocytes without a stable diastolic membrane potential between subsequent cycles of excitation are called pacemaker cells. The electrical excitation is initiated in the sinoatrial node, which is composed of pacemaker cells. The excitation spreads through both atria, causing atrial depolarization, and reaches the atrioventricular node. Subsequently, the excitation travels through the bundle of His and enters the Purkinje network that branches throughout the ventricles.[38]

2.1.2 The vascular system

Systemic and pulmonary circulation

The vascular system can be divided into the systemic and the pulmonary circulation. This division can be found in the heart, that can be seen as composed of two separate pumps, serving one of these circulations. The left heart pumps blood through the

systemic circulation, whereas the right heart serves the pulmonary circulation.[38] The right atrium and ventricle serve the pulmonary circulation by pumping deoxygenated blood into the pulmonary arteries. This blood is brought to the lungs, where it will become oxygenated after passage through the alveoli of the lungs. After oxygenation, the blood is transported back to the heart, where it enters via the left atrium and is pumped into the systemic circulation by the left ventricle. The systemic circulation is composed of parallel vascular circuits. Oxygenated blood enters these vascular circuits through the arteries and deoxygenated blood leaves the vascular circuits through the veins.[38]
The largest vessel present in the human body is the aorta, which originates from the left ventricle at the aortic root. It has a diameter of 2-3 cm in a normal healthy adult and tapers to a diameter of 1 cm at the aorta-iliac bifurcation.[44] A distinction can be made between the thoracic aorta and the abdominal aorta. In the thoracic aorta an ascending and a descending part can be found. The ascending thoracic aorta can be subdivided into different regions: the proximal and distal ascending thoracic aorta and the aortic arch. The aorta and its structure are visualized in Figure 2.2.[51]

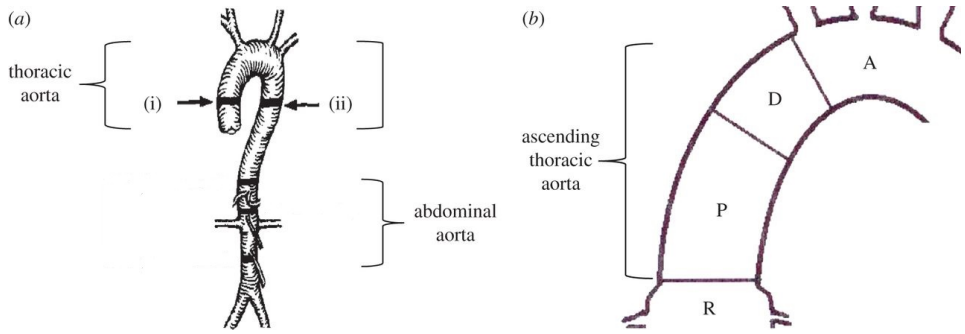

Figure 2.2: The aorta and its structures. (a) The thoracic aorta (consisting of the ascending and descending aorta) and the abdominal aorta. (b) The aortic root (R), The ascending thoracic aorta with the proximal ascending aorta (P), the distal ascending aorta, and the aortic arch (A). Adapted from Tsamis *et al.*[51]

The systemic circulation requires that the heart generates a higher pressure than the pressure necessary in the pulmonary circulation. In humans, the maximum pressure generated in the major systemic arteries is 120 mmHg. The maximum pressure in the pulmonary artery has a value of 25 mmHg.[38]

Characteristics of arteries

Anatomy Three layers can be distinguished in the arterial wall: the intima, the media and the adventitia. Each of these layers will be described shortly. In Figure 2.3 the arterial layers and their constituents are depicted.
The *intima* is the inner layer of the arterial wall and is primarily composed of a single layer of endothelial cells, which rests on a thin basal membrane. This endothelial layer functions as a barrier between the blood and the arterial wall. Other functions of

the endothelial layer include regulating mass transport processes, arterial remodeling processes, and mechanosensing. In young individuals, the intima is very thin and can be discarded in the determination of the solid mechanical properties of the arterial wall. When aging, this intima thickens and stiffens and will become significant in the solid mechanical properties.[21]

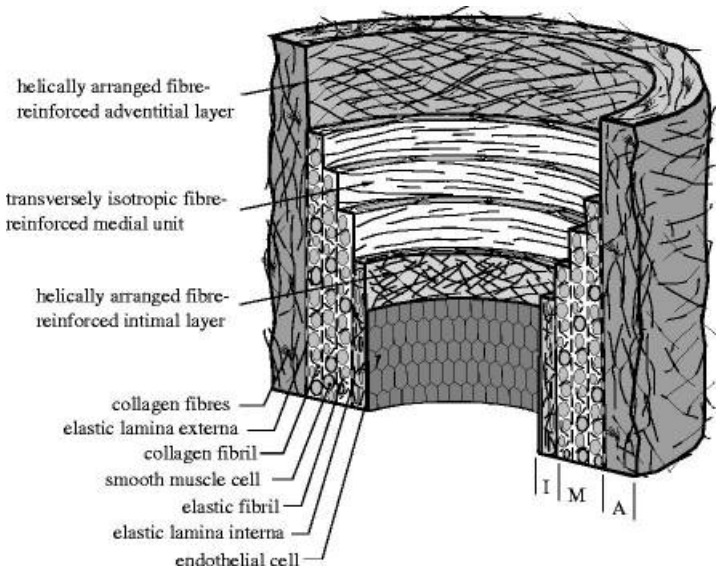

Figure 2.3: The arterial layers: intima (I), media (M), and adventitia (A) [15]

The middle layer of the arterial wall is called the *media*. It is composed of a complex three-dimensional network of elastin, collagen fibers, and smooth muscle cells. The internal elastic lamina separates the media from the intima, and the external elastic lamina separates the media from the adventitia. As can be seen in Figure 2.3 different layers, or lamellar units, can be distinguished in the media. These layers are composed of subgroups of aligned smooth muscle cells, which are reinforced and delimited by elastic fibers.[9] The elastic and collagen fibers, elastic lamina, and smooth muscle cells compose a fibrous helix which gives the media high strength, resilience, and gives the media the ability to withstand loads in the circumferential and longitudinal direction. The collagen fibers are aligned closely with the circumferential direction, which is in contrast with the dispersed collagen fibers in the intima and adventitia layers. Consequently, the media is the most important layer in an artery from a mechanical perspective.[21]
The outermost layer of the arterial wall is the *adventitia* and is composed mostly of fibroblasts and fibrocytes, histological ground substances, and thick bundles of collagen fibrils, making the adventitia a fibrous tissue. Helix structures, composed of wavy collagen fibrils, strengthen the arterial wall and contribute significantly to the stability and strength of the arterial wall. When the artery is subjected to high pressures, the wavy collagen fibrils will straighten and the adventitia will preclude the arterial wall from rupture and overstretch. Loose connective tissue surrounds

the adventitia continuously.[21]
The most important constituents of the sublayers of the arterial wall are collagen, elastin, smooth muscle cells, and other connective tissue. Collagen, a protein with a high Young's modulus, influences the strength of the arterial wall. The elasticity of the arterial wall is determined by the protein elastin. The smooth muscle cells can actively control the diameter of the vessel.[43]

Mechanical Behavior The different layers in the arterial wall contribute to the mechanical behavior. The intima primarily consists of a layer of endothelial cells and can be discarded for the mechanical properties. The media includes collagen fibers oriented in the circumferential direction, providing strength in the circumferential direction. The dispersed collagen fibers in the adventitia preclude the arterial wall from overstretch.[54]
Due to the organized structural arrangement of the arterial wall, it can be considered anisotropic. Furthermore, the arterial wall can be classified as a solid-fluid mixture, where the solid comprises the elastin, the smooth muscle cells, and the collagen. However, the fluid can for many problems be discarded, and the arterial wall can be classified as a homogenized solid. In physiological conditions, the arterial wall can be viewed as incompressible. Arteries are also highly deformable and show a nonlinear strain-stress response. In the strain-stress response a stiffening can be noticed around the physiological strain level, which is believed to be caused by the recruitment of the collagen fibers. Viscoelasticity has been demonstrated in the arterial wall. A hysteresis curve is formed under cyclic loading, as well as creep under constant loading, and stress relaxation under constant deformation.[15]

2.2 Vascular grafts

The surgical treatment of the dilated aortic root of patients with Marfan's syndrome consists of replacing the aortic root with a prosthesis. Recently, a procedure in which a support, the PEARS, is wrapped around the aorta is developed. In this section, the materials most often used for vascular prostheses are discussed, as well as the PEARS.

2.2.1 Materials used for vascular prostheses

Prosthetic materials used in vascular prosthesis should ideally be impermeable, thromboresistant, compliant, biocompatible, durable, resistant to infection, easy to sterilize, easy to implant, cost-effective, and its mechanical properties should match those of arterial tissue. Materials that are commonly used for making vascular grafts are Dacron and Teflon.[50] Dacron is the commercial name for polyethylene terephtalate and Teflon is the commercial name for polytetrafluorethylene.[58], [19]
Vascular grafts can also be constructed as bioprostheses, e.g. bovine pericardium.[50]
The mechanical properties of synthetic materials as arterial grafts have been investigated by Hasegawa *et al.* The layout of their study has been mentioned in Section 2.3.1. They performed uniaxial tests on following materials: knitted and woven

Dacron grafts, knitted and woven Teflon grafts, canine ascending aorta, proximal and distal portions of the canine abdominal aorta, the canine left iliac and the canine femoral arteries, and segments of knitted and woven Dacron and Teflon grafts that were implanted for three weeks in the subcutaneous tissue of canine hind limbs.[17]
Looking at the results of the tests on the synthetic materials, the moduli of elasticity in the circumferential direction were high compared to the elastic moduli in the longitudinal direction. The elastic moduli in the longitudinal direction were low until a certain strain was reached after which the elastic moduli increased and approximated the elastic moduli in the circumferential direction. This difference is a result of the presence of circular crimps. Threads in the longitudinal direction will only be subjected to stretch after these crimps are straightened. When comparing the woven and knitted configuration of the polymers, there can be seen that the distensibility, the reciprocal of the slope of the stress-strain curve, is significantly higher in the knitted design than in the woven design.[17]
The viscoelastic characteristics differ between the different types of synthetic grafts. Stress relaxation was more present in Teflon grafts, compared to Dacron grafts. However, no differences in stress relaxation were present when comparing longitudinal direction with circumferential direction or comparing woven design with knitted design. Relaxation strengths differ between Teflon grafts and Dacron grafts, the former being the largest. However no differences in relaxation strengths can be found comparing the different designs or the different directions.[17]
Comparing the stress-strain relationships of the different synthetic grafts with the ones of the different arterial segments results in the conclusion that in general the woven Teflon graft appeared to be the most similar to the arterial wall. The viscoelastic characteristics of the arterial wall seemed to be dependent on the location of the arterial segment. The Dacron graft had similar relaxation strengths as the proximal aorta, whereas the relaxation strengths of the Teflon graft in circumferential direction were similar to the values of the more distally oriented arterial segments.[17]
Investigating the results of the uniaxial tensile tests on the synthetic grafts that have been implanted for three weeks, leads to the conclusion that the distensibility of the grafts decreased after implantation. This decrease was more pronounced in the longitudinal direction than in the circumferential direction. The knitted Teflon graft had the largest reduction in distensibility.[17]

Tremblay *et al.* conducted a study to evaluate the differences in mechanical properties of different graft materials. The graft materials that have been investigated are bovine pericardium, human pericardium which was either fresh or fixed in a Carpentier solution, and woven Dacron. These materials are compared mechanically with healthy and dilated human ascending aortas. The different materials and tissues have been tested biaxially and the design of the study is discussed in Section 2.3.2.[50]
When comparing the thickness of the different materials, there is noticed that human aortic tissues have a significantly higher thickness than the other materials. These are at least 74% thinner than the healthy and dilated ascending aortas.[50]
The stiffness between the different materials has been investigated as well. The stiffness has been evaluated at a low strain of 7.5% and at a high strain of 25%. At

low strains, the dilated ascending aortas appeared to be 1.3 times stiffer than the healthy aortas. Moreover, Dacron was 21 times stiffer than the dilated aortas, fixed and fresh human pericardium were respectively 4.1 and 5.9 times stiffer than the dilated aortas, and bovine pericardium had a stiffness which was 13.9 times higher than the stiffness of the dilated aorta. At high strain, the difference in stiffness between dilated and healthy ascending aortas was the same, the fixed and fresh human pericardium were respectively 7.1 and 9.5 times stiffer than the dilated aorta. The bovine pericardium and Dacron graft appeared to be respectively 16.4 and 18.4 times stiffer than the dilated aortas.[50]
The anisotropy between the different materials was calculated using the anisotropic index, which is the difference between the stiffness in circumferential and axial direction divided by the average stiffness. This anisotropic index is computed at the low strain (7.5%) and at the high strain (25%). For all materials, the circumferential direction is stiffer than the axial direction. At low strains, the anisotropic index of healthy ascending aorta and bovine pericardium was not significantly different from zero, meaning that these tissues have no directional dependency at low strains. The remaining tissues have an anisotropic index which differs significantly from zero at low strains. At high strains, all the materials showed significant directional dependency with an anisotropic index which was different from zero.[50]

2.2.2 Personalized External Aortic Root Support

Dissection of the ascending aorta is the most lethal symptom in patients with Marfan's syndrome. Therefore, when the aortic root diameter reaches a size of 50 mm, aortic root surgery is performed. This surgery can be the Bentall procedure or the David procedure, or a new surgical option in which the root and aortic valve are maintained. The Bentall and David procedure have been discussed in the Introduction. The new surgical option will be elaborated here. In this new procedure, the patient's aorta is recreated with rapid prototyping techniques based on the MRI images or CT images. This personalized three-dimensional replica of the patient's aorta is used to make a close fitting mesh or the PEARS that covers the aorta from the atrioventricular junction to beyond the brachiocephalic artery. Figure 2.4 shows a PEARS on the template made with rapid prototyping techniques based on MRI images. This PEARS is placed around the patient's aorta. The PEARS subsequently gets incorporated into the adventitia and forms a composite.[49] The PEARS can be made from different materials, e.g. polyester, PTFE or an ultra high molecular weight polyethylene.[16] According to the article of Pepper *et al.* [36] the mesh has a pore size of 0.7 mm, and is made from the same material as the Dacron grafts, PET.[55]

Figure 2.4: A Personalized External Aortic Root Support on the template made by means of rapid prototyping techniques, the mesh has a pore size of 0.7 mm. (Picture from [36])

Verbrugghe *et al.* investigated the use of the external aortic root support histologically and mechanically in sheep. Therefore, a mesh was positioned around the carotid artery of growing sheep. Four to six months after surgery, part of the coronary artery with a sleeved and an unsleeved portion was removed. The histological evaluation was performed by an experienced pathologist. The mechanical evaluation consisted of evaluation of the ultimate tensile strength using an uniaxial tensile test. The intima proved to be preserved, and in four out of five samples the media appeared to be intact. A fibrotic reaction was reported, but no signs of inflammation were present. The diameters of the supported carotid artery were comparable to the diameters of the unsupported arteries. Also, the adventitia had a similar thickness in both groups of arteries. The results of the mechanical analysis led to the conclusion that the ultimate tensile strength and the stiffness increased when supporting the carotid artery with a mesh.[55]
The use of the PEARS has investigated and published in different studies, which will be reviewed shortly.
A preliminary study by Pepper *et al.*, published in 2010, investigated the use of the PEARS in ten patients. These patients underwent a procedure where a PEARS is fitted around their dilated aortic root. MRI images were obtained prior to the operation, six months and twelve months after the operation, and annually thereafter. Also, MRI images of 37 non-operated Marfan patients are obtained and serve as control group. A reduction in aortic diameter was found for eight of the ten patients operated with the PEARS.[34]
In 2010, a follow-up study was published in which 20 patients underwent the procedure with the PEARS. In 19 of the 20 patients the procedure succeeded in its primary objective: reinforcing the ascending aorta while leaving the aortic valve intact and maintaining the interface between blood and endothelium. Also, only in the first patient cardiopulmonary bypass was required, and no anticoagulation therapy was required.[35]
Pepper *et al.* subsequently published another follow-up study in 2013 in which 14 extra patients received the PEARS, bringing the study group to 34 patients. The 34^{th} patient died as a result of an intraoperative accident. The first patient, operated in 2004, had no changes in dimensions of the aortic root. Also, in the first 20 patients, only the first patient required cardiopulmonary bypass, and no myocardial ischemia

is present in patients undergoing this surgery. Moreover, opening of the aorta, with accompanying embolic risks, is not required. No patient is receiving anticoagulant therapy, and no device, aorta, or valve-related events are reported.[37]
One concern that has risen comprises the risk that exists when the coronary arteries leave the support. In 2011, the opportunity has risen to investigate the coronary arteries in a patient who received the PEARS in 2004. This patient developed exercise induced chest pain and an invasive coronary angiography was performed. This coronary angiography made it possible to study the coronary orifices. Both left and right coronary orifice appeared to be normal, as well as the proximal arteries. An atherosclerotic narrowing was found in the left anterior descending coronary artery which was successfully stented.[12]
In the paper by Treasure *et al.* the main findings of the studies discussed above are summarized.[49]

2.3 Mechanical Testing

In order to determine the mechanical behavior of arterial tissue, mechanical tests can be performed, either *in vivo* or *in vitro*. When testing *in vitro*, a distinction between uniaxial and biaxial tests can be made. Different tests to capture the biaxial behavior of the arterial tissue can be used: the biaxial tensile test, the bulge inflation test, and the inflation-extension test.[1]
Determining the stiffness of arterial tissue *in vivo* requires the measurement of the pressure in the artery as well as the inner or outer diameter or the cross-sectional area of the artery. The stiffness of arterial tissue can be quantified by different indices, e.g. the distensibility coefficient, and the pulse wave velocity.[43] However, estimating the material properties of arterial tissue in vivo using non-invasive techniques, requires the use of certain assumptions. In the paper by Smoljkić *et al.* a method to determine material properties of arterial tissue *in vivo* is discussed.[46]
The bulge-inflation test uses square specimens from arterial tissue, which are clamped into the testing devices. The samples form a hermetically sealed cavity in which a fluid is injected at a controllable rate, while measuring the pressures. The deformation of the segment is determined optically.[1] The study conducted by Kim *et al.* gives an example of this type of biaxial testing. In this study, they determine the coefficients of the constitutive model proposed by Holzapfel and a stress value that reflects the stresses at failure for specimens obtained from the ascending aorta of patients with an aneurysm.[26]
In the inflation-extension test, a cylindrical segment of a vessel is pressurized and the corresponding extensions of the segment are registered. This registration is done by first applying markers to the segment, which will be tracked using a video-based tracking technique.[1] An example can be found in another study by Kim *et al.*, who investigated the circumferential variations in mechanical behavior of the porcine thoracic aorta using the inflation test.[25] Since the inflation-extension test closely resembles the motion of the arterial wall during the cardiac cycle, as it preserves the curvature of the sample, and it may include a residual stress analysis, it is the

preferred test by many for estimating the stresses that occur *in vivo*.[1],[25]
In biaxial tensile tests the sample can be square or rectangular, and can be loaded biaxially. During these tests, the strain can be determined using markers fixed in the center of the sample.[1] The markers can be drawn on the sample with alcohol based permanent ink as done by Zemanek *et al.*[60] or ceramic black markers as described in the article by Azadani *et al.*[2]
In uniaxial tests the samples have a rectangular or dogbone shape, and are subjected to extension along their length. During the test, force data as well as displacement data are collected. The displacements can be recorded using markers which can be tracked during the test. The parameters that can deduced from these types of tests are mainly related to tissue stiffness and failure strengths.[1]
According to Holzapfel *et al.* uniaxial tests alone are not sufficient to characterize arterial tissue completely, but can provide some basic information of the tissue.[21] This statement is confirmed by Zemanek *et al.* who state that when the parameters of a hyperelastic constitutive model need to be determined, uniaxial tests are not sufficient, since these models require the use of different types of biaxial stress-strain states.[60] However, due to the attachment techniques that are used for mounting biaxial testing, e.g. using suture wires, and due to the rectangular or square shape of the sample, biaxial tests are less appropriate for assessing the strength of the tissue.[1]
Uniaxial and biaxial test methods and protocols of different studies will be further described in the following sections.

2.3.1 Uniaxial Testing

In the article written by Lally *et al.* the elastic behavior of porcine coronary artery tissue is investigated using uniaxial and biaxial tension tests. The protocol used for uniaxial tests will be described here, the protocol for the biaxial tension tests is described in the following section. Twenty-one arterial samples are harvested from twenty-one pigs for the uniaxial tests. From each of these samples a rectangular shape is cut with a width of 3.5 mm, and is loaded longitudinally during the test. The samples are preconditioned during five preconditioning cycles in which a maximum load of 1N is reached at a strain rate of 60% per minute of the initial length. The initial length is the length the sample has when it has a preload of 0.05 N. After the preconditioning, the sample is loaded to failure at a strain rate of 60% per minute of the initial length.[29]
Okamoto *et al.* investigate the mechanical properties of the dilated human ascending aorta, which can occur in patients with Marfan syndrome. Tissue samples of 64 patients, of whom six had Marfan's syndrome, 33 had bicuspid aortic valve and 15 had tricuspid aortic valve, are investigated. They conduct uniaxial as well as biaxial tests. The latter are described in the following paragraph. The uniaxial tests are used to determine the strength of the tissues in circumferential direction. Samples of approximately 3 cm in length and 1 cm wide are cut from the tissues. The samples are given a dogbone shape, in which the width was smallest in the middle with a value of approximately 4 mm. The biaxial tester is used in a uniaxial setting: the

sample is attached to one direction of the biaxial tester. The samples are emerged in a bath of Krebs-Ringer solution. The protocol starts with 10 preconditioning cycles, triangular waveform with period of 10s going to 0.10 - 0.49 N. Next, the sample was stretched until failure by applying a force ramp of 0.59 N/s for 30s.[33]
The effect of aneurysm formation on the mechanical properties of the ascending aorta is also investigated by Vorp *et al.* From 26 patients samples of the aneurysmatic ascending aorta are obtained. Seventeen longitudinally oriented and 23 circumferentially oriented samples are cut. Control samples are obtained from ten subjects during autopsy, giving seven longitudinal and seven circumferential samples. All samples are mounted in a uniaxial tester and are continuously sprayed with phosphate-buffered saline. The samples are stretched until failure during which the deformation and force are measured.[56]
Carr-White *et al.* examine the mechanical properties of the pulmonary autograft in the aortic root position using uniaxial testing. During autograft surgery specimens of the aorta and pulmonary artery are obtained from nine patients. In addition, specimens are obtained from a patient in whom an autograft of four months is explanted. The specimens are cut into strips which are mounted in clamps. The samples are stretched until failure with an extension rate of 10 mm per minute.[6]
To evaluate the mechanical effect of the external aortic root support on a carotid artery, Verbrugghe *et al.* performed uniaxial tensile tests on segments of the carotid artery with no support of a mesh, and segments around a mesh was fixed six months prior to explantation. Therefore, segments from an unsupported and a supported segment of the carotid artery were obtained from five sheep. Circumferentially oriented strips of 10 mm by 5 mm were cut from these segments. The protocol started with five preconditioning cycles going to a load of 6.67 N/cm^2, with a crosshead speed of 5 mm/s. After which the sample was stretched to failure with the same crosshead speed.[55]
In order to investigate the mechanical properties of synthetic arterial grafts, Hasegawa *et al.* conducted a series of uniaxial tests. Samples were obtained from woven and knitted Dacron grafts, as well as from woven and knitted Teflon grafts. Arterial samples, both in longitudinal and circumferential direction, from the the canine aortic tree were collected at the following segments: ascending aorta, proximal and distal abdominal aorta, the left iliac and the femoral arteries. Furthermore, the four types of synthetic grafts were implanted for three weeks in subcutaneous tissue of canine hind limbs. Two types of tests were conducted to investigate respectively the stress-strain relationship and the stress relaxation pattern on these samples. The test to study the stress-strain relationship consisted of a uniaxial tensile test with a crosshead speed of 5 mm/min. The test to study the stress relaxation pattern used a cross head speed of 500 mm/min, to stretch the sample a fixed amount and keep it fixed at that amount for 5 minutes after which it was quickly released. Samples oriented in the longitudinal direction were stretched to 50% of their initial length, whereas samples oriented in the circumferential direction were stretched to 10% of their initial length. The results of this study have been reviewed in Section 2.2.1.[17]

2.3.2 Biaxial Testing

Lally *et al.* describe biaxial tests to determine the elastic behavior of porcine coronary artery tissue. Therefore, eight samples are harvested from five pigs. These samples are cut into squares of 5 mm x 5 mm. Markers are applied on the samples using water-resistant, oil-based, quick drying ink. Five preconditioning cycles are applied in which the samples reach a maximum load of 0.5 N a strain rate of 60% per minute of the initial length, which is determined at a preload of 0.05 N. The preconditioning is followed by loading at a constant strain rate of 60% per minute of the initial length until tears are detected in the sample.[29]
The mechanical properties of different graft materials used in reconstruction of the aortic arch and the mechanical properties of the healthy and dilated human ascending aorta are investigated by Tremblay *et al.* Four samples from 30 healthy and 14 dilated ascending aortas are taken, as well as from 34 human pericardial sections. From commercial bovine pericardium square samples are also cut in order to compare them with Dacron grafts. Three gelatin impregnated Dacron grafts are cut into square samples. All the samples are squares of 15 mm x 15 mm and are tested biaxially. The samples are mounted into the biaxial tester using sutures. After which they are placed in bath of 37°C of Krebs-Ringer buffered solution. A preload of 0.05 N is applied to both sides of the square sample. The protocol starts with 10 preconditioning cycles to 30% strain, followed by three runs to 30%.[50]
Okamoto *et al.* investigate the mechanical properties of the dilated human ascending aorta. The used tissues are described above. From these tissues, square samples of 2 cm - 2.5 cm are cut. Four markers are attached using glue in the central region of the samples. These samples are mounted in the biaxial tester using suture wires and are placed in a bath of Krebs-Ringer solution at room temperature. Preconditioning consists of 10 cycles of 10% equibiaxial stretch. For different prescribed stretch ratios, with a baseline of 2% stretch, three ratios of stretch are applied. First, the sample is stretched in one direction while the other is held constant. Second, the direction which previously was held constant is stretched and the other direction is held constant. Finally, both directions are stretched equibiaxially. The strain rates vary between 2% per second to 4% per second.[33]
In the Ross operation, the pulmonary autograft is used as replacement for the aortic valve. The study by Azadani *et al.* has as objective the comparison of human pulmonary and aortic roots in terms of their mechanical properties. Healthy human aortic root and pulmonary root specimens are obtained from 21 patients. Square samples are cut from these specimens. Five black ceramic markers are attached to the center of the samples, resulting in a 3 mm x 3 mm grid in the center of the sample. The square samples are mounted on the biaxial tester using suture wires, and are emerged in a bath with saline solution at room temperature. The equibiaxial displacement control starts with 10 preconditioning cycles at 10% stretch, with a triangular waveform of period 2s. Next, the sample is repeatedly stretched up to 55% peak strain.[2]
The properties of porcine pulmonary and aortic root are compared in a study by Matthews *et al.* In this study, 10 porcine hearts and one human heart are obtained

and from both aortic and pulmonary roots five samples are cut. These samples receive five black ceramic markers in the center of the sample resulting in a grid of 3 mm x 3 mm. The samples are mounted using suture wires and float in a saline solution at a temperature of 20°C. The equibiaxial displacement controlled protocol starts with ten preconditioning cycles using a triangular waveform at 0.5 Hz at a stretch level of 10%. Next, the biaxial tester stretches the sample consecutively to 20%, 35%, and 55% peak strain.[31]
Martin *et al.* conducted a study to compare the differences in material properties between aged human and porcine tissues. Eight human hearts and six nine months old porcine hearts are tested. From each heart samples from the ascending aorta, right coronary sinus, left coronary sinus, and non-coronary sinus are cut with dimensions respectively 21.5 ± 3.5 mm, 13.7 ± 1.8 mm, 13.4 ± 1.1 mm, and 14.1 ± 2.6 mm. In order to measure the strain, the researchers placed four graphite markers on each of these samples in a square of 3 mm x 3 mm. After preparation of the samples, the samples are placed in a bath with 0,9% NaCl solution at room temperature. In contrast with the above studies, the researchers used a stress controlled protocol in which the stress components $T_{11} : T_{22}$ are kept constant and the stress components T_{12} and T_{21} have a zero value. The protocol starts with 20 preconditioning cycles. Each of the samples are tested at the highest load level possible without damaging the tissue. At this level the following ratios are used to test the sample: $T_{11} : T_{22}$= 0.75:1, 0.5:1, 0.3:1, 1:1, 1:0.75, 1:0.5 and 1:0.3.[30]

2.4 Conclusion

The use of a PEARS for a dilated aortic root in patients with Marfan's syndrome has been studied and published. However, most of these papers report solely clinical results, and no mechanical aspects have been investigated.[34], [35], [37] A mechanical analysis of the use of a PEARS is given in the paper by Verbrugghe *et al.* In this paper, the PEARS is positioned around the carotid artery of growing sheep. The authors performed uniaxial tests to quantify the ultimate tensile strength and the stiffness. Both quantities increased when a reinforcement was added to the carotid. As such, a mechanical analysis of the PEARS positioned around the aorta is lacking. Apart from the uniaxial tests on the PEARS in carotid position, no mechanical tests on the PEARS are reported. Moreover, no study on this reinforcement, when used in the Ross procedure, has been found. A mechanical analysis on the PEARS when used in the Ross procedure has not yet been done, and will be undertaken in this thesis.
When undertaking a mechanical analysis, a decision regarding the mechanical tests needs to be made. As was explained in Section 2.1.2, the artery consists of a matrix in which fibers are dispersed. The direction of this fibers differs in the different arterial layers. Due to the presence of these fibers, there is expected that the mechanical behavior of the artery will be different in different directions. Performing only uniaxial tests will not be sufficient. Thus, both uniaxial and biaxial tests will be performed. The test protocols for both types of mechanical tests start with preconditioning, as is

done by Okamoto *et al.*[33] Furthermore, markers will be attached on the samples for uniaxial and biaxial tests by glueing small parts of suture wires onto the sample. The uniaxial tests are performed to be able to quantify the ultimate tensile strength. After the preconditioning cycle in the uniaxial test protocol, the sample will be stretched until failure. The biaxial test protocol can be either displacement-controlled, e.g. the protocol used by Azadani *et al.*[2], or force-controlled, e.g. the protocol used by Martin *et al.*[30] Both type of protocols will be used.

Chapter 3

Mechanical Testing

This thesis aims to mechanically characterize the use of a PEARS in Ross procedure and to examine the influence of this wrapping on this procedure. Therefore, tests investigating the mechanical behavior need to be performed. In the literature overview, several types of mechanical tests are described, with the main focus on biaxial and uniaxial tests. These two types of tests will be performed in order to obtain force-displacement curves that can be used to determine material characteristics describing the mechanical behavior of the tissue.
This chapter describes the different mechanical tests that have been performed. It starts by outlining the surgical procedure, followed by a short calculation of the stresses and strains that are present in physiological conditions. Thereafter, the protocol used for uniaxial testing and the protocol for biaxial testing is explained. Some steps in these methods are identical for both types of mechanical testing, e.g. measuring the thickness. A brief overview of the results is given.

3.1 Materials and Methods

3.1.1 Surgical Procedure

Seven female Lovenaar sheep have underwent a simplified version of the Ross procedure, followed by a reinforcement with the PEARS textile. In the simplified version of the Ross procedure a section of the truncus pulmonalis is used to replace a part of the thoracic aorta descendens. Afterwards, the truncus pulmonalis replacing part of the thoracic aorta is reinforced using the PEARS textile. During this procedure a section of the pulmonalis has been harvested. Six months after the procedure, the sheep are sacrificed. Samples from the following tissues are collected: unreinforced aorta, reinforced aorta, and reinforced pulmonalis in aorta position, and are mechanically tested. Furthermore, one control sheep, namely sheep BE77572-321, has been treated by replacing a part of the thoracic aorta descendens with a section of the truncus pulmonalis, but without reinforcing the truncus pulmonalis in aortic position. After six months, this sheep is sacrificed and samples from the following tissues are obtained: unreinforced aorta and unreinforced pulmonalis in aorta position. The

details of the eight sheep can be found in Appendix A.

After removing the different tissue types, the tissues are frozen either in a physiological PBS solution or in a physiological NaCl solution, and are stored at a temperature of $-80°C$.
Overnight, the tissues are thawed in a refrigerator at $4°C$. After thawing, the tissue is divided into different samples, either meant for biaxial tests or for uniaxial tests, which will be discussed in the following sections.

3.1.2 Physiological conditions

Before starting mechanical testing, it is important to calculate the stresses and strains to which the aorta and truncus pulmonalis are subjected to in physiological conditions. These values will serve as an indication for determining the different force- and displacement- values used in the protocols of the uniaxial and biaxial tests. In normal physiological conditions, a vessel is subjected to shear stress and a stress resulting from the dynamic pressure exerted by the blood on the vessel wall. The shear stress is directed longitudinally along the vessel, whereas the stress due to the pressure works in the circumferential direction. The wall shear stress is several orders of magnitude lower than the circumferential stress, and will be neglected. [43] The stress as a result of the blood pressure will be calculated using the law of Laplace. The law of Laplace, illustrated in Figure 3.1, states that in a thin-walled cylinder the stress in circumferential direction can be related to the pressure inside the cylinder using following equation:

$$\sigma_{circumferential} = \frac{P \cdot r}{t} \tag{3.1}$$

In this equation, P is the blood pressure, r the radius of the blood vessel, and t the thickness of the vessel. Values for these parameters are taken from the literature. According to Bia *et al.*, the mean systolic blood pressure in sheep is 96.7 ± 9.3 mmHg at the aorta, with a corresponding mean diameter of 15.7 ± 2.2 mm. The diastolic blood pressure has a value of 74.8 ± 9.1 mmHg with a corresponding diastolic diameter of 14.7 ± 2.3 mm.[4]

Furthermore, the stress can not be used as a value to enter in a protocol for mechanical tests. Protocols are either force-controlled or displacement-controlled. Therefore, a value for the force required to result in the circumferential stress from equation 3.1 needs to be calculated. From Figure 3.1 can be seen that a force can be calculated from the following equation:

$$\sigma_{circumferential} = \frac{F_{circumferential}}{A_{circumferential}} = \frac{F_{circumferential}}{t \cdot h}$$

$$\Rightarrow F_{circumferential} = \sigma_{circumferential} \cdot t \cdot h = \frac{P \cdot r}{t} \cdot t \cdot h = P \cdot r \cdot h \tag{3.2}$$

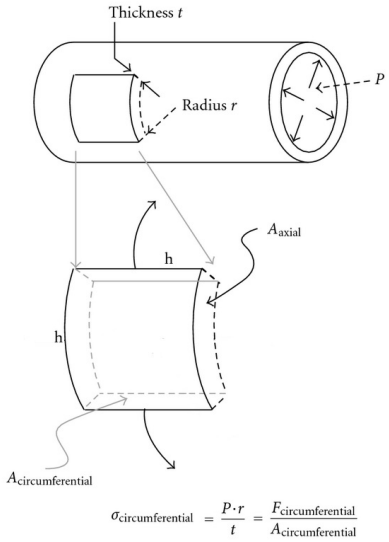

Figure 3.1: The law of Laplace, with P the pressure inside the vessel, r the radius of the vessels, and t the thickness of the vessel. (Figure adapted from [42])

In equation 3.2, the parameter h determines the size of the square sample. As will be explained in the section on biaxial testing, the samples will have a size of 6 mm x 6 mm after mounting them on the biaxial tester. Entering the numerical values of the parameters in equation 3.2, leads to:

$$F_{circ,sys} = 96.7mmHg \cdot 133.322 \frac{Pa}{mmHg} \cdot 7.85mm \cdot 6.00mm = 0.61N = 610mN \quad (3.3)$$

$$F_{circ,dia} = 74.8mmHg \cdot 133.322 \frac{Pa}{mmHg} \cdot 7.85mm \cdot 6.00mm = 0.47N = 470mN \quad (3.4)$$

The strains to which the aorta is subjected will be calculated as follows:

$$\epsilon = \frac{D_{sys} - D_{dia}}{D_{dia}} \quad (3.5)$$

Using the values for the systolic and diastolic diameter from Bia *et al.*, respectively 15.7 ± 2.2 mm and 14.7 ± 2.3 mm, leads to

$$\epsilon = \frac{15.7 - 14.7}{15.7} = 0.068 = 6.8\% \quad (3.6)$$

The last quantity that will be needed for the protocols is the loading rate under physiological conditions. This will be calculated using the force under systolic and diastolic conditions, as well as the heart rate under normal conditions, which is taken as 114 bpm or 1.9 beats per second according to Bia *et al.*[4].

$$loadingrate = \frac{F_{circ,systole} - F_{circ,diastole}}{\frac{1}{HR}} = \frac{0.61N - 0.47N}{\frac{1}{1.9}} = 0.27\frac{N}{s} \quad (3.7)$$

3.1.3 Uniaxial Testing

Sample Preparation

After thawing of the tissue, different samples are cut from this tissue. Samples for uniaxial tests are required to have a dogbone shape and are directed either in the longitudinal or circumferential direction of the tissue. This shape ensures that the sample will rupture at the middle, where its cross-section is the smallest.

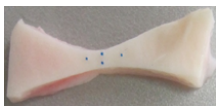

Figure 3.2: Dogbone shaped aortic sample with four markers placed in diamond configuration

On this sample, four markers are placed using small fragments of surgical suture wire in a diamond like configuration. This configuration enables the tracking of the extension of the sample along its length and the thinning of the sample in the orthogonal direction. However, only the extension along the length of the sample will be used. An example of a dogbone sample with the four markers can be found in Figure 3.2.

Thickness Measurements

To measure the thickness of the sample, the tissue is placed between two metal plates of which the thicknesses are known. This set-up is photographed from the side, and through image analysis of the picture in *MatLab 2013*, the thickness is determined. This set-up is demonstrated in Figure 3.3. The thickness of the samples, prepared for biaxial tests, is measured using the same set-up.

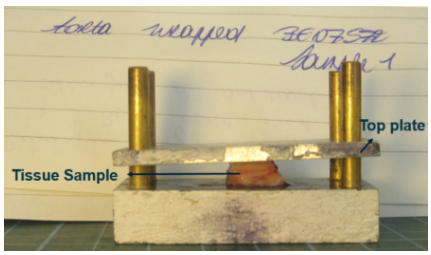

Figure 3.3: A biaxial sample of the reinforced aortic tissue placed in the set-up used for thickness measurements.

Hardware

The dogbone samples are clamped in the Instron 5943 device and the whole experiment is registered using the Limess Snap Shot Bluehill camera at a frequency of 30 Hz.

Protocol

When mounting the sample, a preload of 0.05 N is applied. Firstly the sample is subjected to 10 preconditioning cycles: the sample is stretched to half the physiological strain 3.4%, calculated in Section 3.1.2, at a rate of 40 mm/min, and is subsequently released. After preconditioning, the sample is stretched at the same rate until rupture.

3.1.4 Biaxial Testing

Sample Preparation

After thawing of the tissue, different samples are obtained from the tissue. For uniaxial tests, these samples had a dogbone shape and the markers are placed in a diamond configuration. Biaxial tests, on the other hand, require square samples. These samples have a size of 8 mm x 8 mm, and two of the edges are directed longitudinally and subsequently two of the edges are directed circumferentially. The markers, small fragments of surgical suture wire, are glued in the center region of the sample, where the stresses and strains are the most homogeneous. Four markers are placed at the corners of a square, and a fifth marker is placed in the center of this square. This configuration enables to track the deformation of the sample in the longitudinal and circumferential direction of the sample. In Figure 3.4, an example of a biaxial sample, mounted in the biaxial tensile tester, can be found.

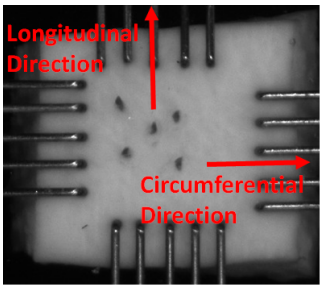

Figure 3.4: Biaxial sample of the aorta of sheep BE07572-73 mounted in the Biotester

Hardware

The biaxial tests have been performed on the BioTester, the biaxial tensile test system of CellScale, visualized in Figure 3.5. As can be seen from the right part of this figure, the BioTester has two main axes, namely the x- and y-axis. When mounting the sample, care is taken that the circumferential direction of the sample is aligned with the x-direction, and the longitudinal direction of the sample is aligned with the y-direction of the BioTester.
On each of the axes, two actuators are present. These pairs of actuators can be operated separately, thereby allowing the sample to be stretched with a different force- or stretch in the x-direction than the force or stretch in the y-direction. Furthermore,

one load cell is positioned on each of the axes in order to measure the forces along that axis. The load cells used during the tests have a maximum load of 23 N and have an accuracy of 46 mN.
The mounting of the sample is done by means of BioRakes. The BioRakes can be described as being five sharp pins, with a spacing of 1 mm, that will be pierced through the tissue. The five pins of one BioRake will be piercing through one edge of the square sample, implying that four BioRakes are required for mounting one sample.
The sample, mounted by means of the BioRakes, will be suspended in a fluid bath filled with a 0.9 % NaCl solution. By heating of the fluid bath, the solution can be brought to the physiological temperature of 37°C. In Figure 3.6, a mounted sample is visualized.

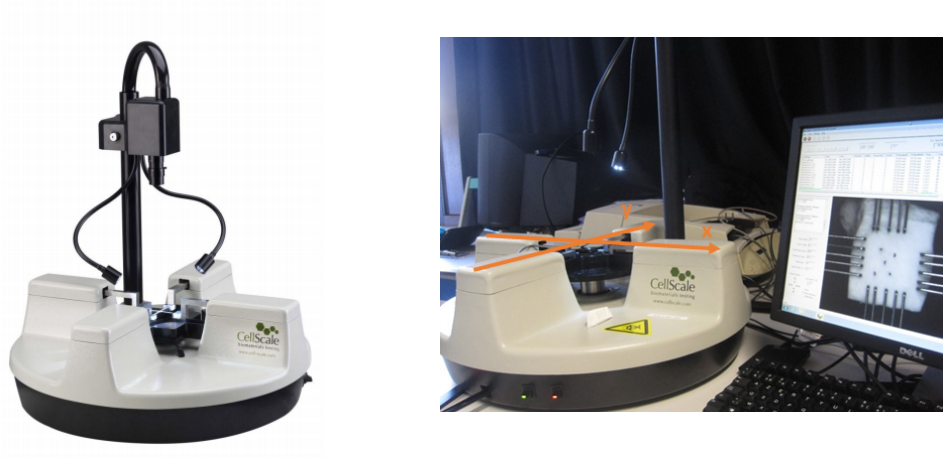

Figure 3.5: The BioTester [8](left), and the set-up of the Biotester, with x the circumferential direction and y the longitudinal direction (right)

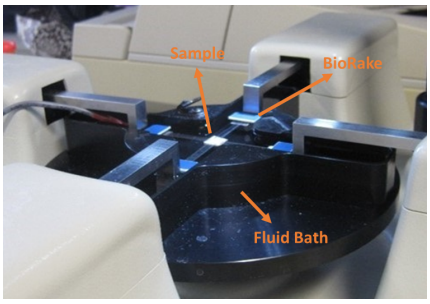

Figure 3.6: Visualization of a mounted sample in the BioTester

The test will be registered using the high-resolution CCD camera at a frequency of 30 Hz, mounted on the BioTester. The images obtained from this camera will be used for tracking the markers during the test.

Protocol

Two types of protocols can be used for biaxial tensile tests: force-controlled protocol or displacement-controlled protocol. Displacement-controlled tests have a major disadvantage compared to force-controlled tests. In these types of test, the imposed stretches are influenced by the connection between the sample and the actuator, implying that there is no direct link between the imposed stretches and the resulting strains in the sample.[54] However, both types of protocols are used for the biaxial tests, when a sufficient number of samples is available. When the number of samples is limited, the displacement-protocol is chosen, since the biaxial tester has proven to be more reliable when using displacement-controlled protocols.
Before, elaborating on the details of the protocols, the terminology regarding the experiments needs to be explained. The same terminology is followed as in Van den Abbeele *et al.*[54] In this work, a test is divided into different test sequences, which are composed of different test sets. Each of these test sets comprises several test cycles. The application of a force or a displacement, followed by the subsequent release, composes one test cycle. The structure of an experimental protocol is displayed in Figure 3.7.

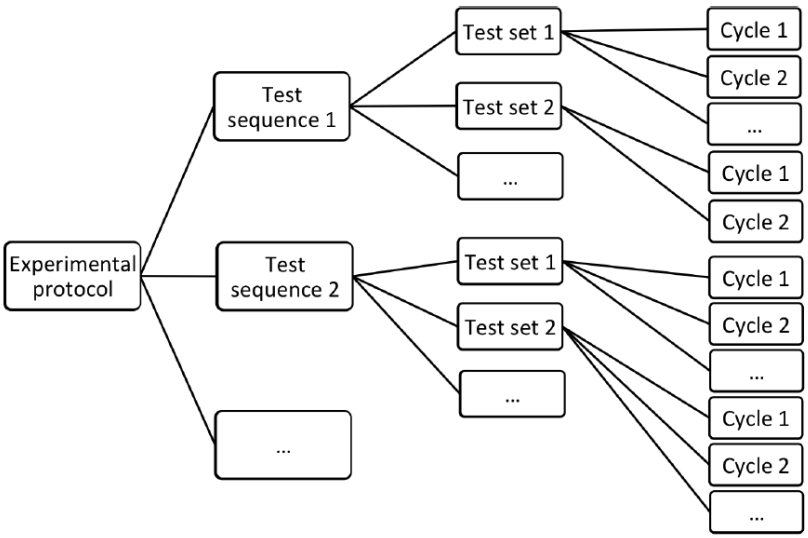

Figure 3.7: The structure of an experiment [54]

During one test set, the ratio of the applied force or stretch between the x- and y-direction remains constant. This ratio can change from test set to test set. The maximum applied force or stretch differs between test sequences. Before the start of each test cycle, the sample is preloaded with a force of 70 mN in both directions to prevent sagging.
Each experimental protocol starts with preconditioning.

Force-controlled protocol The force-controlled protocol starts with a preconditioning phase. The preconditioning phase comprises 10 test cycles where the sample is loaded until 300 mN, half of the physiological load calculated in Section 3.1.2.
The preconditioning phase is followed with a first test sequence, in which the sample is loaded up to 600 mN. The test sets in these test sequence determine the ratio with which this load is applied to the sample. Firstly, the load is applied with a ratio 1:1, meaning that both directions are subjected to a load of 600 mN. Secondly, the x-direction is subjected to a load of 600 mN, and the y-direction to a load of 300 mN. Subsequently, the ratio is reversed, and a load of 300 mN is exerted in the x-direction, and a load of 600 mN in the y-direction. The test sequence ends with subjecting the x- and y-direction both to a load of 600 mN.
The following test sequence has a maximal load of two times the physiological load, 1200 mN. The ratios of loading of the test sets in this test sequence are the same as in the previous test sequence. First, both directions are subjected to 1200 mN. Next, the load in the y-direction is half of the load in the x-direction. This ratio is reversed in the next test set. The test sequence ends with loading both directions with 1200 mN.
The consecutive test sequences have a higher maximal load, which is a multitude of the physiological load, than the previous test sequences. In the third test sequence, the maximal load is three times the physiological load, resulting in a maximal load of 1800 mN. Four times the physiological load, 2400 mN, is maximally exerted in the fourth test sequence. The next test sequence subjects the sample to six times the physiological load, 3600 mN. The experimental protocol, without the preconditioning phase, is given in Table 3.1.

Table 3.1: The different test sequences with the different test sets for the force-controlled protocol

Maximal load [mN]	Ratio 1:1 [mN]	Ratio 1:0.5 [mN]	Ratio 0.5:1 [mN]	Ratio 1:1[mN]
1 x physiological force	600:600	600:300	300:600	600:600
2 x physiological force	1200:1200	1200:600	600:1200	1200:1200
3 x physiological force	1800:1800	1800:900	900:1800	1800:1800
4 x physiological force	2400:2400	2400:1200	1200:2400	2400:2400
6 x physiological force	3600:3600	3600:1800	3600:1800	3600:3600
8 x physiological force	4800:4800	4800:2400	2400:4800	4800:4800
10 x physiological force	6000:6000	6000:3000	3000:6000	6000:6000

During each test sequence, the maximal load is increased. The test ends either when the end of the protocol is reached or when the sample ruptures. The last test sequence the sample has completely undergone, is taken as the test sequence used for the calculations. When increasing the imposed load, the dataset available increases. When the imposed load is higher, it takes more time before this load has been reached and therefore more data points are available. By starting the imposed load at the physiological load, followed by test sets in which the imposed load is increased in a steplike manner, ensures that there is at least one dataset available per sample, as it is not expected that the sample will rupture when submitted to physiological conditions.

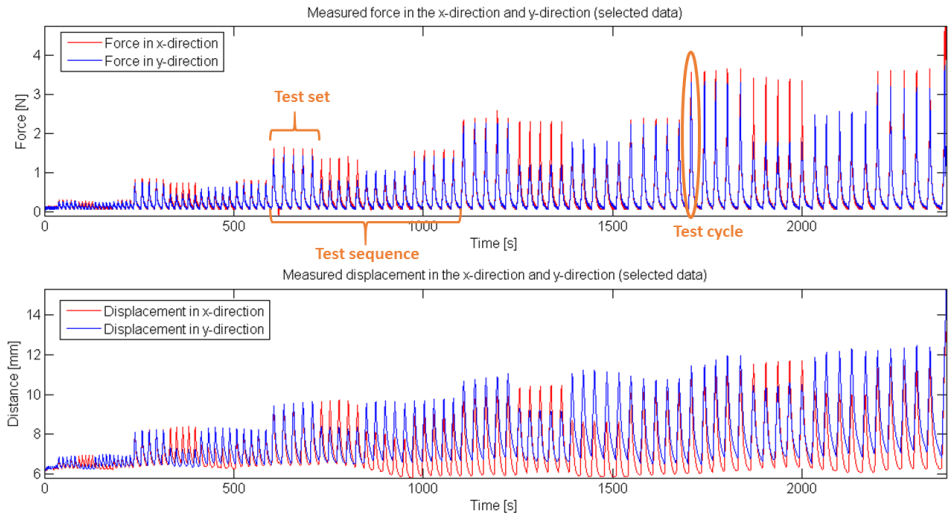

Figure 3.8: Force and displacement measured of an aortic tissue sample of sheep BE07572 – 73 after a force-controlled experiment.

In Figure 3.8, the output of an experiment is shown. In this figure, the different ratios of the force imposed by the protocol in subsequent test sets are visible. The highlighted test cycle in this figure is shown enlarged in Figure 3.9. The stretching phase and subsequent recovery phase of one test cycle are clearly visible in this figure.

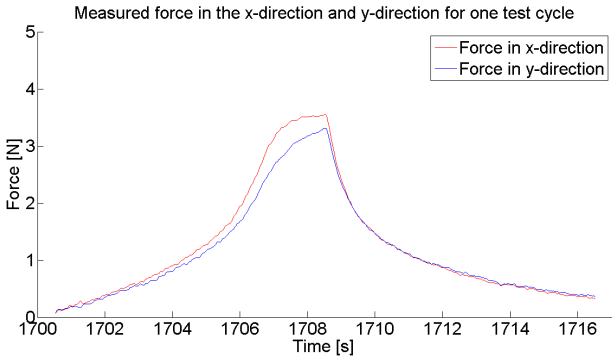

Figure 3.9: Force measured during one test cycle in a force-controlled experiment on an aortic tissue sample of sheep BE07572 – 73

Displacement-controlled The displacement-controlled protocol has a similar layout as the force-controlled protocol. However, not a multitude of the physiological load is imposed, but a multitude of the physiological displacement is imposed.
Similar to the force-controlled protocol, the displacement-controlled protocol commences with a preconditioning phase, in which the sample is stretched to a strain equal to half the physiological strain. In Section 3.1.2 the physiological strain was calculated to have a value of 6.8%. The preconditioning phase imposes a displacement of 3.4%.
The first test sequence will impose a maximal displacement of 6.8%, with the test sets having the following ratios: 1:1, 1:0.5, 0.5:1 and 1:1. The following test sequences all impose a multitude of the physiological displacement as the maximal displacement in the same ratios as the first test sequence. The experimental protocol, excluding the preconditioning phase, is described in Table 3.2.

Table 3.2: The different test sequences with the different test sets for the displacement-controlled protocol

Maximal displacement [%]	Ratio 1:1 [%]	Ratio 1:0.5 [%]	Ratio 0.5:1 [%]	Ratio 1:1 [%]
1 x physiological displacement	6.8:6.8	6.8:3.4	3.4:6.8	6.8:6.8
5 x physiological displacement	34:34	34:17	6.8:1200	1200:1200
10 x physiological displacement	68:68	68:34	34:68	68:68
15 x physiological displacement	102:102	102:51	51:102	102:102
20 x physiological displacement	136:136	136:68	136:68	136:136

During each test sequence, the maximal displacement is increased. The test ends either when the end of the protocol is reached or when the sample ruptures. The last test sequence the sample has completely undergone, is taken as the test sequence used for the calculations.

3.2 Results

3.2.1 Sample Preparation

Previously stated, four types of tissues have been obtained from seven different sheep. From each tissue segment, different samples have been prepared and tested. A total of 63 samples have been tested biaxially, of which 32 aorta samples, eight pulmonalis samples, ten reinforced aorta samples, and 13 reinforced pulmonalis samples. Furthermore, a total of 37 uniaxial samples have been tested, including 15 aorta samples, 15 pulmonalis samples, three reinforced aorta samples, and four reinforced pulmonalis samples. However, all the pulmonary tissues as well as the reinforced pulmonalis of sheep BE47572-393, have been tested by M. Van Den Abbeele, author of [54].
The first step of the experimental phase consisted of the sample preparation, in which samples for uniaxial and biaxial test are cut from a tissue segment. An example of the position of the different samples on a tissue segment of the aorta is given in Figure 3.10. In Appendix B the positioning of all the samples is given.

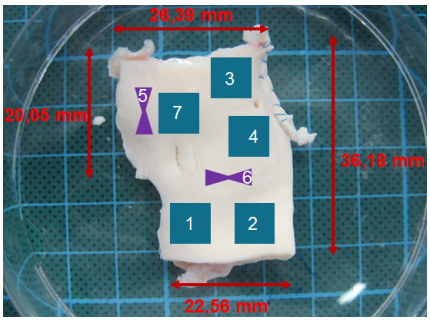

Figure 3.10: Positioning of the biaxial and uniaxial samples on the aortic tissue from Sheep BE37572-418

3.2.2 Thickness Measurements

After cutting the sample, its thickness was measured. The thickness of the samples used for biaxial testing can be found in Appendix D in the last column of each table.

3.2.3 Biaxial and uniaxial tests

The sample is mounted in the biaxial tester or in the uniaxial tester, depending on the shape of the sample. An example of a force-displacement curve typically obtained from the biaxial tester can be found in Figure 3.8 in the previous section. Furthermore, the displacement data from the biaxial tester is not used for calculating the stresses and strains, but the displacements found by markertracking are used. From the uniaxial tests, force-displacement curves are found as well, but have a different shape, and Figure 3.11 shows an example of these types of curves.

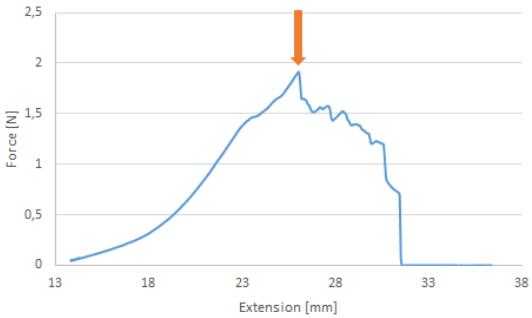

Figure 3.11: Force-extension curve of a uniaxial test of the aorta of Sheep BE07572-73. The orange arrow indicates the moment of failure of the sample

3.3 Discussion

3.3.1 Thickness Measurements

The values of the thickness for each biaxial sample are reported in Appendix D. When comparing the values of the thickness of the aorta with those of the pulmonalis, a possible trend may be observed. In many cases the thickness of the pulmonalis is smaller than the thickness of the aorta. This is similar to what Van den Abbeele *et al.* found, who stated that the thickness of the human aorta, with an average thickness of 2.44 mm, was significantly different from the thickness of the human pulmonalis, with an average value of 1.88 mm.[54] Furthermore, the thicknesses of the reinforced pulmonalis are in many cases higher than those of the unreinforced pulmonalis. However, a similar trend is not as evidently present when comparing the thickness of the reinforced aorta with the unreinforced aorta. Demonstrating these observations statistically is beyond the scope of this thesis.

3.3.2 Uniaxial Tests

Uniaxial tests have been performed to be able to determine the strength of the different tissues. This can be done by determining the ultimate tensile stress and ultimate tensile strain for each tissue. This is done for one sample of each type of tissue: unreinforced aorta, reinforced aorta, unreinforced pulmonalis, and reinforced pulmonalis. The ultimate tensile stress and ultimate tensile strain correspond to the stress and strain present in the sample at the moment of failure. A figure is made in which the stress-strain curve for one sample of each tissue type is plotted. The final point of each curve corresponds to the moment of failure. The result is shown in Figure 3.12.

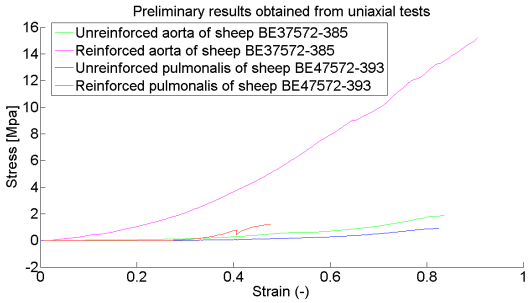

Figure 3.12: The stress-strain curves obtained from uniaxial tests for one sample in circumferential direction of each tissue type: unreinforced aorta, reinforced aorta, unreinforced pulmonalis, and reinforced pulmonalis

However, for no sheep successful uniaxial tests have been performed for all four tissues. There are two distinct reasons. The first reason pertains to the size and shape of the tissue sections available. For the reinforced tissues, often not enough tissue was available to obtain the dogbone samples for uniaxial tests. The second reason is that not every uniaxial test has been successful. In a few cases, the sample

did not rupture, but slipped out the clamping system, resulting in an incomplete test.
Figure 3.12 visualizes preliminary results from the uniaxial tests. From this figure can be seen that failure occurs for a much higher stress for the reinforced tissues when compared to the corresponding unreinforced tissues. However, not enough samples have been tested to draw a general conclusion regarding the tensile strength of the different reinforced tissues, only one uniaxial sample of the reinforced aorta was successfully tested, and only three samples of the reinforced pulmonalis were successfully tested. Of the unreinforced tissues, enough samples have been successfully tested to perform a further analysis regarding their tensile strength. A total of 12 aorta samples and 15 pulmonalis samples have been successfully tested uniaxially. This analysis is beyond the scope of this thesis.

3.3.3 Biaxial Tests

Biaxial tests are more appropriate to model the anisotropic behavior of tissues compared to uniaxial tests, which are more appropriate for quantifying the strength of the material.

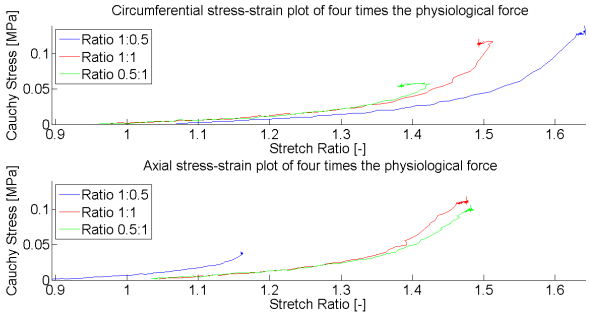

Figure 3.13: The stress-strain curves of a sample for the pulmonalis of sheep BE07572-73. A curl at the end of the curves can be observed, as well as a cumulation of datapoints

As previously mentioned, some samples have been tested by Van den Abbeele. For these samples not the exact same protocol has been followed, and one problem regarding these tests was observed. When the stress-strain curves of these samples are plotted, it can be noticed that a curl at the end of the curves is present, combined with a cumulation of datapoints. An example is given in Figure 3.13. There is assumed that this problem is related to the speed at which the sample is stretched, and it has been resolved by reducing this speed.

3.4 Conclusion

In this section, the experimental part of this thesis is discussed, starting with an explanation on the used materials and methods, and ending with a brief exposition on the different results obtained from these experiments. Both biaxial and uniaxial tests are performed. However, only the data obtained from the biaxial tests will be used further on. The uniaxial tests have been performed to ensure completeness with respect of characterizing the mechanical behavior of the different tissue types, and this data can be analyzed in the future.

Chapter 4

Parameter Fitting to the Gasser-Holzapfel-Ogden Model

The results of the mechanical tests consist of force-displacement curves for each tested sample. In this chapter, this force-displacement curves are used to determine material characteristics of the sample. The curves are used to calculate stress-strain curves, which serve as input for the Gasser-Holzapfel-Ogden model. The GHO model is a constitutive law characterizing the mechanical behavior of arterial tissue, using a set of parameters. Determining these parameters comprises a large section of this chapter.
This chapter starts by describing the GHO model. In a second section there is explained how the different material parameters of this model are calculated. Furthermore, the methods tested to find a representative set of parameters for each tissue type tested, are reported in this section. In the third section the determined parameters are given, as well as the results pertaining to the methods for finding a representative set of parameters. Finally a discussion on the results concludes this chapter.

4.1 Description of the GHO model

The GHO model is a constitutive law which describes the mechanical response of arterial tissue. The artery is viewed as a cylindrical tube, with two layers: the media and adventitia. Since the intima can be discarded in the determination of solid mechanical properties, this layer is not taken into account. This assumption is valid for healthy young arteries, where the intima is thin. However, the intima becomes stiffer and thicker with age, and it may contribute to the mechanical behavior. Taking the intima into account in the GHO model is similar to the other two layers, and is therefore not difficult.
The adventitia and the media are described as fiber-reinforced material, consisting of a non-collagenous matrix and collagenous fibers. The anisotropy in the mechanical response is a consequence of the presence of these fibers.[21]
A few assumptions have been made in the construction of this model. There is

assumed that when an arterial ring is cut and it springs open, the configuration in which it is sprung open is stress free. The residual stresses in the axial direction are not taken into account.[21]
Both arterial layers are modeled with the same form of the strain-energy function with different material parameters for each layer. The strain-energy function is divided into a part that models isotropic deformations and a part that models anisotropic deformations.

$$\Psi(\boldsymbol{C}, \mathbf{a}_{01}, \mathbf{a}_{02}) = \Psi_{iso}(\boldsymbol{C}) + \Psi_{aniso}(\boldsymbol{C}, \mathbf{a}_{01}, \mathbf{a}_{02}) \tag{4.1}$$

In this equation the vectors $\mathbf{a}_{01}$ and $\mathbf{a}_{02}$ correspond to the directions of the collagen fibers, and $\mathbf{C}$ is the right Cauchy-Green tensor.[21]
The isotropic part of the strain-energy function is associated with the mechanical response of the matrix, and therefore does not include the directions of the collagen fibers. The anisotropic part of the strain energy function models the response of the collagenous fibers, which become stretched at high pressures, and does include the direction vectors of the collagen fibers.[21]
The isotropic part of the strain-energy function can be determined using the classical Neo-Hookean model. This equation uses the first invariant of the Cauchy-Green tensor $\mathbf{C}$ and can be calculated as $I_1(\mathbf{C}) = tr\mathbf{C}$.

$$\Psi_{iso}(I_1) = \frac{\mu}{2}(I_1 - 3), \tag{4.2}$$

with μ a stress-like parameter, representing the stiffness of the matrix. The parameter C_{10} can also represent the stiffness of the matrix and equals $\mu/2$.
The anisotropic part is determined using,

$$\Psi_{aniso}(I_4, I_6) = \frac{k_1}{2k_2} \sum_{i=4,6} \left\{ exp\left[k_2(I_i - 1)^2\right] - 1 \right\}, \tag{4.3}$$

where I_4, I_6 correspond to the fourth and sixth invariant of the Cauchy-Green tensor $\mathbf{C}$ and can be found as:

$$I_4(\mathbf{C}, \mathbf{a}_{01}) = \mathbf{C} : (\mathbf{a}_{01} \otimes \mathbf{a}_{01}) \tag{4.4}$$

$$I_6(\mathbf{C}, \mathbf{a}_{02}) = \mathbf{C} : (\mathbf{a}_{02} \otimes \mathbf{a}_{02}) \tag{4.5}$$

The parameter k_1 is related to the stiffness of the fibers, while k_2 is linked to the nonlinear behavior of the sample.[21] The model has been generalized by Gasser *et al.*[15] by including the effect of dispersion in fiber orientation. Two families of collagen fibers are present in each of the different layers of arterial tissue. An assumption is made by characterizing these collagen families as parallel aligned fibers within each family. Furthermore there is assumed that both families of collagen fibers are symmetrically embedded in the non-collageneous matrix with a mean orientation given by a_{0i} (i=1,2). The fiber angle α corresponds to the angle the mean orientation makes with the circumferential direction.[15]

To include the effect of dispersion of the collagen fibers a new parameter κ has been introduced, which expresses the degree of anisotropy in the arterial layer. Two extreme values can be found for κ: $\kappa = 0$ which corresponds to no fiber dispersion, thus the fibers are aligned, and $\kappa = 1/3$ which corresponds to an isotropic fiber distribution.[15] In Figure 4.1 the parameters κ and α are visualized.[54]

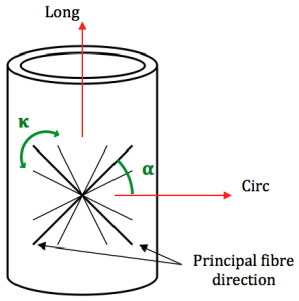

Figure 4.1: Visualization of the parameters α and κ of the GHO model [54]

The principal stretches in the axial and circumferential directions are noted as λ_z and λ_θ. The invariants I_4 and I_6 can be written in terms of this principal stretches:

$$I_4 = I_6 = \lambda_\theta^2 cos^2\alpha + \lambda_z^2 sin^2\alpha \tag{4.6}$$

In the generalized model, the term I_i in the summation in the anisotropic strain-energy function is replaced by: $\kappa I_1 + (1 - 3\kappa)I_i$, which results in:

$$\Psi_{aniso} = \frac{k_1}{k_2}\left\{exp\left[k_2(\kappa I_1 + (1-3\kappa)I_4 - 1)^2\right] - 1\right\}, \tag{4.7}$$

[32], [15]

Reporting parameters According to Robertson *et al.* reporting of average parameters of nonlinear constitutive models can produce unreliable results. Using average parameters in nonlinear models can lead to errors for three reasons.
Firstly, according to probability theory, linear functions satisfy following properties: the homogeneity property: $E(aX + b) = aE(X) + b$, and the additive property: $E(g(X, Y)) = g(E(X), E(Y))$. These properties imply that for linear functions the expected value can be calculated by evaluating the linear function at the average value of the input values. Unfortunately, this is only valid for *linear* functions. In *nonlinear* functions, using the average value of the inputs as input will generally not lead to an average output. Secondly, sometimes piecewise constitutive equations are used for modeling, in which specific conditions need to be fulfilled at the interface between adjacent regions. When the parameters are obtained experimentally they will automatically satisfy these conditions. However, this is not guaranteed for the average parameters. Finally, the distribution of the parameters is often not known, which may lead to problems. Using the average for the normal distribution is

appropriate, as opposed to for skewed distributions, in which experimental samples will shift the average to the tail of the distribution.
The authors suggest two different ways of reporting parameters of nonlinear constitutive models. Reporting individual sets of parameters for each set would be the ideal case and is recommended by the authors. Instead of averaging the parameters, the curves that are used as input for the model can be averaged, and the parameters of the average curve are reported.[41]

4.2 Materials and Methods

4.2.1 Parameter fitting

The GHO model will be used to characterize the different tissues obtained from the sheep. In the description in the Section 4.1, is stated that this constitutive law determines parameters for the adventitia and media separately. However, in this study these layers are not considered separately, since the samples that are tested include all three layers: intima, media, and adventitia, and the reinforced samples even include a wrapping layer. One set of parameters which characterizes the tissue as a whole is determined for each sample.
The input of the constitutive modeling step is composed out of the force-displacement data obtained after the biaxial tensile test and the coordinates of the markers, calculated in the marker tracking step. However, not all the data are used, only the stretch part of the last test cycle of each test set of the last complete test sequence is used, e.g. the upward part of the curve in Figure 3.9 in the previous chapter. For example, when the sample has ruptured when eight times the biaxial force was imposed, the stretch part of the last test cycle of three test sets of the test sequence which imposes six times the biaxial force are used as input. By taking the highest complete test sequence, there is ensured that the largest possible dataset is used.
The obtained force data, the coordinates of the markers as well as the thickness of the sample are used to calculate the principal stretches, the Cauchy stresses and the first Piola Kirchhoff stresses.
The principal stretches, or stretch ratios, in a certain direction can be calculated by taking the ratio of the current length in that direction l_i and the corresponding original length $l_{i,0}$: $\lambda_{ii} = \frac{l_i}{l_{i,0}}$. Moreover, the tissue is assumed to be incompressible, which means that the determinant of the deformation gradient can be considered to be equal to 1, and : $det(\boldsymbol{F}) = \lambda_{11}\lambda_{22}\lambda_{33} = 1 \Rightarrow \lambda_{33} = \frac{1}{\lambda_{11}\lambda_{22}}$. Both λ_{11} and λ_{22} are calculated by taking the relative displacement of the markers in the corresponding directions compared to the original length in that direction, while λ_{33} is calculated by using the formula described above. Furthermore, there is assumed that shear stresses can be neglected, which results in a deformation gradient in which only elements on the diagonal are present.
Subsequently, the deformation gradient is composed. The deformation gradient can be thought of as being composed of a stretch and rotation tensor: $\boldsymbol{F} = \boldsymbol{R} \cdot \boldsymbol{U}$. In the loading situation as imposed by a biaxial test, the rotation tensor equals the identity matrix and $\boldsymbol{U}$ equals a diagonal matrix with the principal stretches the diagonal

elements:

$$\boldsymbol{F} = \boldsymbol{U} = \begin{bmatrix} \lambda_{11} & 0 & 0 \\ 0 & \lambda_{22} & 0 \\ 0 & 0 & \lambda_{33} \end{bmatrix} \tag{4.8}$$

These deformation gradient can be used to determine the Cauchy-Green tensor, since $\boldsymbol{C} = \boldsymbol{F}^T \cdot \boldsymbol{F}$.
Thereafter, the Cauchy stress tensor $\boldsymbol{\sigma}$ needs to be determined. Since the Cauchy stress can be calculated from the first Piola Kirchhoff $\boldsymbol{T}$ stress using the following formula: $\boldsymbol{\sigma} = J\sigma\mathbf{F}^{-T}$, the first Piola Kirchhoff stress is determined. The first Piola Kirchhoff stress is a stress tensor which is referenced to the initial configuration, as opposed to the Cauchy stress which is referenced to the deformed configuration. The first Piola Kirchhoff stress present in the sample during a biaxial tensile test can be calculated as:

$$\boldsymbol{T} = \begin{bmatrix} \frac{L_{j,1}}{A_1} & 0 & 0 \\ 0 & \frac{L_{j,2}}{A_2} & 0 \\ 0 & 0 & 0 \end{bmatrix} \tag{4.9}$$

In this equation, $L_{j,i}$ is the load in the i^{th}-direction present at instant j. The parameters A_i are the initial surfaces in the i^{th}-direction. This first Piola Kirchhoff stress will be used to calculate the Cauchy stress. An example of the calculated Cauchy stress in function of the stretch ratio is shown in Figure 4.2.

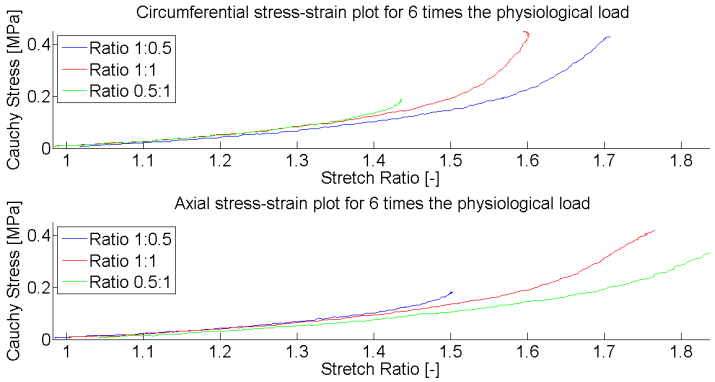

Figure 4.2: Cauchy stress in function of stretch ratios for the test sets with ratios 1:1, 0.5:1 and 1:0.5 for 6 times the physiological load for a sample of the aorta of sheep BE07572-73 in the circumferential and longitudinal direction

The Cauchy stress tensor and the deformation tensor comprise the input of the GHO model. The deformation tensor combined with an initial guess of the parameter set of the GHO model will be used to calculate an initial guess of the modeled Cauchy stress tensor, $\boldsymbol{\sigma_{mod}}$. The correct parameter set will be determined by trying to minimize the squared difference between the experimental measured Cauchy stress and the modeled Cauchy stress by varying the parameter set that is used to determine the

modeled Cauchy stress. When the difference between the experimental and modeled stress is sufficiently small a valid parameter set for the data set has been found.

4.2.2 Determining a representative set of parameters

The parameters are identified for every sample that has been tested. However, often more samples could have been obtained from one tissue type extracted out of one sheep, e.g. five samples have been collected out of the given aorta extract of sheep BE07572-73. This leads to the following step in which an attempt has been made to determine a representative set of parameters for every tissue type per sheep, e.g. determining one representative set of parameters for the five aortic samples of sheep BE07572-73. When applying the different methods to determine a representative set, summarizing figures are made to visualize the result when using this representative set. In these figures, a curve is modeled by applying the obtained set of representative set of parameters on the smallest set of strains. This smallest set of strains is calculated by first determining all the upper- and lower values of the strains for each dataset. Subsequently, all the sets of strains are reduced by removing all the values higher than the lowest uppervalue and all the values lower than the highest uppervalue. The smallest strain set is then chosen as the reduced strain set with the smallest number of datapoints.
Before undertaking an attempt to find a representative set of parameters, an overview of the different stress-strain curves of the different samples is constructed. Two types of graphs are made for this purpose: graphs in which all the samples of all the different tissue types are plotted, in which every tissue receives a different color, and graphs with the stress-strain curves for a specific tissue type, in which the samples of a sheep receive a specific color. The first type of graphs allows to visualize the difference in mechanical behavior between the different tissue types. The second type of graphs illustrates the intervariability and the intravariability of the mechanical behavior of the different tissue types.
Subsequently, the following methods have been performed: averaging of all the parameter sets pertaining to all the samples of one tissue type of one sheep, averaging the Cauchy stress curves in function of the stretch ratios of all the parameter sets pertaining to all the samples of one tissue type of one sheep, and performing the fitting procedure by using all the Cauchy stress tensors and deformation tensors of all the samples pertaining to one tissue type of one sheep. All these methods will be described further.

Averaging of parameters

The first method used to determine a representative set of parameters for all the samples pertaining to one tissue type of one sheep, consists of averaging the corresponding parameters of all the samples. In Table 4.1, this has been done for the five samples extracted from the aortic tissue of sheep BE07572-73.

Curve Averaging

Averaging the Cauchy stress curve in function of the stretch ratios comprises the second method that has been performed in order to determine a representative set of parameters for all the samples of the tissue type of one sheep. This average curve serves as input for the parameter fitting, described in Section 4.2.1.
The input for curve averaging comprises the Cauchy stress curves in function of the stretch ratio. Firstly, the stretch ratios of the smallest data set are chosen as the reference stretch ratios to which all the other data sets will be interpolated. The smallest set is chosen to avoid extrapolation. Secondly, the Cauchy stress of the remaining samples are interpolated to the values of the reference stretch ratios using the MatLab function *interp1*. This function interpolates linearly and is chosen since it results in NaN (Not a Number) when it is asked to extrapolate. Subsequently, there is checked in the interpolated Cauchy stresses if the value NaN is present. In case this value is found, this point is removed from all the data sets. After this step, interpolated values for the Cauchy stresses at the reference stretch ratios are obtained for all the samples. Finally, at every reference stretch ratio the corresponding Cauchy stress values are averaged, and an average curve for the Cauchy stress curve in function of the stretch ratios is obtained.

Table 4.1: parameters, average parameters, parameters of the average curve, and parameters obtained by fitting all samples together of the five samples of the aortic tissue of sheep BE37572-73

Sample No	C_{10} $[MPa]$	k_1 $[MPa]$	k_2 $[-]$	α $[rad]$	κ $[-]$
Sample 1	0.0221	0.0129	1.704	1.57	0.28
Sample 2	0.0137	0.0122	1.7152	1.57	0.32
Sample 3	0.0109	0.0211	0.4315	1.57	0.30
Sample 4	0.0107	0.0308	0.8307	1.57	0.31
Sample 5	0.0163	0.0452	0.8307	1.57	0.31
Average	0.0147	0.0244	0.9644	1.57	0.31
Average Curve	0.0088	0.0186	$2.22e^{-14}$	0.78	$2.92e^{-10}$
All samples together	0.0114	0.0429	0.0048	1.57	0.31

By using these average Cauchy stresses and reference stretch ratios as input in the parameter fitting, a summarizing set of parameters can be found for a series of samples pertaining to one tissue type of one sheep. An example of such a set can be found in Table 4.1.

Fitting all samples together

The last method that has been utilized to determine a representative set of parameters for all samples of one tissue type of one sheep consists of using the Cauchy stresses and deformation gradients of all the samples of one tissue type of one sheep as input for the parameter fitting. An example of the obtained set is given in Table 4.1.

4.3 Results

The results section in this chapter can be divided into two different sections: one pertaining to the parameter fitting and one pertaining to finding a representative set of parameters for one tissue type.

4.3.1 Parameter fitting

In total, four types of tissues are extracted from seven sheep. From most of these tissue extracts, more than one sample is obtained. Therefore, the complete parameter sets with the root mean squared error and corresponding range of stresses and strains for each sample can be found in Appendix D.

4.3.2 Determining a representative parameter set

Before starting the different methods, described above, the different sets of Cauchy stresses in function of the stretch ratios for all the samples of the four tissue types for all the sheep are visualized in Figures 4.3, 4.4, and 4.5. These figures give an overview of the different mechanical behaviors of the different tissue types.
Furthermore, in Figures 4.6, 4.7, and 4.8, the different samples for every sheep of the aorta are visualized. These figures are also created for the samples of the pulmonalis, the reinforced aorta samples, and the reinforced pulmonalis samples, and can be found in Appendix E. These figures are created to visualize and compare the intervariability and intravariability between the samples of the different sheep.

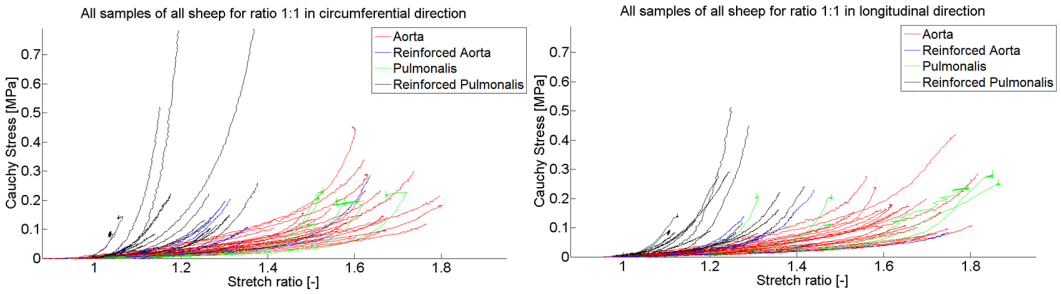

(a) Circumferential direction

(b) Longitudinal direction

Figure 4.3: Cauchy stress in function of the stretch ratio in the circumferential and longitudinal direction for the test set with ratio 1:1 for all the biaxially tested samples. The reinforced aorta and pulmonalis samples appear to be grouped together, as well as the unreinforced aorta and pulmonalis. The distinction between reinforced and unreinforced samples is not outspoken.

The methods of determining a representative set of parameters have been tested on the aorta samples of sheep BE37572-73.
Averaging of the parameter comprises the first method used for determining a representative set of parameters. The calculated parameters can be found in Table 4.1 and the result is visualized in Figures 4.9, 4.10, and 4.11.

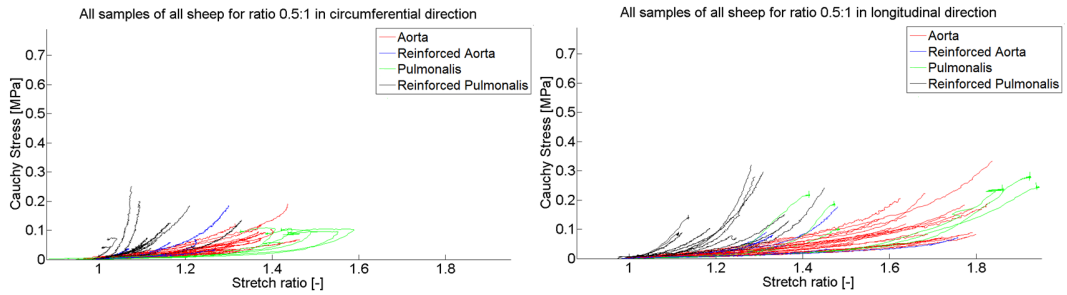

(a) Circumferential direction (b) Longitudinal direction

Figure 4.4: Cauchy stress in function of the stretch ratio in the circumferential and longitudinal direction for the test set with ratio 0.5:1 for all the biaxially tested samples. The reinforced aorta and pulmonalis samples appear to be grouped together, as well as the unreinforced aorta and pulmonalis. The distinction between reinforced and unreinforced samples is not outspoken.

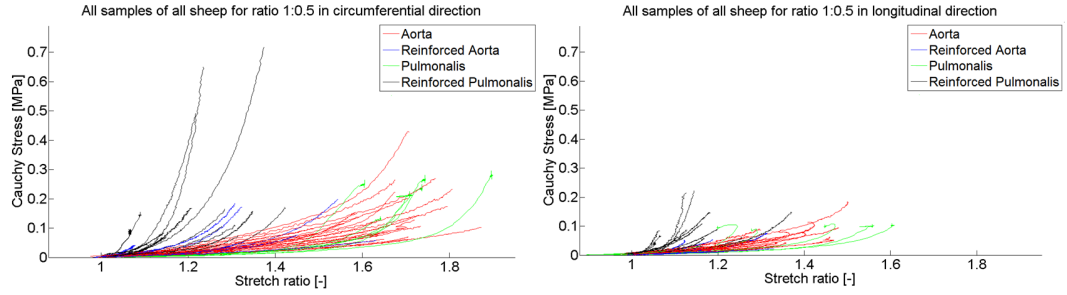

(a) Circumferential direction (b) Longitudinal direction

Figure 4.5: Cauchy stress in function of the stretch ratio in the circumferential and longitudinal direction for the test set with ratio 1:0.5 for all the biaxially tested samples. The reinforced aorta and pulmonalis samples appear to be grouped together, as well as the unreinforced aorta and pulmonalis. The distinction between reinforced and unreinforced samples is not outspoken.

The second method consists of determining a set of parameters which models the average curve. The average curve of all the aortic samples of sheep BE37572-73 is shown in Figures 4.12, 4.13, and 4.14. The fitted set of parameters of the average curve can be found in Table 4.1.

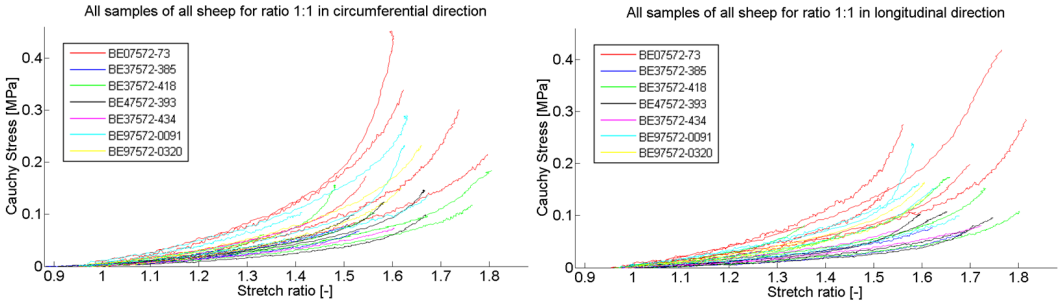

(a) Circumferential direction (b) Longitudinal direction

Figure 4.6: Cauchy stress in function of the stretch ratio in the circumferential and longitudinal direction for all the samples of the aorta for the test set with ratio 1:1. The curves belonging to one sheep are dispersed between the curves belonging to the other sheep. The variability between the samples of one sheep, intravariability, is not very different from the variability between the samples of the different sheep, intervariability.

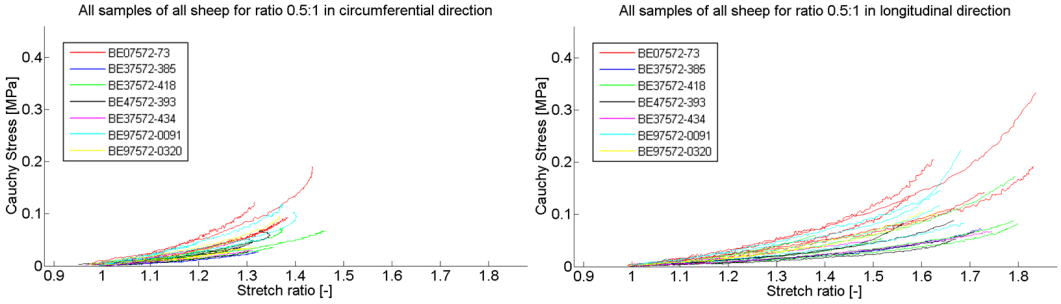

(a) Circumferential direction (b) Longitudinal direction

Figure 4.7: Cauchy stress in function of the stretch ratio in the circumferential and longitudinal direction for all the samples of the aorta for the test set with ratio 0.5:1. The curves belonging to one sheep are dispersed between the curves belonging to the other sheep. The variability between the samples of one sheep, intravariability, is not very different from the variability between the samples of the different sheep, intervariability.

The third method tries to fit all the stress-strain curves simultaneously. The obtained parameters can be found in Table 4.1 and are also used to model a stress-strain curve. The Figures 4.15, 4.16, and 4.17 visualize the result of modeling this stress-strain curve.

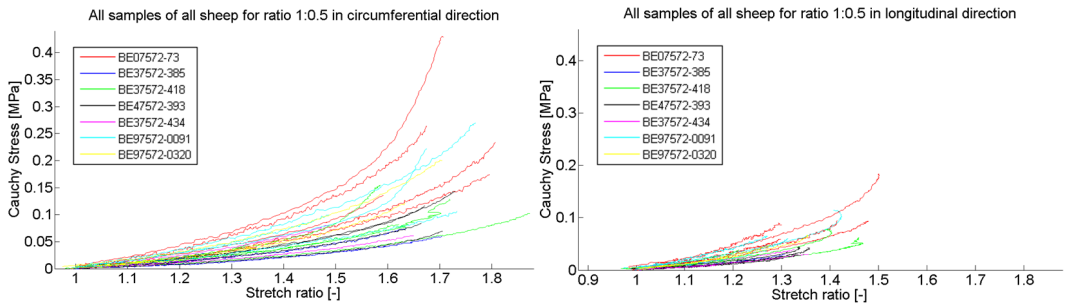

(a) Circumferential direction (b) Longitudinal direction

Figure 4.8: Cauchy stress in function of the stretch ratio in the circumferential and longitudinal direction for all the samples of the aorta for the test set with ratio 1:0.5. The curves belonging to one sheep are dispersed between the curves belonging to the other sheep. The variability between the samples of one sheep, intravariability, is not very different from the variability between the samples of the different sheep, intervariability.

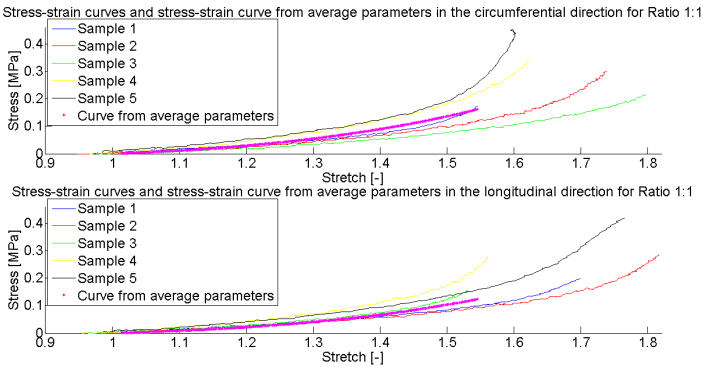

Figure 4.9: The experimentally determined stress-strain curves for all the aortic samples of sheep BE37572-73 and the stress-strain curve modeled using the average parameters for the test set with ratio 1:1

4.4 Discussion

This chapter deals with determining the parameters of the GHO model from the stress-strain curves obtained from biaxial testing. Firstly, the parameters of all the samples are determined. Secondly, an attempt to find a representative set of parameters for the different tissue types has been undertaken.

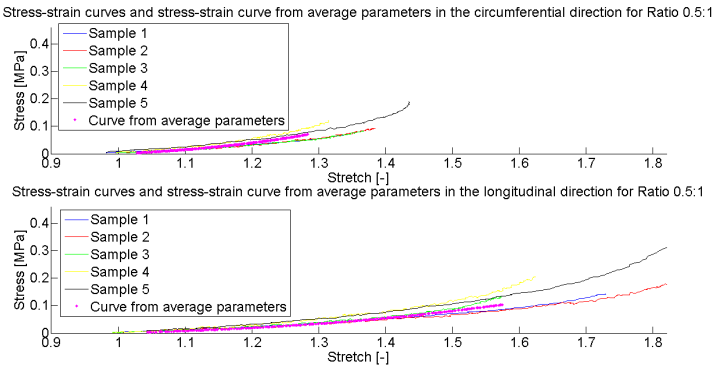

Figure 4.10: The experimentally determined stress-strain curves for all the aortic samples of sheep BE37572-73 and the stress-strain curve modeled using the average parameters for the test set with ratio 0.5:1

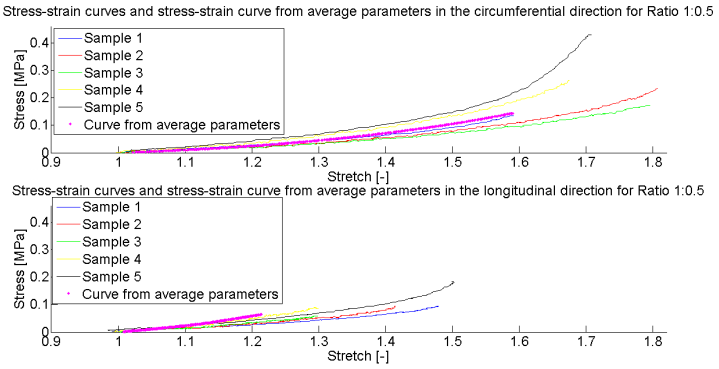

Figure 4.11: The experimentally determined stress-strain curves for all the aortic samples of sheep BE37572-73 and the stress-strain curve modeled using the average parameters for the test set with ratio 1:0.5

4.4.1 Parameter fitting

The result of the parameter fitting of all the samples can be found in Appendix D. From these sets of parameters can be noticed that several parameters tend to go to their limit. As explained in the beginning of this chapter, the parameters include: C_{10},k_1, k_2, α, and κ. The last two parameters have respectively the following limits: α can range from 0° to 90° or $\pi/2$ radials, whereas κ can have values between $0 - \frac{1}{3}$. The remaining parameters may, in theory, take values between 0 and infinity.
The value that most often goes to one of its limit values is α. As can be seen from the tables in Appendix D, this value goes to the limit for 43 of the 63 samples. This value expresses the angle under which the fibers are oriented. There can be thought of two different scenarios for this curiosity. The first has to do with the unreinforced samples, namely the aorta and pulmonalis samples. These samples consist of the three different layers that can be found in an artery.

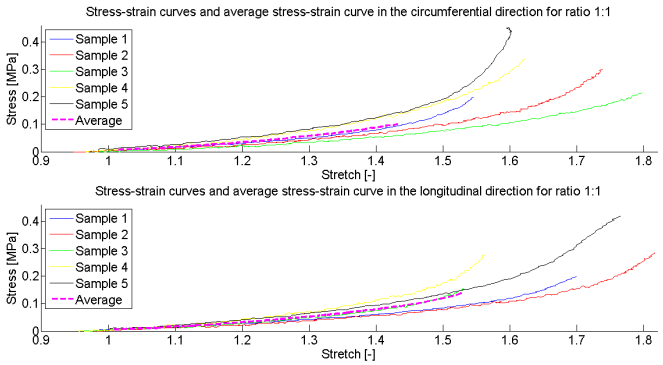

Figure 4.12: The average curve of the stress-strain curves for the test set with ratio 1:1 from the aortic samples of sheep BE37572-73. The average curve approximates a straight line, and thus behaves linear, resulting in a low value for the parameter k_2

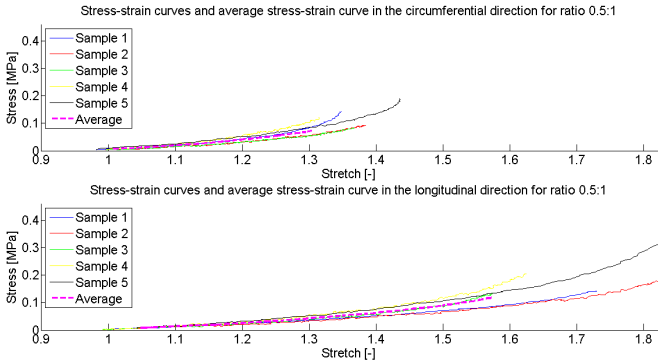

Figure 4.13: The average curve of the stress-strain curves for the test set with ratio 0.5:1 from the aortic samples of sheep BE37572-73. The average curve approximates a straight line, and thus behaves linear, resulting in a low value for the parameter k_2

However, the GHO model is designed to model these different layers separately. Furthermore, the alignment of the fibers differs in the separate arterial layers. The collagen fibers are closely aligned to the circumferential direction, which corresponds to an α equal to zero, whereas in the intima and adventitia the collagen fibers are more dispersed. This different alignment may lead to difficulties for fitting this parameter. This phenomenon has been readily described by Haskett *et al.* They measured the fiber angle using a small-angle light scattering technique, which gives the true fiber angle of their samples. Furthermore, they determined the fiber angle by testing their samples biaxially and fit their data on the GHO model. The fiber angle determined from the GHO model did not correspond to the measured fiber angle. The authors concluded that the fiber angle derived from the GHO model loses its physical meaning.[18]

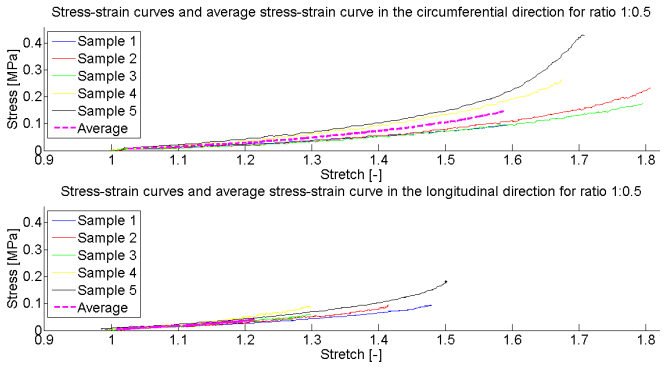

Figure 4.14: The average curve of the stress-strain curves for the test set with ratio 1:0.5 from the aortic samples of sheep BE37572-73. The average curve approximates a straight line, and thus behaves linear, resulting in a low value for the parameter k_2

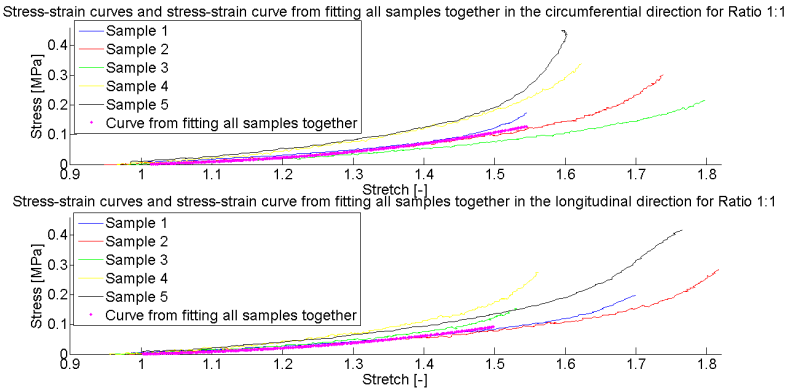

Figure 4.15: The stress-strain curves for the test set with ratio 1:1 of the aortic samples of sheep BE37572-73 with the curve modeled from the parameters obtained by fitting all the stress-strain curves simultaneously

The second scenario that may occur, takes place in the reinforced samples: the reinforced aorta and the reinforced pulmonalis. In these samples, a wrapping is incorporated into the arterial tissue. These wrapping consists of a mesh in which two distinct fiber directions may be noticed. A close-up of the wrapping can be found in Figure 4.18. There can be reasoned that the mechanical behavior of this wrapping will dominate the mechanical behavior of the sample, moreover that the fiber direction of the fibers of the wrapping dominates over the fibers of the arterial tissue. Following this reasoning is expected that the found fiber angle has a value around 45°. Nevertheless, this is not the case. This problem may be resolved by determining the fiber direction microscopically for the unreinforced samples, and by fixing the fiber direction to be the same as the one of the wrapping for the reinforced samples.

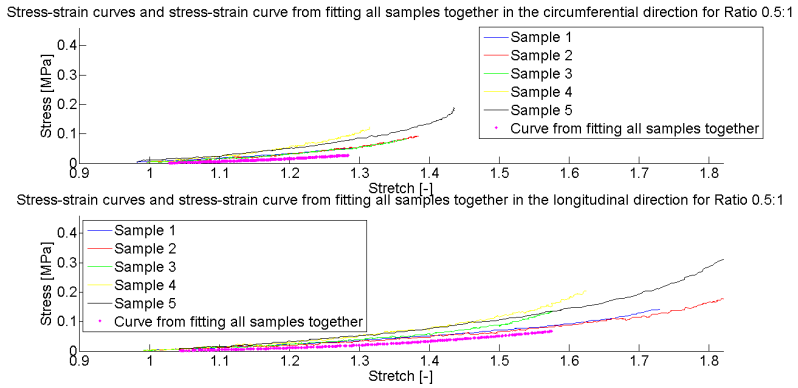

Figure 4.16: The stress-strain curves for the test set with ratio 0.5:1 of the aortic samples of sheep BE37572-73 with the curve modeled from the parameters obtained by fitting all the stress-strain curves simultaneously

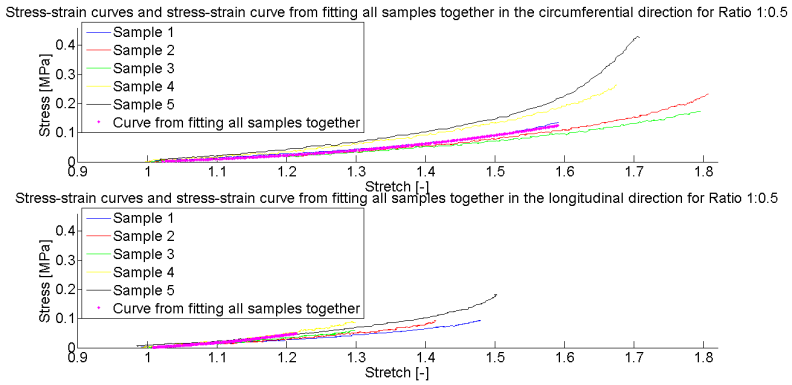

Figure 4.17: The stress-strain curves for the test set with ratio 1:0.5 of the aortic samples of sheep BE37572-73 with the curve modeled from the parameters obtained by fitting all the stress-strain curves simultaneously

Figure 4.18: The wrapping which reinforces the pulmonalis

The second value that often goes to its limits is κ, which expresses the dispersion of the fibers around their direction. For this case the same reasoning as for α may be followed. For the unreinforced samples, this may be a consequence of the fact that the model is intended for the different layers separately while the model is applied on the three layers simultaneously. The limit value of $\frac{1}{3}$ corresponds to a random distribution of the fibers, while the value zero corresponds to no dispersion of the fibers. Since the adventitia and the intima have a rather random distribution of the fibers, a value going to $\frac{1}{3}$ for the unreinforced samples is not remarkable.

However, for the reinforced samples, the fibers of the wrapping have clearly no dispersion, meaning that a low value for κ may be expected. Nevertheless, both for the reinforced and the unreinforced samples, values going to 0 or $\frac{1}{3}$ have been found. The parameter that is related to the stiffness of the matrix is C_{10}. This value converges for 10 samples to zero. When this parameter has a low value, the matrix in which the collagen fibers are dispersed, does not contribute significantly to the mechanical behavior. When the wrapping is present, there can be assumed that the wrapping dominates the mechanical behavior. This wrapping consists solely of fibers and does not contain a matrix in which these are dispersed. The only matrix that is present in the reinforced samples is the matrix of the arterial tissue. Therefore, a value of C_{10} going to zero is not that unexpected for the reinforced samples. However, it may be remarkable when this convergence to zero occurs for the unreinforced samples.
The remaining two parameters are k_1 and k_2. The former is related to the stiffness of the fibers, whereas the latter is a dimensionless parameter, which is used to describe the nonlinearity of the experimentally found stress-strain curve. When this parameter has a low value, the behavior is more linear when compared to when this parameter has a high value. For example, the fourth sample of the aorta of sheep BE47572-393 has a value of $2.60e^{-14}$ for k_2. Thus, the mechanical behavior may be expected to be more linear. When looking at the stress-strain curves of these samples, shown in Figure 4.19, it can be seen that the modeled stress-strain curves are more or less straight lines, which explains the low value of k_2.

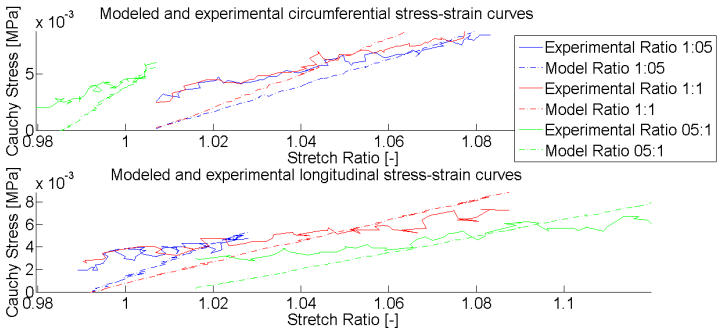

Figure 4.19: The experimental and modeled stress strain curves for the three test sets of the fourth sample of the aorta of sheep BE47572-393. The modeled stress-strain curves are more or less straight lines due to the low value of k_2

After investigating all the found parameter sets, it may be thought that the GHO model may not be appropriate as a model for the samples investigated in this thesis.

4.4.2 Determining a representative set of parameters

Before, attempts to find a representative set have been undertaken, several important figures have been constructed. Firstly, all the samples that have been biaxially tested are visualized all together for the three test sets 1:1, 0.5:1, and 1:0.5, both for the

circumferential and longitudinal directions in Figures 4.3, 4.4, and 4.5. From these figures can be seen that the reinforced aorta and pulmonalis samples appear to be grouped together, whereas the unreinforced aorta and pulmonalis seem to do the same. Nevertheless, the distinction between reinforced and unreinforced samples is not outspoken.
Subsequently, all the samples pertaining to a specific tissue type haven been plotted for all the sheep for each test set, both in circumferential and longitudinal direction. The resulting graphs for the aorta are shown in Figure 4.6, 4.7, and 4.8. There can be seen that the curves belonging to one sheep are dispersed between the curves belonging to the other sheep. Moreover, there can be seen that the variability between the samples of one sheep, intravariability, is not very different from the variability between the samples of the different sheep, intervariability. Thus, an attempt to find a set of parameters which represents all the aortic samples of all the sheep may be undertaken.
Previously, the methods tested to find a representative set have been explained. The results have been shown as well. In the last part of this chapter, the results of each of the methods and the accompanying reservations will be briefly discussed.

Averaging of parameters

The most straightforward method to find a representative set comprises averaging of the parameters. The main advantage of this method is that it is very easy and straightforward. Nevertheless, according to Robertson *et al.* the use of average parameters is not allowed due to the fact that averaging is a linear operation whereas the constitutive model clearly behaves nonlinear. However, in literature averaging of parameters is still often done, as was explained by Robertson *et al.*[41] Thus, averaging of the parameters is renounced.

Curve Averaging

Following the article of Robertson *et al.*, the curves rather than the parameters, have been averaged. Robertson *et al.* argue that the use of individual sets of nonlinear parameters is the best practice and that parameter averaging should be avoided. However, when the central tendency needs to be found, curve averaging is advised. Thus, the curve averaging method has been applied to the data of the aortic samples of sheep BE37572-73. When looking at the average curve in Figure 4.12, 4.13, and 4.14, there can be noticed that the average curve can only be calculated in the domain of the stretch ratio where values exist for the stress-strain curves of all the samples. One disadvantage of the use of this method is the loss of datapoints.
The obtained parameter set after fitting the average curve contains two values that go to their limit, namely a value of $2.22e^{-14}$ for k_2, and a value of $2.92e^{-10}$ for κ. The low value of k_2 can be easily explained. This parameter is related to the nonlinearity of the stress-strain curve. The higher its value, the more nonlinear the curve is. As stated before, a lot of data can not be used to construct the average curve. Furthermore, the data that is lost, appears to be the data that represents the

nonlinearity of the stress-strain curve. The average curve approximates a straight line, and thus behaves linear. Another disadvantage of the method with curve averaging is that the method for averaging a curve is not clearly described in the literature. Consequently, the method will not be used.

Fitting all parameters together

Using the stress-strain curves of all the samples simultaneously is the last method that has been attempted. The advantage of this method is that it is easy compared to the method with curve averaging. However, this method has an important disadvantage, namely that the set with the most datapoints will receive a higher weight and will have a larger influence on the outcome. This disadvantage may be resolved by resampling the datasets to contain the same number of points as the curve with the smallest number. Nevertheless, if this resampling is performed, again datapoints are lost.

4.5 Conclusion

From this chapter can be concluded that the GHO model may not be optimal for the obtained samples and that using a representative parameter set is allowed, but finding it is not straightforward. Consequently, no representative set of parameters will be used in the rest of this thesis. To summarize the different methods for obtaining a representative set of parameters, a table with the advantages and disadvantages of each of the method is given in Table 4.2.

Table 4.2: The advantages and disadvantages of the different methods for determining a representative set of parameters

Method	Advantages	Disadvantages
Averaging parameters	Easy Often done in literature	Not allowed [41]
Curve Averaging	Advised by Robertson *et al.* [41]	Parameters go to the limit Loose datapoints Method for averaging curves not clearly described
Fitting all stress-strain curves simultaneously	Easy	Stress-strain curves with more datapoints receive higher weight

Future work will comprise the determination of an appropriate material model, which should be capable of modeling the mechanical behavior of the wrapping, as well as the mechanical behavior of the complete arterial tissue. The latter is in contrast with the GHO model which is appropriate for use when determining the behavior of the separate arterial layer.

Chapter 5

Finite Element Modeling

Three different types of finite element models are constructed. The first model entails a section of an aorta or a pulmonalis. The second model represents the Ross procedure and consists of an aorta with a pulmonary section. The altered Ross procedure, where a reinforcement is added, is modeled by an aortic section combined with a reinforced aortic and reinforced pulmonary section.
The parameter sets of two different sheep are applied to the third model type to visualize the influence of different parameter sets on the model. Moreover, the parameter sets of one sheep are chosen to investigate the influence of the wrapping on the Ross procedure.
This chapter starts by describing the different methods used to construct the model, starting with information on the different types of residual stresses present in arterial tissue. In this section, the manner in which the mesh convergence analysis is executed is described. In the second section, the results of the finite element analysis are described, and these will be discussed in the third section. The last section will conclude the chapter by reciting the most important findings.

5.1 Materials and Methods

5.1.1 Constructing the model

Residual Stresses

Before constructing the finite element model, two types of different residual stresses need to be clarified: circumferential residual stresses and axial residual stresses. The latter can be quantified by determining the shortening resulting when excising a part of a vessel from the body. This can be done by attaching two suture wires as reference point before excising the artery. Firstly, the length between the two reference points is determined. Subsequently, part of the artery is removed and the length between the two points is measured after this excision. The ratio of the *in situ* length and the length after removal quantifies this axial prestretch.[22]
By determining the opening angle of a vessel, the circumferential stresses can be measured. This is done by removing an arterial ring from a vessel. When this arterial

ring is cut, it will open. After 15 minutes it reaches a steady state condition and the opening angle is determined as shown in Figure 5.1.[14]

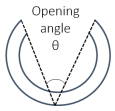

Figure 5.1: Opening angle

Both types of residual stresses are present in the aorta and the pulmonalis and are included in the finite element model. However, no determination of these stresses has taken place for the samples used in this thesis, and the values are therefore taken from literature. According to Valdez-Jasso *et al.* the aorta is stretched 20% *in situ* compared to the excised condition.[53] The circumferential stress is quantified by the use of an opening angle. This opening angle is chosen arbitrarily at a value of 120°. The influence of both types of stresses should be investigated further.

Model

Three types of models are constructed in *Abaqus Standard 6.13*. The first model entails a section of an aorta or a pulmonalis. The second model represents the Ross procedure and consists of an aorta with a pulmonary section. The altered Ross procedure, where a reinforcement is added, is modeled by an aortic section combined with a reinforced aortic and reinforced pulmonary section. The three models are schematically visualized in Figure 5.2.

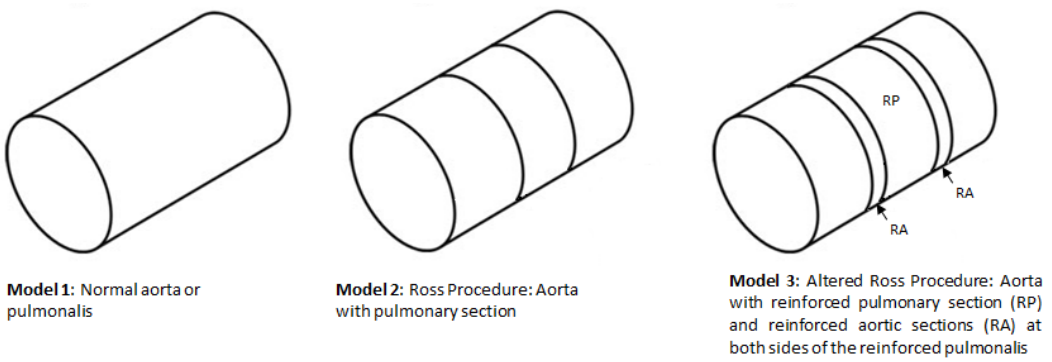

Figure 5.2: The three types of models. Model 1 consists of a normal aorta or pulmonalis, depending on which material properties are assigned. Model 2 visualizes the Ross Procedure where a pulmonary section is inserted into the aorta. Model 3 represents the altered Ross Procedure in which a wrapping is applied around the pulmonary section.

Before the construction of the models, the dimensions are determined from the CT scans of one sheep, shown in Figure 5.3, to have an estimate for the geometry of the model. Since the CT scans are taken when the sheep was anesthesized, there is assumed that the diameter is the diameter during diastole. Thus, the model needs to have a diameter of ±24 mm when applying diastolic pressure. The last dimension that is needed, is the thickness of the aorta in unloaded condition. The average thickness of the aortic samples, used for the mechanical testing, gives a good estimate for this geometric feature, and has a value of 3.66 mm. Furthermore, the vessel in all three types of model will be constructed as half a cylinder, since there can be assumed that the behavior is symmetrically in both sides of the cylinder.

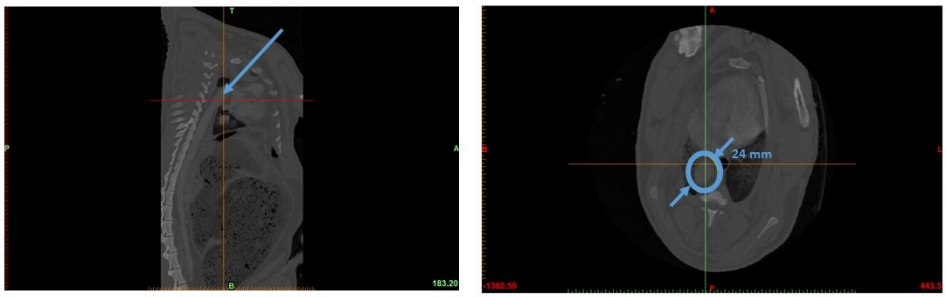

Figure 5.3: Determining the diameter of the aorta from CT scans

In the three models, different steps take place in order to model the different types of residual stresses as well as to model the loading conditions. The different steps include modeling the circumferential stress, modeling the axial prestretch, modeling the diastolic condition and the systolic condition. In the third model, an extra step is implemented after applying the circumferential stresses, necessary to model the reinforced pulmonary and aortic section. In the altered Ross procedure, there is assumed that the wrapping is applied loosely around the pulmonary section, and that the wrapping dominates the mechanical behavior. Therefore, there is assumed that the wrapping part has no circumferential prestress, resulting in an extra step in the model, in which a part with circumferential stresses is combined with a part with no circumferential stresses. Below the steps used in the different models will be outlined, a more detailed description of the model and the used boundary conditions can be found in Appendix F.
The first step in all three types of models consists of creating circumferential stresses. Using the opening angle, an initial shape for the model is constructed, which can be described as being half a cylinder that is not complete, illustrated in Figure 5.4.
The first step in the model comprises the application of circumferential stresses, which is done by closing the initial shape until it has the shape of half a cylinder. This step results in the existence of circumferential stresses. Figure 5.5 depicts the result of this closing step. The next step is only present in the third model and consists of coupling a part with circumferential stresses, the unreinforced part, and a part without circumferential stresses, the reinforced part, as shown in Figure 5.6.

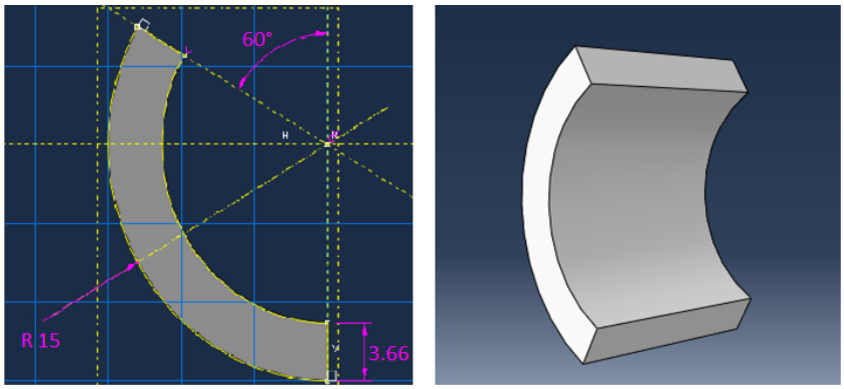

Figure A: sketch of model

Figure B: Initial shape of model

Figure 5.4: Figure A depicts the dimensions of the initial state of the model. Figure B visualizes the initial condition of the model

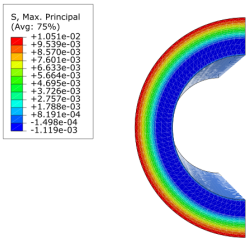

Figure 5.5: Circumferential stresses present in the model after the closing step

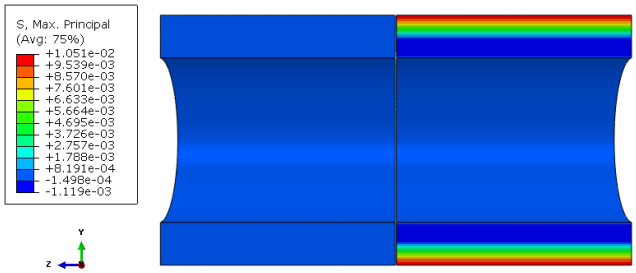

Figure 5.6: The configuration before the coupling step, which is only present in the third model, in which a part without circumferential stresses and a part with circumferential stresses will be attached to each other

Subsequently, the residual stresses in the axial direction are modeled. This step takes place in all three types of models. The result of the axial prestretch step for the third model is shown in Figure 5.7.

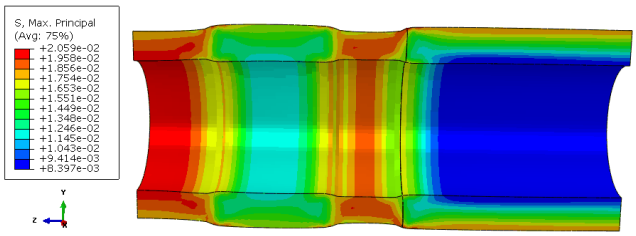

Figure 5.7: Model 3 after applying axial prestretch

In this step, the different mechanical behaviors of the different material types present in the third type of the models become apparent. The section on the right behaves as a normal aorta, where as the middle part of the left section has the properties of the reinforced pulmonalis. The parts on the left and right of this reinforced pulmonalis have the material parameters belonging to the reinforced aorta.

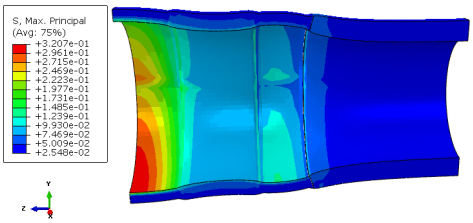

(a) Application of the diastolic pressure

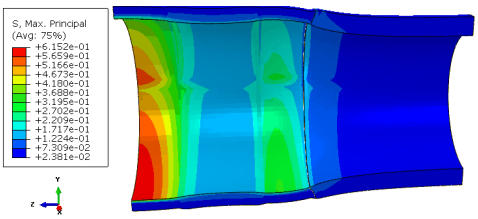

(b) Application of the systolic pressure

Figure 5.8: The third model after application of the diastolic pressure, and after application of the systolic pressure

Both types of residual stresses have now been modeled. Thereafter, diastolic and the subsequent systolic pressures are applied to the model. The results of both steps for the third model type are shown in Figure 5.8.

5.1.2 Mesh Convergence

Important in a finite element model is the determination of the right size for the mesh, which is the objective of a convergence analysis. The first step in such a convergence analysis comprises the choice of a good convergence criterion, which according to Kurowski *et al.* is the global strain-energy.[28]
After determining the convergence criterion, the simulation is performed for different mesh sizes. The mesh size is defined by the number of elements that are found through the thickness of the model, e.g. when the edge length of an element is 3.66 mm only one element can be found through the thickness of the model. The result of this convergence analysis can be found in Figure 5.9. From this figure can be seen that the strain-energy significantly changes when the number of elements through the thickness changes from one element to four elements. Since the strain-energy appears

not to change largely when increasing the number of elements through the thickness from six elements to seven elements, more precisely the strain-energy has changed with 0.06%. Therefore, there is chosen for a mesh size in which seven elements through the thickness can be found, corresponding to an edge length of 0.52 mm.

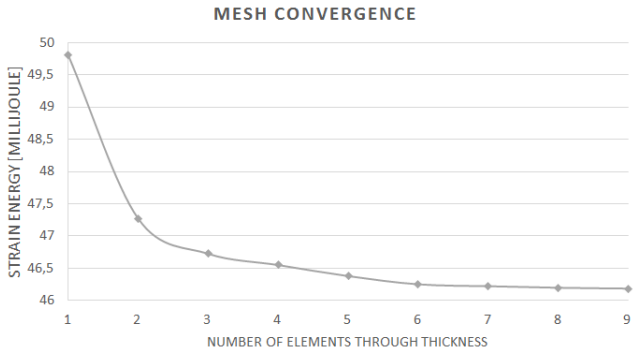

Figure 5.9: The result of the mesh convergence analysis, with the strain-energy for the whole model as convergence criterion. There is opted for a model with seven elements through the thickness.

5.1.3 Applying different material parameters

In a first step, the difference between two different sheep, namely sheep BE07572-73 and BE47572-393 is visualized by assigning the obtained material parameters to the corresponding section of the third model. This is done since no representative set of parameters could be found. Furthermore, as found in the previous section, several parameters tend to go to the limit. Moreover, a value of zero for the parameters C_{10}, k_1, and k_2 is not accepted by Abaqus, which limits the number of parameter sets that can be used. However, in the previous chapter is concluded that for the reinforced tissues the mechanical properties are dominated by the fibers of the wrapping. Thus, new parameter sets have been determined for the reinforced tissues of the two sheep by fixing the fiber angle to have a value equal to the fiber angle of the wrapping, namely 50°. The coefficients used in the finite element model are given in Tables 5.1 and 5.2.
After running the simulations, the profile of the models are visualized together. The profiles are determined by plotting the coordinate in the vertical direction of the highest edge of the model in function of the number of nodes, where node 1 corresponds to the node on the far right of the model.
Secondly, to investigate the influence of the wrapping, there is solely looked at the three types of models with the parameter sets of sheep BE07572-73. From the results of these different simulations, the following output is obtained: the profile of each simulation, as well as the stresses at the outside and inside in the three directions.

5.2 Results

As explained in the previous section, the number of parameter sets used is limited to the sets of sheep BE07572-73 and BE47572-393 and the obtained profiles are visualized simultaneously in Figure 5.10. In Figure 5.11 the obtained profiles with only the parameter sets of sheep BE07572-73 can be found whereas Figure 5.12 visualizes the profiles of sheep BE47572-393. The used parameter sets can be found in Tables 5.1 and 5.2. In Figures 5.11 and 5.12 the legend shows the used combination of parameters, e.g. 393-A5-RA2-RP1 uses the parameters of the fifth sample of the aorta, the parameters of the second sample of the reinforced aorta, and the parameters of the first sample of the reinforced pulmonalis. The second step in the finite element analysis entails the examination of the influence of the wrapping.

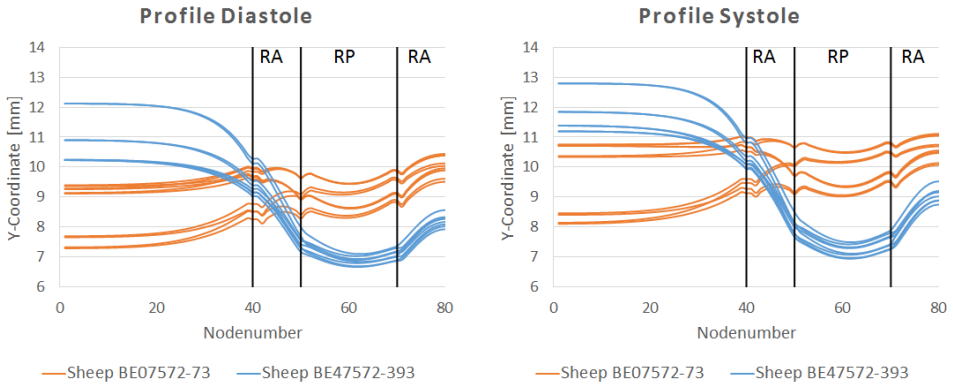

Figure 5.10: The profile of the third model with all the parameter combinations for sheep BE07572-73 and sheep BE47572-393. RA corresponds to the section with the material parameters of the reinforced aorta, RP of the reinforced pulmonalis, and the rest of the model has the material properties of the normal aorta. The profiles differ between both sheep.

Of all the parameter sets used in Figures 5.11 and 5.12, one parameter set is chosen to be used further on to examine the influence of the wrapping on the simplified Ross procedure, namely the parameters determined by fitting the first aorta sample, the first reinforced aorta sample, the first reinforced pulmonary sample, and the pulmonary sample of sheep BE07572-73 (73-A1-RA1-RP1). These parameter sets are assigned to the three different model types, which leads to four different simulations. An important remark regarding these parameter sets needs to be made. The pulmonary parameters are determined from a sample which was harvested from the pulmonalis. It has not been implanted in aorta position and did consequently not undergo any remodeling processes. Ideally, the pulmonalis needs to be implanted in aorta position for six months before harvesting this tissue. The parameters of the reinforced tissues have been determined from tissues that have been implanted for six months and did undergo remodeling processes.
In the first simulation, the normal aorta is modeled under physiological conditions. The same is done for modeling the pulmonalis under its normal conditions.

Table 5.1: Coefficients of constitutive modeling for sheep BE47572-393

Sample Type	Sample No	C_{10} $[MPa]$	k_1 $[MPa]$	k_2 $[-]$	α $[rad]$	κ $[-]$
Aorta	Sample 2	0.0039	0.0073	0.5823	1.57	0.28
	Sample 3	0.0068	0.0154	0.6312	1.57	0.29
	Sample 4	0.0069	0.0099	$2.60e^{-14}$	0.96	$2.40e^{-9}$
	Sample 5	0.0031	0.0065	0.2008	0.89	0.05
	Sample 6	0.0047	0.009	0.1764	0.94	0.09
Pulmonalis	Sample 1	0.0078	0.0292	2.9407	$2.31e^{-7}$	0.30
Aorta Wrapped	Sample 1	$2.7660e^{-14}$	0.0252	1.4938	0.87	0.19
	Sample 2	0.0082	0.0021	5.4932	0.87	0.22
Pulmonalis Wrapped	Sample 1	0.0603	0.03326	71.9443	0.87	0.19
	Sample2	0.0860	0.0268	51.6535	0.87	0.30

Table 5.2: Coefficients of constitutive modeling for sheep BE07572-73

Sample Type	Sample No	C_{10} $[MPa]$	k_1 $[MPa]$	k_2 $[-]$	α $[rad]$	κ $[-]$
Aorta	Sample 1	0.0221	0.0129	1.704	1.57	0.28
	Sample 2	0.0137	0.0122	1.7152	1.57	0.32
	Sample 3	0.0109	0.0211	0.4315	1.57	0.30
	Sample 4	0.0107	0.0308	0.1407	1.57	0.33
	Sample 5	0.0163	0.0452	0.8307	1.57	0.31
Pulmonalis	Sample 1	0.0027	0.039	1.7443	1.57	0.32
Aorta Wrapped	Sample 1	0.0055	0.0003	7.5479	0.87	0.26
Pulmonalis Wrapped	Sample 1	0.01923	0.003692	4.4073	0.87	0.30
	Sample 2	0.02286	0.01261	11.5073	0.87	0.30
	Sample 3	$1.2271e^{-11}$	0.0726	1.7111	0.87	0.22

The diastolic and systolic pressure for the aorta are taken as 74.8 mmHg and 96.7 mmHg according to Bia *et al.*, whereas the diastolic and systolic pressure in the pulmonalis are respectively 10.7 mmHg and 20.6 mmHg.[4] The third simulation represents the simplified Ross procedure without reinforcement, where a pulmonalis section is placed in the aorta. The last simulation represents the simplified Ross procedure in which a wrapping is positioned around the pulmonary autograft.

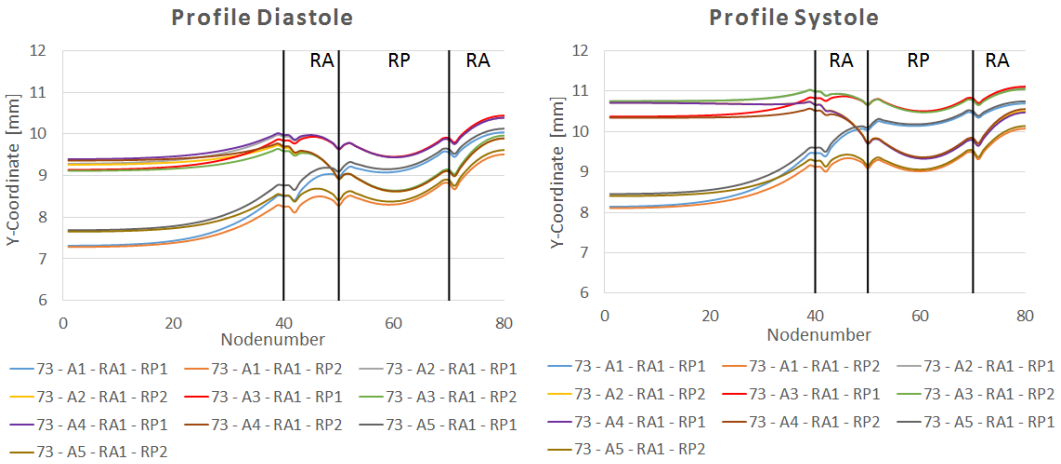

Figure 5.11: The profile of the third model with all the parameter combinations for sheep BE07572-73. RA corresponds to the section with the material parameters of the reinforced aorta, RP of the reinforced pulmonalis, and the rest of the model has the material properties of the normal aorta.

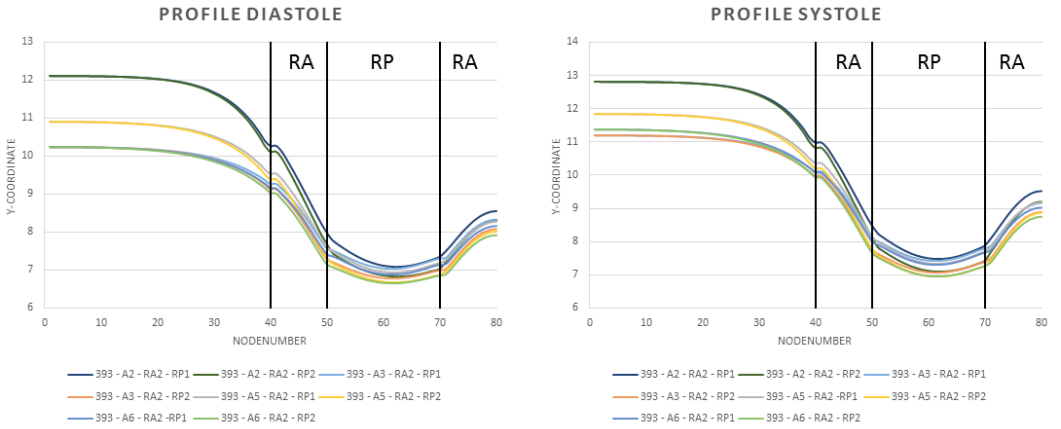

Figure 5.12: The profile of the third model with all the parameter combinations for sheep BE47572-393. RA corresponds to the section with the material parameters of the reinforced aorta, RP of the reinforced pulmonalis, and the rest of the model has the material properties of the normal aorta.

Figures 5.13, 5.14, and 5.15 show the results of the four simulations after imposing systolic pressure, respectively in the x-direction, the y-direction, and the z-direction.

Next, the stresses at the upperedge, as well at the loweredge of the topsurface are visualized together. The stresses at upperedge are representative for the stresses at the outside of the vessel, whereas the stresses at the loweredge of the topsurface can represent the stresses at the inside of the vessel.

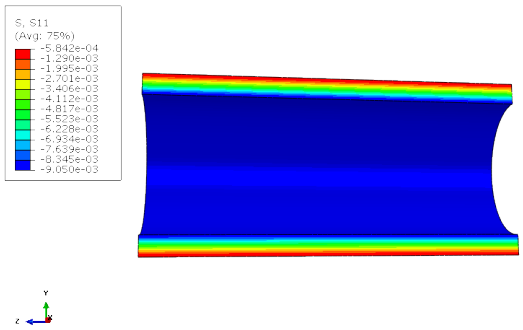

(a) The stresses in the x-direction of the finite element model of the aorta under systolic pressure [MPa]

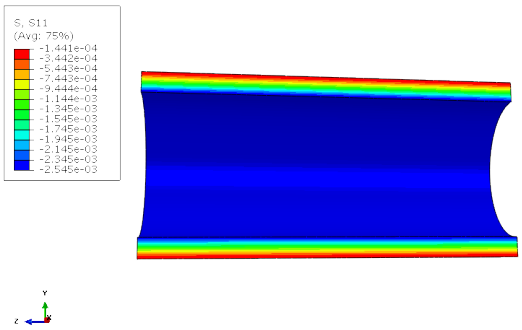

(b) The stresses in the x-direction of the finite element model of the pulmonalis under systolic pressure [MPa]

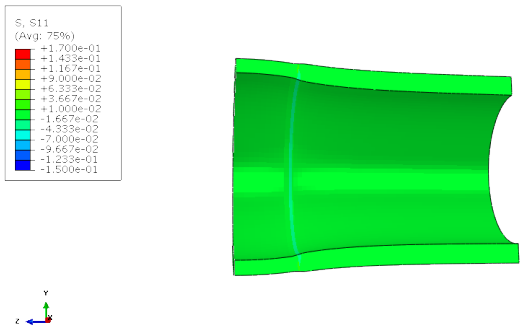

(c) The stresses in the x-direction of the finite element model of the simplified Ross procedure without reinforcement under systolic pressure [MPa]

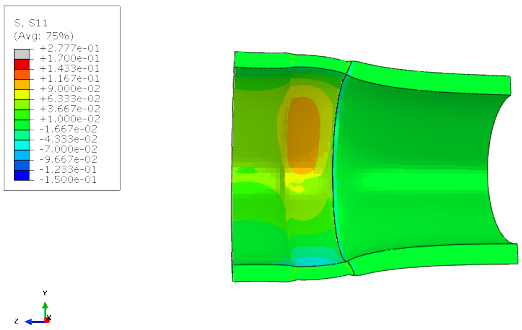

(d) The stresses in the x-direction of the finite element model of the simplified Ross procedure with reinforcement under systolic pressure [MPa]

Figure 5.13: The stresses in the x-direction, with the parameter set of the aorta sample 1, reinforced aorta sample 1, pulmonalis sample 1 and reinforced pulmonalis sample 1 of sheep BE07572-73, during systole. The Ross procedure with and without reinforcement changes the stress pattern compared to the initial configuration.

5.3 Discussion

5.3.1 Profile

Figure 5.10 visualizes the profiles of the different simulations with the different parameter sets of the sheep BE07572-73 and sheep BE47572-393. Both in systole and diastole, the profiles of sheep BE07572-73 have a similar shape, whereas the profiles of the second sheep also have a similar shape, but differ from the profiles of the first sheep. Moreover, the profiles of sheep BE47572-393 have a smaller diameter at the reinforced pulmonalis section and this difference becomes more apparent during systolic conditions.

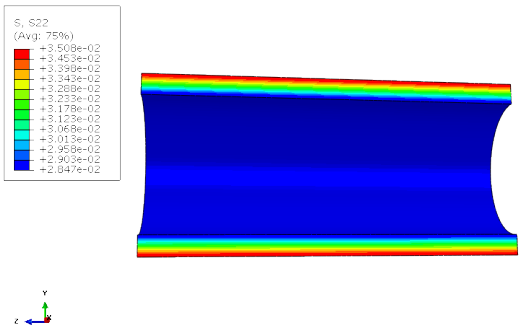

(a) The stresses in the y-direction of the finite element model of the aorta under systolic pressure [MPa]

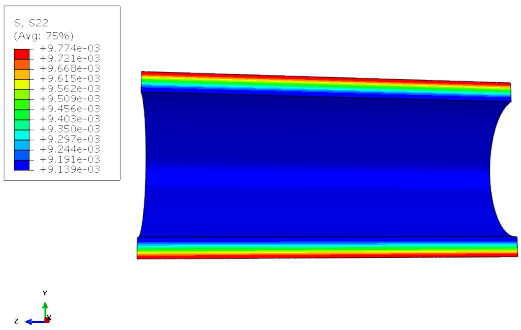

(b) The stresses in the y-direction of the finite element model of the pulmonalis under systolic pressure [MPa]

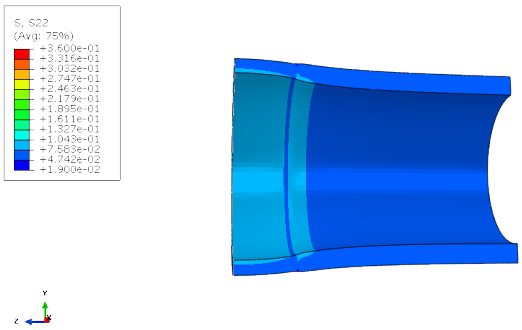

(c) The stresses in the y-direction of the finite element model of the simplified Ross procedure without reinforcement under systolic pressure [MPa]

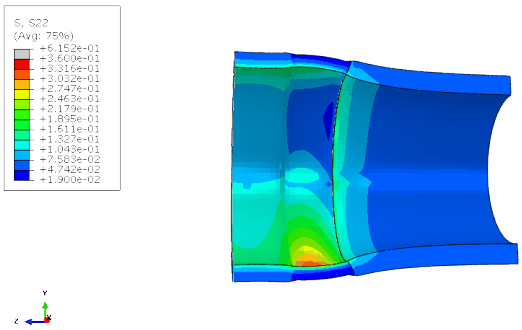

(d) The stresses in the y-direction of the finite element model of the simplified Ross procedure with reinforcement under systolic pressure [MPa]

Figure 5.14: The stresses in the y-direction, with the parameter set of the aorta sample 1, reinforced aorta sample 1, pulmonalis sample 1 and reinforced pulmonalis sample 1 of sheep BE07572-73, during systole. The Ross procedure with and without reinforcement changes the stress pattern compared to the initial configuration.

Looking at the different parameters of both sheep, leads to the observation that the k_2 parameter differs severely between both sheep: sheep BE07572-73 has a value for k_2 equal to 4.407, whereas k_2 for sheep BE47572-393 has a value of 71.944. As explained before, this parameter quantifies the nonlinearity of the mechanical behavior of the material. When this parameter has a higher value, e.g. for reinforced pulmonalis sheep BE47572-393, the stiffness of the material increases faster compared to the situation with a lower value, e.g. for sheep reinforced pulmonalis BE07572-73. This explains that when applying the same pressure to the reinforced pulmonary section of sheep BE47572-393 the diameter at that point is smaller than in the pulmonary section of sheep BE07572-73.

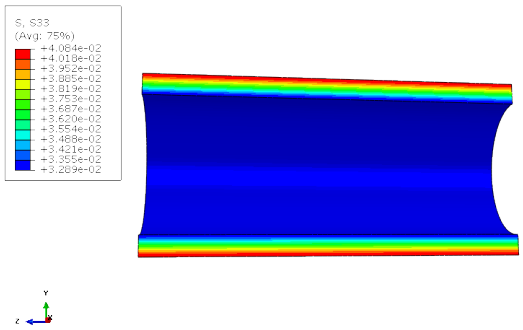

(a) The stresses in the z-direction of the finite element model of the aorta under systolic pressure [MPa]

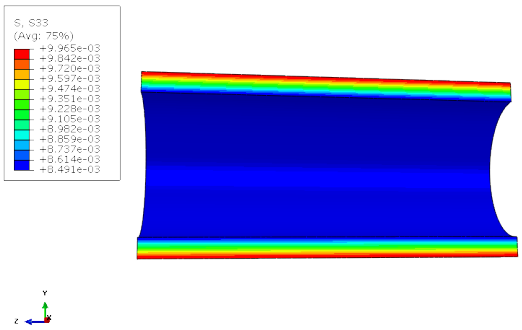

(b) The stresses in the z-direction of the finite element model of the pulmonalis under systolic pressure [MPa]

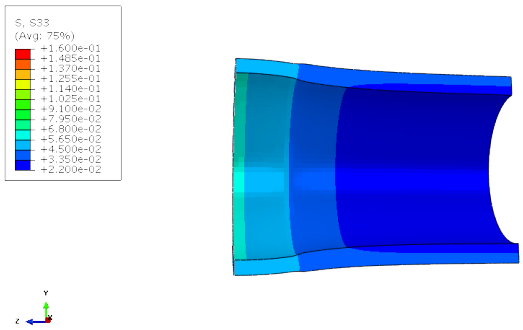

(c) The stresses in the z-direction of the finite element model of the simplified Ross procedure without reinforcement under systolic pressure [MPa]

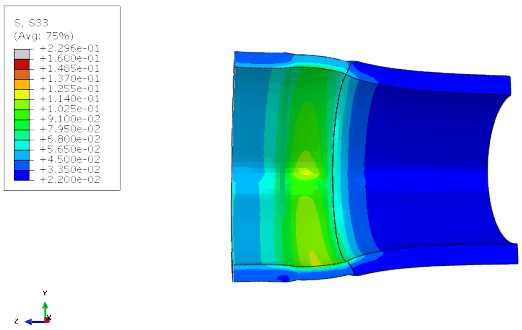

(d) The stresses in the z-direction of the finite element model of the simplified Ross procedure with reinforcement under systolic pressure [MPa]

Figure 5.15: The stresses in the z-direction, with the parameter set of the aorta sample 1, reinforced aorta sample 1, pulmonalis sample 1 and reinforced pulmonalis sample 1 of sheep BE07572-73, during systole. The Ross procedure with and without reinforcement changes the stress pattern compared to the initial configuration.

There can also be noticed in Figures 5.11 and 5.12 that changing the parameters of one section has an influence on the profile of the other sections. For example, in Figure 5.11 the simulation 73-A1-RA1-RP1 has a different parameter set in the reinforced pulmonary section compared to simulation 73-A1-RA1-RP2. However, the profile differs in the aorta section and the reinforced aorta section, and not only in the reinforced pulmonary section.

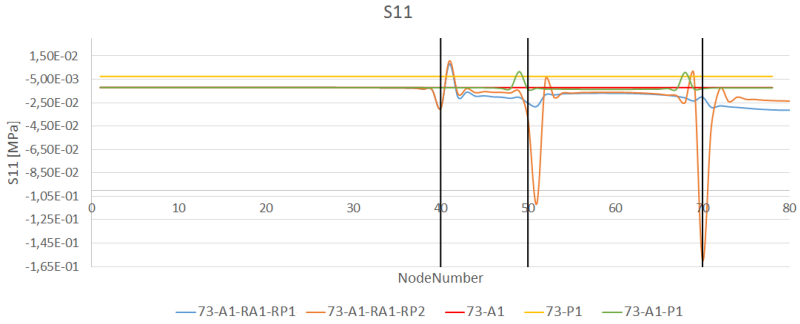

Figure 5.16: The stresses in the x-direction at the loweredge of the topsurface. RA corresponds to the section with the material parameters of the reinforced aorta, RP of the reinforced pulmonalis, and the rest of the model has the material properties of the normal aorta

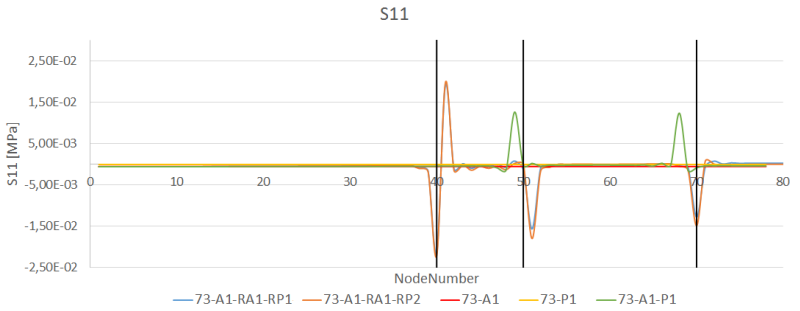

Figure 5.17: The stresses in the x-direction at the upperedge. RA corresponds to the section with the material parameters of the reinforced aorta, RP of the reinforced pulmonalis, and the rest of the model has the material properties of the normal aorta

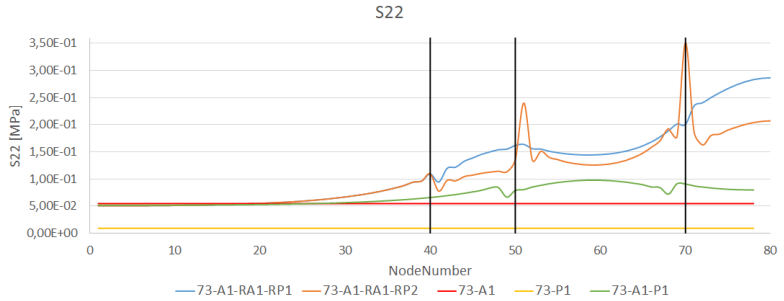

Figure 5.18: The stresses in the y-direction at the loweredge of the topsurface. RA corresponds to the section with the material parameters of the reinforced aorta, RP of the reinforced pulmonalis, and the rest of the model has the material properties of the normal aorta

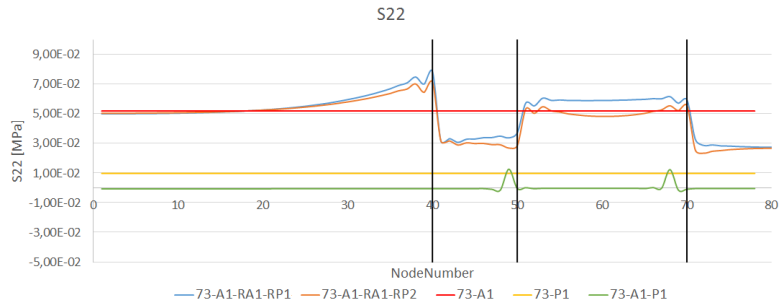

Figure 5.19: The stresses in the y-direction at the upperedge. RA corresponds to the section with the material parameters of the reinforced aorta, RP of the reinforced pulmonalis, and the rest of the model has the material properties of the normal aorta

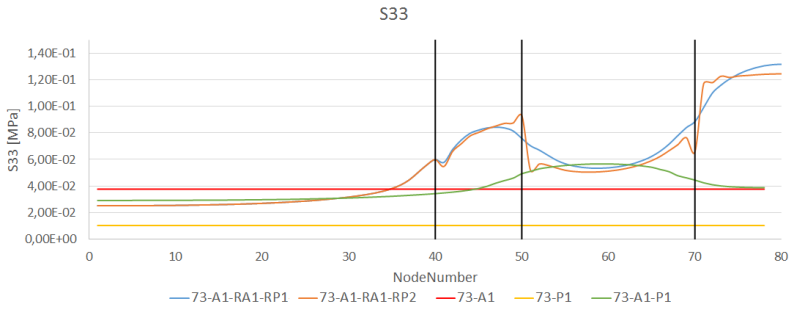

Figure 5.20: The stresses in the z-direction at the loweredge of the topsurface. RA corresponds to the section with the material parameters of the reinforced aorta, RP of the reinforced pulmonalis, and the rest of the model has the material properties of the normal aorta

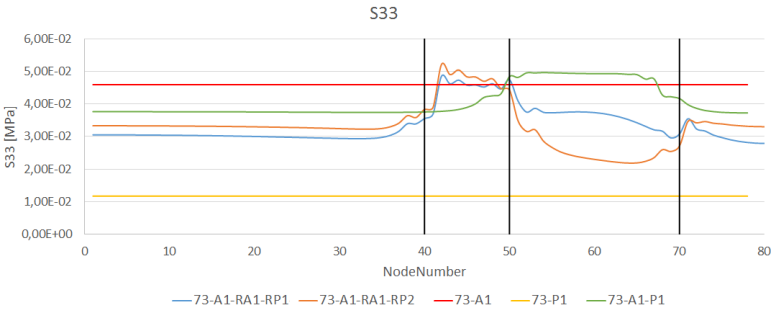

Figure 5.21: The stresses in the z-direction at the upperedge. RA corresponds to the section with the material parameters of the reinforced aorta, RP of the reinforced pulmonalis, and the rest of the model has the material properties of the normal aorta

Furthermore, it appears that changing the parameter sets of the aorta section changes the diameter at the beginning of the aorta section. However, even if the aorta section starts with a different diameter, the diameter at the reinforced pulmonary sections

appears to be mainly determined by the reinforced pulmonary parameters.
This is illustrated by comparing simulations 73-A1-RA1-RP1, 73-A1-RA1-RP2, 73-A4-RA1-RP1, and 73-A4-RA1-RP2.
The diameter at the beginning of the aorta section does not differ significantly between simulation 73-A1-RA1-RP1 and 73-A1-RA1-RP2, and between 73-A4-RA1-RP1 and 73-A4-RA1-RP2. This is expected since both pairs have the same parameters for the aorta section.
However, looking at the reinforced sections, the simulations with the same parameter set for the reinforced sections are closer together, e.g. 73-A1-RA1-RP1 and 73-A4-RA1-RP1. From this reasoning can be concluded that the combination of the parameter set determines the mechanical behavior of the complete model, rather than the individual sets separately.

5.3.2 Stresses

In Figure 5.22 the stresses in the x-direction of the simulation in which the reinforced simplified Ross procedure is modeled, are visualized.

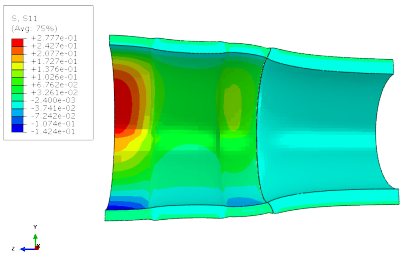

Figure 5.22: The stresses in the x-direction in the simulation of the reinforced simplified Ross procedure

At the left side, a high stress concentration can be noticed. Nevertheless, in the third model in Figure 5.2 the following sequence of tissues can be seen: aorta - reinforced aorta - reinforced pulmonalis - reinforced aorta - aorta. Ideally, this model should be symmetrical with respect to the middle of the reinforced pulmonary section and an aorta part should be added on the left side to obtain this symmetry. Therefore, the results are shown by cutting the model in the middle of the reinforced pulmonary section and are assumed to be symmetric. An improvement that should be made in this model is the addition of an extra part aorta on the left side. The high stress concentration is expected to disappear when adding this improvement and will be disregarded further.
The influence of complementing the simplified Ross procedure with the positioning of a wrapping or reinforcement is examined by means of different figures. Figures 5.13, 5.14, and 5.15 visualize the stress patterns obtained in the three directions in the four different simulations. A few observations can be made from these figures. In the three figures, the aorta and pulmonalis have a circular stress distribution

where the inside of the vessel experiences a lower stress than the outside of the vessel. However, both in the simplified procedure without wrapping as in the procedure with the wrapping, this stress pattern changes and is no longer circular.
Looking Figure 5.13c, there can be seen that a stress concentration occurs at the boundaries of the pulmonary section. Figure 5.14c also shows an altered stress pattern, where the middle section of the pulmonary autograft shows the highest stress combined with a high stress concentration at the boundaries of the autograft. The higher stress in the middle of the autograft is also observed looking at the stress distribution in the axial direction, Figure 5.15c.
To further compare the differences in stresses between the four different models, there is looked at Figures 5.16 to 5.21.
Looking at Figure 5.16 shows that the stresses in the x-direction at the inside of the vessel are in absolute value an order of magnitude higher for the aortic tissue both in the unreinforced as in the reinforced Ross procedure. There can also be seen that the difference in stresses for the pulmonary sections of both types of procedures and the pulmonalis in normal conditions appears to be small. Looking at the stresses in the x-direction at the upperedge in Figure 5.17, the differences between the stresses in the aorta in both procedures and the stresses in the aorta under normal circumstances become smaller. The same is true for the pulmonary stresses. However, in both figures, peaks in the stresses can be observed. These peaks occur in the zones where the material changes. By increasing the mesh density in those zones, there can be seen that the peaks are attenuated. Consequently, these peaks may be the result of a numerical problem. The figures which compare the normal model with the model with a local higher mesh density can be found in Appendix G.
Figure 5.16 visualizes the stresses of the four simulations in the x-direction at the loweredge of the top-surface simultaneously. There can be seen that the stresses in the pulmonary artery in aortic position without reinforcement (section RP of the green line) are higher in absolute value than the stresses the pulmonalis experiences in its physiological configuration (yellow line). Adding a reinforcement around this pulmonalis, appears to increase the stresses slightly. The stresses in the reinforced aorta section increase in absolute value by adding the wrapping. This increase in stresses is not expected. However, the pulmonalis tissue has been harvested when the procedure was performed, whereas the other tissues have been harvested six months after the procedure. The tissues that have been harvested after six months had the opportunity to remodel, whereas the pulmonalis did not undergo any remodeling processes. Ideally, the pulmonalis should be implanted six months in the aortic position before determining its material parameters. There is expected that these material parameters will be different from the current parameters due to possible remodeling processes.
Also, stress peaks can be noticed in the unreinforced and reinforced Ross-procedure. These stress peaks are thought to be a consequence of the material parameter mismatch that occur at these points.
The stresses at the upperedge of the topsurface in the x-direction are shown in Figure 5.17. In this figure, the effect of the different stresses in the different sections is less outspoken, but the peaks due to the parameter mismatch are still noticeable.

Similar figures for the stresses in the y-direction can be found in Figures 5.18 and 5.19. Placing the pulmonary artery in the aorta position without adding a reinforcement leads to increased stresses in the loweredge of the topsurface. If a reinforcement is added, this effect increases further. In the upperedge, placing the pulmonary artery in the aorta position decreases the stresses present in the uppperedge. When this pulmonary artery is reinforced, the stresses in the reinforced pulmonary section are higher than the stresses in the pulmonary artery in its normal configuration. The stresses in the reinforced artery sections on the other hand, decrease with respect to the normal aorta stresses.
The stresses in the z-direction for the lower- and upperedge of the topsurface are visualized in Figures 5.20 and 5.21. In the loweredge, the stresses in the pulmonary artery in aorta position without reinforcement are higher compared to its normal configuration. However, adding a wrapping decreases these stresses, but these stresses are still higher than in the normal configuration. The stresses in the reinforced aorta are also higher compared to the stresses present in the normal aorta. In the upperedge, the addition of a reinforcement to the pulmonalis in aorta position decreases the stresses in this section, but increases the stresses present in the reinforced aorta position compared to the unreinforced case and the normal configuration.

5.4 Conclusion

From the finite element analysis can be concluded that inserting a pulmonary section in the aorta position, alters the stress pattern. Adding a reinforcement changes the stress pattern compared to the unreinforced simulation and compared to the normal situation. This reinforcement lowers the stresses in the axial direction and brings them closer to the value of the normal configuration. However, this is not the case for the stresses in the x- and y-direction. This change in stress pattern and stress values is important since changing mechanical loads on tissues can trigger growth and remodeling of these tissues. In blood vessels, a change in shear stress and blood pressure is known to cause remodeling. Two types of cells are present in vessels which are influenced by the mechanical loads: endothelial cells and smooth muscle cells. These endothelial cells form the inner lining of the vessel, and are the main constituent of the intima. These cells form the barrier between the blood and the arterial wall. The smooth muscle cells can be mainly found in the media. The endothelial cells are subjected to loads due to two phenomena: the cyclic load due to the pressure and the shear stress due to the blood flow. The smooth muscle cells are only influenced by the pulsatile pressure. An abnormal loading condition on a cell, either an endothelial cell or a smooth muscle cell, may cause a change in cell function and alter the composition and structure of the extracellular matrix.[57] Thus, this change in stresses imposed on the pulmonary autograft may have an influence on the long-term results of the procedure.

5.4.1 Future work

Currently, care must be taken when examining the results of the finite element analysis, since improvements can be made to the models of the unreinforced and reinforced simplified Ross procedure. Ideally, these models should be symmetrically, as was schematically visualized in Figure 5.2. Thus, an extra aortic section needs to be added to these models. Furthermore, the value for the opening angle is chosen arbitrarily since no opening angle was measured. The influence of this parameter needs to be investigated further. Also, the value for the axial residual stress is taken from literature. Determining these values for this situation would be better. Since the surgeon can alter the axial residual stress present in the unreinforced pulmonary section or in the wrapping, an investigation of the influence of the axial residual stress is advised.

Chapter 6

Conclusion

The goal of this thesis consists of mechanically characterizing the PEARS when used in the Ross procedure and examining the influence of the addition of this reinforcement in the Ross procedure. After a simplified version of the Ross procedure is performed on sheep, several types of tissues are obtained: aorta, reinforced aorta, pulmonalis, reinforced pulmonalis. Mechanical tests are performed on each tissue type, and the output of these tests serves as input for determining the parameters of the GHO model. These parameters are then used to construct a FEM which simulates the simplified Ross procedure with and without the reinforcement.
This thesis started by defining two objectives. The first objective stated that the different tissue types had to be mechanically characterized by performing experimental tests and using the outcome to determine the material parameters of the GHO model. The second objective comprised the investigation of the addition of the reinforcement on the Ross procedure by means of a FEM. This chapter will summarize the main thoughts and conclusions of the mechanical tests, the use of the GHO model, and the FEA.

6.1 Mechanical Tests

The performed mechanical tests entailed uniaxial and biaxial tests. Both types of tests have been executed since the uniaxial tests are better for determining strength, whereas biaxial tests are more appropriate to capture anisotropic behavior.
Both force-controlled and displacement-controlled tests have been performed on the samples of the different tissues. According Van Den Abbeele *et al.* the use of force-controlled protocols is preferred, since in the displacement-controlled protocols the stretches are influenced by the connection to the system. However, the biaxial test device showed to be more reliable when using displacement-controlled protocols. Thus, both types of protocols are used.
The obtained data from these tests consisted of force-displacement curves. The force was determined by the force sensors in the testing device, whereas the displacements were calculated by means of tracking the markers attached to each sample.

6.2 Gasser-Holzapfel-Ogden model

After performing the mechanical tests, the obtained force-displacement curves are used to calculate the stress-strain curves which serve as input for determining the parameters of the GHO model, thereby characterizing the material. A few remarks need to be made with respect to this parameter fitting step. The GHO model normally calculates the material parameters pertaining the layers separately. However, the input force-displacement curves are determined from samples in which all the arterial layers are tested together. Furthermore, in the reinforced samples, an extra layer, the wrapping, is added to these three layers. Consequently, the obtained parameters loose part of their physiological meaning. For example, the parameter α quantifies the angle under which the fibers can be found in a layer. However, the fibers are directed differently in the different layers and in the wrapping. In the reinforced samples, it is thought that the wrapping dominates the mechanical behavior of the sample. Determining a single angle for the different layers in each sample is not physiologically meaningful. From the parameter fitting step, it may be concluded that the GHO model is not the ideal model for the samples tested in this thesis.
Furthermore, an attempt to determine a representative parameter set for each tissue type is made. Four tissue types of seven sheep are obtained. Of every tissue extract, one or more samples are cut and tested. Thus, several sets of parameters for one tissue type can be found. The following methods are performed: averaging of the parameter, curve averaging, and fitting all parameters together. All three methods had their advantages and disadvantages, and no ideal method was found. Consequently, no representative set of parameters has been defined. Nevertheless, a concise sensitivity analysis of the parameters in the finite element model has been performed.
In future work, a more appropriate material model as opposed to the GHO model needs to be found.

6.3 Finite element modeling

The finite element analysis comprises the final step of this thesis. In this step, four different types of simulations have been done. The first two simulations modeled the aorta or pulmonary artery in their respective physiological configuration. The third type of simulation models the simplified version of the Ross procedure without reinforcement. The simplified Ross procedure with reinforcement is modeled in the fourth simulation.
In a first step, the parameters pertaining to two different sheep are applied to the fourth type of simulation, and there can be found that the combination of parameters is important.
Secondly, the simulation is focused on one sheep to examine the influence of the reinforcement in the simplified Ross procedure. Performing the simplified Ross procedure with and without the reinforcement, alters the stress pattern clearly. This change in stress pattern and stress values is important since changing mechanical loads on tissues can trigger growth and remodeling of these tissues. The change in stress

imposed on the pulmonalis in the aorta position with and without reinforcement, may have an influence on the long-term results of this procedure. Furthermore, the Ross procedure without reinforcement results in a larger diameter where the pulmonalis is positioned, while the wrapping appears to constrain the pulmonary section.
Regarding the FEM, a few important remarks need to be made. As was briefly explained, the constructed model for the simplified Ross procedure with reinforcement is not symmetrically. Ideally, symmetry in this model is obtained. Furthermore, the value for the axial prestretch is taken from literature, since no quantification thereof has been done in the sheep used for this study. Also, currently when positioning the wrapping, no attention is given in prestretching the wrapping. Thus, quantifying the axial prestretch as well as investigating the influence of this parameter on the finite element model needs to be done in the future. The circumferential residual stress, quantified by the opening angle, is taken arbitrarily in the model, since no value was determined in the sheep. The influence of this parameter needs to be examined as well.
Thus, it can be concluded that there is still a lot of work to be done, especially in the areas of material representation and FEM. Furthermore, the results of performed analysis using the FEM need to be interpreted with care. The investigated situation is complex, and the influence of several parameters is not known, e.g. the influence of the opening angle. Moreover, the simulation depends on the combination of the parameter sets and a stable result has not yet been determined. Modeling the wrapping separately and using growth- and remodeling-algorithms may resolve this problem.

Appendices

Appendix A

Details of the sheep

Table A.1: Details pertaining to the seven sheep

Sheep	Date of birth	Date of surgery	Date of sacrifice	Weeks implanted
BE97572 – 0091	28/03/2012	25/10/2012	26/06/2013	34, 9
BE07572 – 73	25/03/2012	28/02/2013	23/09/2013	29, 6
BE37572 – 385	14/08/2012	29/03/2013	26/09/2013	25, 9
BE47572 – 393	17/08/2012	05/04/2013	04/10/2013	26, 0
BE57572 – 434	18/08/2012	26/06/2013	07/01/2014	27, 9
BE97572 – 0320	23/08/2012	04/07/2013	07/01/2014	26, 7
BE37572 – 418	21/08/2012	17/07/2013		

Appendix B

Positioning of samples

B.1 Sheep BE77572-321

Aorta

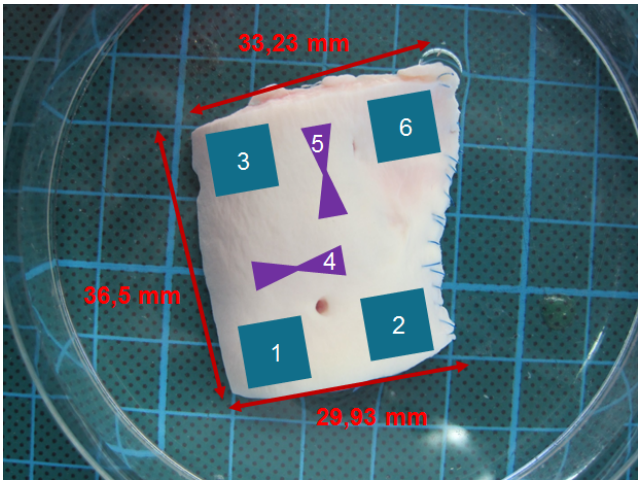

Figure B.1: The positioning of the samples on the aorta section of sheep BE77572-321

B.2 Sheep BE37572-418

Aorta

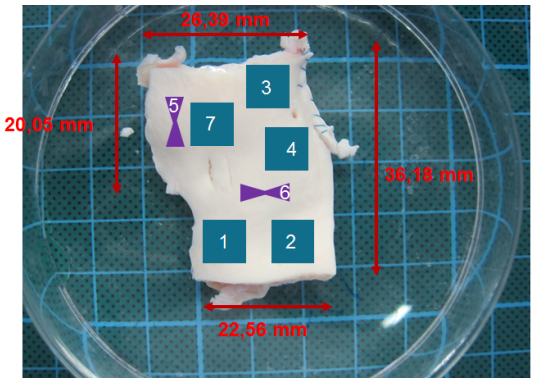

Figure B.2: The positioning of the samples on the aorta section of sheep BE37572-418

Reinforced Aorta

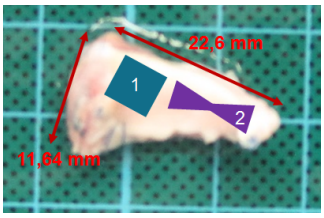

Figure B.3: The positioning of the samples on the reinforced aorta section of sheep BE37572-418

Reinforced Pulmonalis

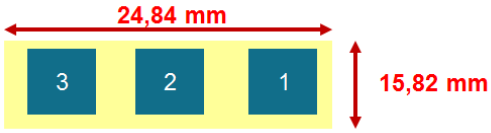

Figure B.4: The positioning of the samples on the reinforced pulmonary section of sheep BE37572-418

B.3 Sheep BE97572-320

Aorta

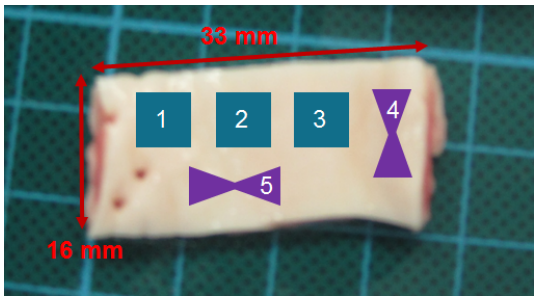

Figure B.5: The positioning of the samples on the aorta section of sheep BE97572-320

Reinforced Aorta

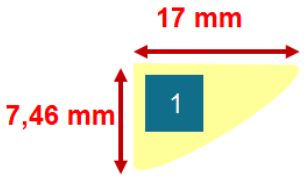

Figure B.6: The positioning of the samples on the reinforced aorta section of sheep BE97572-320

Reinforced Pulmonalis

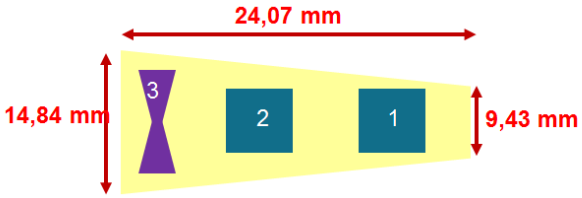

Figure B.7: The positioning of the samples on the reinforced pulmonary section of sheep BE97572-320

B.4 Sheep BE57572-434

Aorta

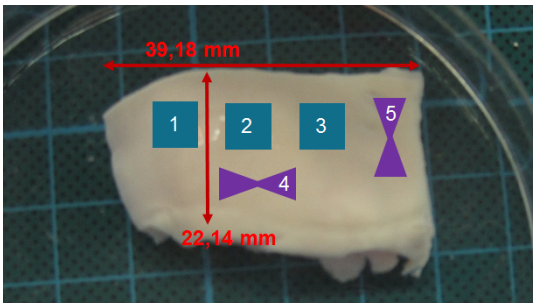

Figure B.8: The positioning of the samples on the aorta section of sheep BE57572-434

Reinforced Aorta

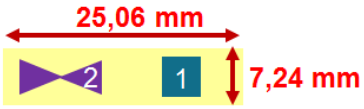

Figure B.9: The positioning of the samples on the reinforced aorta section of sheep BE57572-434

Reinforced Pulmonalis

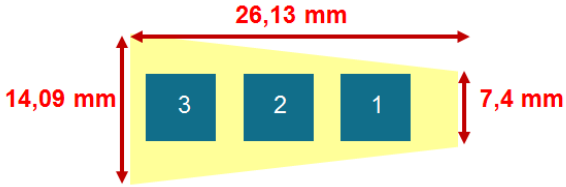

Figure B.10: The positioning of the samples on the reinforced pulmonary section of sheep BE57572-434

B.5 Sheep BE97572-0091

Aorta

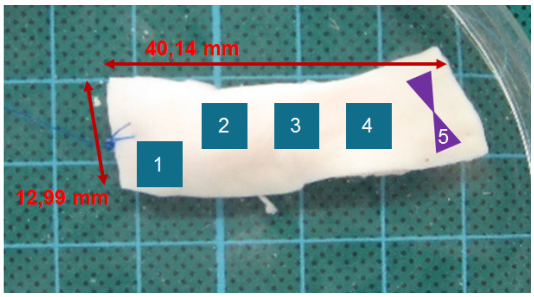

Figure B.11: The positioning of the samples on the aorta section of sheep BE97572-0091

Reinforced Aorta

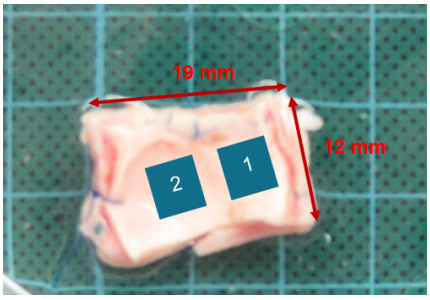

Figure B.12: The positioning of the samples on the reinforced aorta section of sheep BE97572-0091

Reinforced Pulmonalis

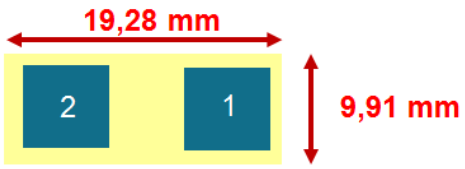

Figure B.13: The positioning of the samples on the reinforced pulmonary section of sheep BE97572-0091

B.6 Sheep BE47572-393

Aorta

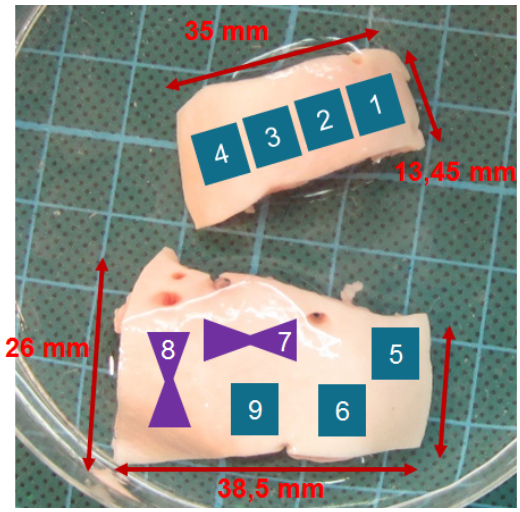

Figure B.14: The positioning of the samples on the aorta section of sheep BE47572-393

Reinforced Aorta

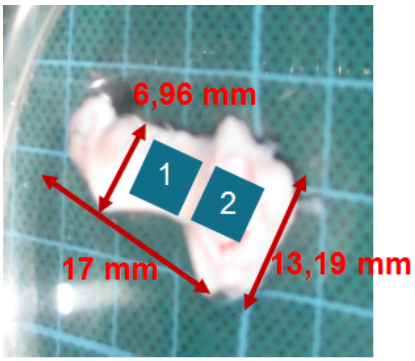

Figure B.15: The positioning of the samples on the reinforced aorta section of sheep BE47572-393

B.7 Sheep BE07572-73

Aorta

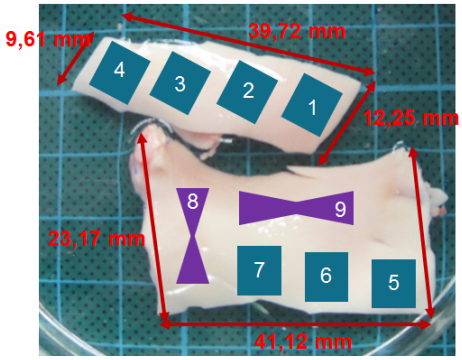

Figure B.16: The positioning of the samples on the aorta section of sheep BE07572-73

Reinforced Aorta

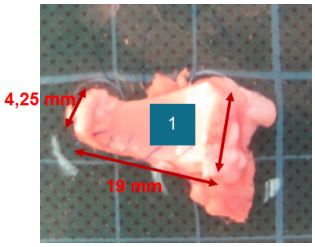

Figure B.17: The positioning of the samples on the reinforced aorta section of sheep BE07572-73

Reinforced Pulmonalis

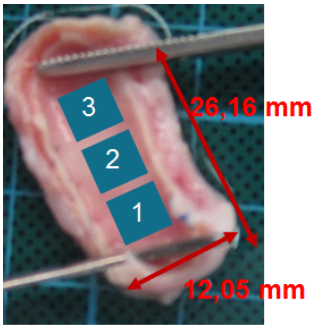

Figure B.18: The positioning of the samples on the reinforced pulmonary section of sheep BE07572-73

B.8 Sheep BE37572-385

Aorta

Figure B.19: The positioning of the samples on the aorta section of Sheep BE37572-385

Reinforced Aorta

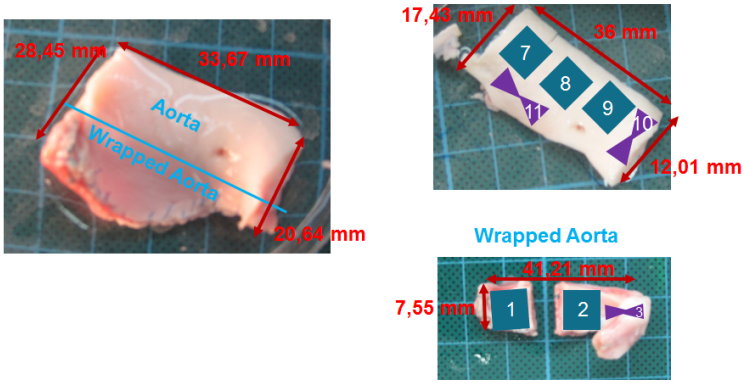

Figure B.20: The positioning of the samples on the reinforced aorta section of Sheep BE37572-385

Reinforced Pulmonalis

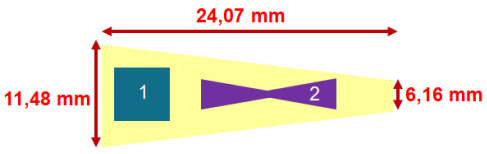

Figure B.21: The positioning of the samples on the reinforced pulmonary section of Sheep BE37572-385

Appendix C

Introduction to continuummechanics

Biological tissues, e.g. arterial tissues, can be thought of as being nonlinear and anisotropic. Therefore, the mechanical behavior of these tissues can be described based on continuummmechanics.[32] A short introduction to continuummechanics is given in this appendix.

C.1 Kinematics

Assume a body in initial state is transformed into the deformed configuration by applying loads onto it. This situation is visualized in Figure C.1.[23]

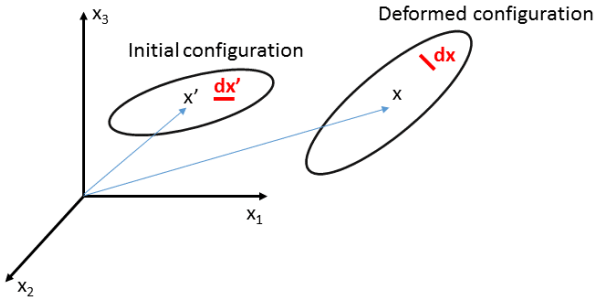

Figure C.1: The deformation of a body in an initial state to a deformed state

A material point in the initial configuration is labeled **x'** and in the deformed configuration this point is labeled **x**. The deformation can thus be described by the function χ which represents the mapping of the material point in the initial configuration **x'** onto the material point in the deformed configuration:

$$\boldsymbol{x} = \chi\left(\boldsymbol{x'}\right) \tag{C.1}$$

[32] The relationship between a material point in the initial configuration x_i and the corresponding material point in the deformed configuration x_i', is the displacement vector, and the following holds for every material point in the body.[23]

$$\boldsymbol{x_i'} = \boldsymbol{x_i} + \boldsymbol{u_i} \tag{C.2}$$

In a next step, there is looked at the transformation of an infinitesimal material vector from the initial configuration to the deformed configuration, visualized in Figure C.1 as the infinitesimal vector **dx'** in the initial state and the corresponding infinitesimal vector **dx** in the deformed configuration. These infinitesimal vectors can be related as:

$$\boldsymbol{dx} = \boldsymbol{F} \cdot \boldsymbol{dx'} \tag{C.3}$$

In the above equation, $\boldsymbol{F}$ represents the *deformation gradient*. Also, since **x** depends on **x'**, the chainrule states:

$$\boldsymbol{dx} = \frac{\delta \boldsymbol{x}}{\delta \boldsymbol{x'}} \cdot d\boldsymbol{x} \tag{C.4}$$

Thus, $\boldsymbol{F}$ satisfies the following equation:

$$\boldsymbol{F} = \frac{\delta \boldsymbol{x}}{\delta \boldsymbol{x'}} \tag{C.5}$$

The determinant of the deformation gradient can be denoted as the Jacobian J and $J = det\boldsymbol{F} = dV/dV'$. In this equation V represents the volume in the deformed configuration, and V' is the volume in the initial configuration. Often biological tissues are considered incompressible, meaning that $J = det\boldsymbol{F} = 1$.
Since the deformation of a body from an initial configuration to a deformed configuration can consist of a translation, deformation or a combination of both, the deformation gradient tensor **F** can be decomposed into a stretch and rotation tensor in two ways. If there is assumed that the the body is first deformed and then rotated, the first equation holds. When the assumption is made that the body is first rotated and then stretched, the second equation is valid.

$$\boldsymbol{F} = \boldsymbol{R} \cdot \boldsymbol{U} \tag{C.6}$$

$$\boldsymbol{F} = \boldsymbol{V} \cdot \boldsymbol{R} \tag{C.7}$$

In the above equations, the rotation tensor **R** is orthogonal [23] and the eigenvalues of **U** and **V** are equal, and are called the principal stretches $\lambda_{11}, \lambda_{22}$, and λ_{33}. These are the stretches associated with the deformations in the direction of the three reference axes.[32]
The deformation can be defined as well using two other measures, namely the *right* and *left Cauchy-Green deformation tensors*, which are respectively:

$$\boldsymbol{C} = \boldsymbol{F^T} \cdot \boldsymbol{F} = \boldsymbol{U^T} \cdot \boldsymbol{R^T} \cdot \boldsymbol{R} \cdot \boldsymbol{U} = \boldsymbol{U^2} \tag{C.8}$$

$$\boldsymbol{B} = \boldsymbol{F} \cdot \boldsymbol{F^T} = \boldsymbol{V} \cdot \boldsymbol{R} \cdot \boldsymbol{R^T} \cdot \boldsymbol{V^T} = \boldsymbol{V^2} \tag{C.9}$$

There should be noted that $\boldsymbol{C}$ is expressed in the initial configuration, whereas $\boldsymbol{B}$ is expressed in the deformed configuration.[23] With $\boldsymbol{C}$ and $\boldsymbol{B}$ principal invariants are associated, which can be determined as:

$$I_1 = tr\left(\boldsymbol{C}\right) = \lambda_{11}^2 + \lambda_{22}^2 + \lambda_{33}^2 \tag{C.10}$$

$$I_2 = \frac{1}{2}\left[I_1^2 - tr\left(\bar{\boldsymbol{C}}^2\right)\right] = \lambda_{11}^2\lambda_{22}^2 + \lambda_{22}^2\lambda_{33}^2 + \lambda_{11}^2\lambda_{33}^2 \tag{C.11}$$

$$I_3 = det\left(\boldsymbol{C}\right) = \lambda_1^2\lambda_2^2\lambda_3^2 \tag{C.12}$$

[54], [32]

The Green strain tensor, one of the most used strain tensors, is defined as:

$$\boldsymbol{E} = \frac{1}{2}\left(\bar{\boldsymbol{C}} - \boldsymbol{I}\right) \tag{C.13}$$

Entering equation C.2 in equation C.5, leads to:

$$\boldsymbol{F} = \frac{\delta\left(\boldsymbol{x'} + \boldsymbol{u}\right)}{\delta x'} = \boldsymbol{I} + \boldsymbol{H} \qquad where \qquad \boldsymbol{H} = \frac{\delta \boldsymbol{u}}{\delta x'} \tag{C.14}$$

Subsequently, equation C.14 is combined with equation C.13 and equation C.8, which results in:

$$\boldsymbol{E} = \frac{1}{2}\left(\boldsymbol{H} + \boldsymbol{H^T} + \boldsymbol{H^T} \cdot \boldsymbol{H}\right) \tag{C.15}$$

Equation C.15 can be simplified with the assumption that when deformations and rigid body motions are small, the quadratic term can be neglected, which leads to:

$$\boldsymbol{\epsilon} = \frac{1}{2}\left(\boldsymbol{H} + \boldsymbol{H^T}\right) \tag{C.16}$$

or with equation C.14:

$$\boldsymbol{\epsilon} = \frac{1}{2}\left(\boldsymbol{F} + \boldsymbol{F^T}\right) - \boldsymbol{I} \tag{C.17}$$

In the above equations $\boldsymbol{\epsilon}$ is called the linearized strain tensor.[23]

C.2 Stress

Assume a cube of material on which external forces are exerted. According to Newton's law, the cube of material must develop internal forces to maintain equilibrium between the external and internal forces. These internal forces can be seen as traction vectors that act in a random direction on the surfaces of the cube. Since the traction force is a vector in three dimensions, this vector can be decomposed into three components in the direction of the axes. These nine components are the components of a second order stress tensor called the Cauchy stress tensor. Note that this tensor

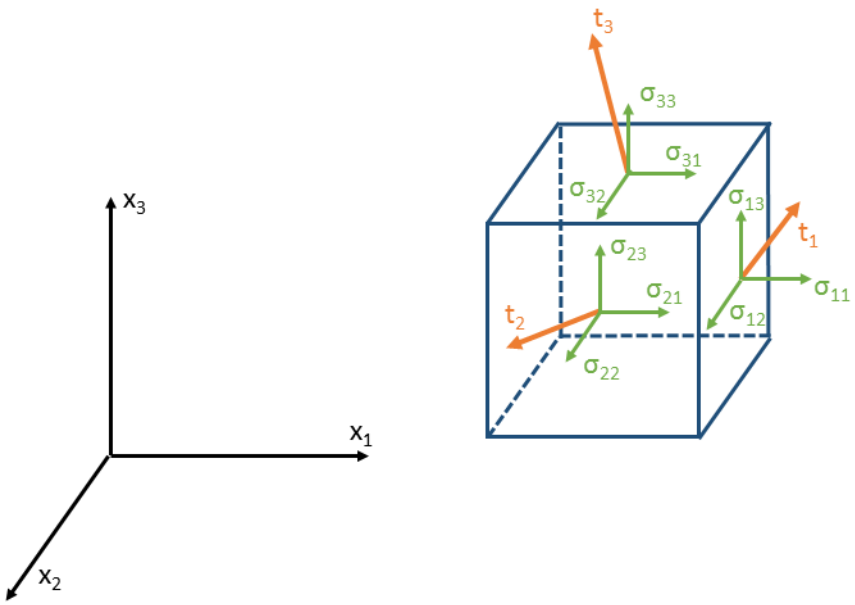

Figure C.2: Definition of the Cauchy stress tensor, with t_i the components of the traction vector and σ_{ij} the components of the stress tensor

is always expressed with reference to the deformed configuration. The definition of the stress tensor is visualized in Figure C.2.[20] With $\boldsymbol{n}$ the vector that represents the outward unit normal vector in the deformed state, $\boldsymbol{t}$ the traction vector, and $\boldsymbol{\sigma}$ the Cauchy stress tensor, then the following holds:

$$\boldsymbol{t} = \boldsymbol{n} \cdot \boldsymbol{\sigma} \tag{C.18}$$

The traction vector $\boldsymbol{t}$ can be found as $\boldsymbol{t} = \frac{df}{dA}$ with df the differential force vector which acts on the differential area dA in the deformed configuration. [23]
However, it is not always easy or possible to know beforehand the deformed configuration, which makes a stress measure which is referenced to the initial configuration more convenient. Two measures that are often used are the *first Piola-Kirchoff stress tensor* and the *second Piola-Kirchoff stress tensor*.
Assume that $\boldsymbol{N}$ represents the outward unit normal vector in the initial configuration, then the first Piola-Kirchoff stress tensor is defined as the stress tensor, $\boldsymbol{T}$ which is defined according the following equation:

$$\boldsymbol{t'} = \boldsymbol{N} \cdot \boldsymbol{T} \qquad \text{with } \boldsymbol{t'} = \frac{df'}{dA'} \tag{C.19}$$

In this equation the infinitesimal force df' equals the infinitesimal force df that is translated from the deformed configuration to the initial configuration, and dA' is the infinitesimal area in the initial configuration.
The first Piola-Kirchoff stress is expressed in terms of the Cauchy stress tensor:

$$\boldsymbol{T} = J\boldsymbol{\sigma}\boldsymbol{F}^{-T} \tag{C.20}$$

The second Piola-Kirchoff stress, $\boldsymbol{P}$, tensor can be defined as:

$$\boldsymbol{P} = J\boldsymbol{F}^{-1}\boldsymbol{\sigma}\boldsymbol{F}^{-T} \tag{C.21}$$

The first Piola-Kirchoff stress can be expressed in terms of the second Piola-Kirchoff stress:

$$\boldsymbol{T} = \boldsymbol{F}\boldsymbol{P} \tag{C.22}$$

C.3 Constitutive Equations

Above, strain formulations as well as stress formulations are expressed. However, no relationship between the defined strain formulations and defined stress formulations is given. This relationship is expressed by a phenomenological mathematical model, which is called a constitutive equation. These mathematical models consist of unknown parameters that need to be determined by fitting experimental data, and measures of deformation.[23]
Arterial tissue can be assumed to behave hyperelastically. Consequently, the state is independent of the history of motion, because in elasticity the deformed configuration is important. Moreover, the tissue can be thought of being homogeneous, leading to the conclusion that the constitutive behavior does not explicitly depend on the location in the tissue. Therefore, the deformation gradient is the only state variable taken into account.[23]
To find the constitutive equation, the second of law of thermodynamics, written in the Clausius-Duhem equation needs to be considered:

$$-\rho_0\left(\frac{d\psi}{dt} + \mu\frac{dT}{dt}\right) + \boldsymbol{T}^T : \frac{d\boldsymbol{F}}{dt} - \frac{1}{T}\boldsymbol{q}_0 \cdot \nabla_0 T \geq 0 \tag{C.23}$$

Furthermore, assume that the process is isothermal with no heat transfer:

$$-\rho_0\left(\frac{d\psi}{dt}\right) + \boldsymbol{T}^T : \frac{d\boldsymbol{F}}{dt} \geq 0 \tag{C.24}$$

The only state variable present is the deformation gradient $\mathbf{F}$, both the Helmholtz free energy, ψ, and the first Piola-kirchoff stress, $\mathbf{T}$ depend on this state variable.

$$\frac{d\psi}{dt} = \frac{\delta\psi}{\delta\boldsymbol{F}} : \frac{d\boldsymbol{F}}{dt} \tag{C.25}$$

Substituting equation C.25 in equation C.24, and the process is reversible (meaning that the inequality can be replaced by an equality) results in:

$$\left(-\rho_0\frac{\delta\psi}{\delta\boldsymbol{F}} + \boldsymbol{T}^T\right) : \frac{d\boldsymbol{F}}{dt} = 0 \tag{C.26}$$

Since the equation above needs to be satisfied for all possible deformation gradients, the term between brackets needs to equal zero:

$$\boldsymbol{T}^T = \rho_0\frac{\delta\psi}{\delta\boldsymbol{F}} \quad \Leftrightarrow \quad \boldsymbol{T} = \rho_0\frac{\delta\psi}{\delta\boldsymbol{F}^T} \tag{C.27}$$

[23] This is an important equation since this reveals that only one scalar constitutive function $\psi = \psi(\boldsymbol{F})$ needs to be found to describe the hyperelastic behavior of the tissue.
Remember equation C.8, which implies that searching for the constitutive equation in the form $\psi = \psi(\boldsymbol{C})$ is also reasonable.

$$\boldsymbol{T} = 2\rho_0 \frac{\delta\psi}{\delta \boldsymbol{C}} \cdot \boldsymbol{F}^T \tag{C.28}$$

Remark that ψ stands for the Helmholtz free energy. [23]

Appendix D

Parameters of the Gasser-Holzapfel-Ogden Model

In the tabels below, the calculated parameters of the GHO model for every sample of every sheep are given. Furthermore, the range of the stress-strain curve is given. Also, the root mean squared error is determined between the experimental stress-strain curve and the stress-strain curve which is modeled using the experimental strains and the obtained parameters. The last column of each table gives the thickness of each sample.

Sheep BE77572-321

Table D.1: Coefficients of constitutive modeling for sheep BE77572-321

Sample Type	Sample No	C_{10} $[MPa]$	k_1 $[MPa]$	k_2 $[-]$	α $[rad]$	κ $[-]$	Range stress $[MPa]$	Range strain $[-]$	RMSE $[-]$	t $[mm]$
Force-Controlled										
Aorta	Sample 1	0.0187	$8.41e^{-4}$	4.9892	1.57	0.017	$0 - 0.0849$	$0.98 - 1.43$	0.0082	1.53
	Sample 2	0.0228	0.007978	38.747	1.57	0.33	$0.0064 - 0.0722$	$0.99 - 1.31$	0.0030	1.93
Pulmonalis	Sample 1	$2.15e^{-11}$	0.1351	1.4208	1.57	0.32	$0.0025 - 0.3830$	$0.89 - 1.62$	0.0371	0.83
	Sample 2	$9.07e^{-4}$	0.04	0.9141	$7.30e^{-6}$	0.3158	$0 - 0.1835$	$0.97 - 1.74$	0.0178	2.42
Displacement-Controlled										
Aorta	Sample 3	0.0367	0.085	0.2119	$2.40e^{-5}$	0.32	$0 - 1.022$	$0.97 - 1.84$	0.0252	0.86

Sheep BE37572-418

Table D.2: Coefficients of constitutive modeling for sheep BE37572-418

Sample Type	Sample No	C_{10} $[MPa]$	k_1 $[MPa]$	k_2 $[-]$	α $[rad]$	κ $[-]$	Range stress $[MPa]$	Range strain $[-]$	RMSE $[-]$	t $[mm]$
Force-Controlled										
Aorta	Sample 2	0.0165	0.0012	5.3772	1.57	0.26	$0.0035 - 0.1892$	$0.98 - 1.79$	0.0116	3.05
	Sample 3	0.0095	0.011	3.3427	0.59	0.19	$0.0032 - 0.0817$	$0.98 - 1.38$	0.0024	3.74
Pulmonalis	Sample 1	$1.80e^{-9}$	0.0273	0.4499	1.57	0.33	$4.7402e^{-4} - 0.2949$	$0.95 - 1.94$	0.0317	2.26
Pulmonalis Wrapped	Sample 2	$4.00e^{-14}$	0.2006	2.9804	0.39	0.21	$0.0019 - 0.2951$	$0.96 - 1.31$	0.0128	4.05
Displacement-Controlled										
Aorta	Sample 4	0.0044	0.0111	0.1526	1.57	0.30	$-3.0806e^{-6} - 0.1182$	$0.95 - 1.87$	0.0028	5.5
	Sample 7	0.0061	0.0182	0.7838	1.57	0.29	$0 - 0.1029$	$0.96 - 1.62$	0.0025	4.26
Aorta Wrapped	Sample 1	0.0081	0.0611	1.1929	$4.41e^{-5}$	0.33	$-0.001 - 0.2845$	$0.98 - 1.64$	0.0176	4.05
Pulmonalis Wrapped	Sample 1	$2.24e^{-14}$	0.1879	12.1609	0.50	0.29	$-3.677e^{-4} - 0.2845$	$0.96 - 1.42$	0.0115	4.50
	Sample 3	$9.69e^{-14}$	1.2084	16.4396	1.57	0.30	$-0.0041 - 0.5194$	$0.95 - 1.29$	0.017	3.97

Sheep BE97572-0320

Table D.3: Coefficients of constitutive modeling for sheep BE97572-0320

Sample Type	Sample No	C_{10} $[MPa]$	k_1 $[MPa]$	k_2 $[-]$	α $[rad]$	κ $[-]$	Range stress $[MPa]$	Range strain $[-]$	RMSE $[-]$	t $[mm]$
Force-Controlled										
Aorta	Sample 1	0.0091	0.0054	2.725	1.04	0.17	$0.0026 - 0.062$	$0.97 - 1.41$	0.0036	3.82
Pulmonalis	Sample 1	0.006	0.0222	3.433	0.27	0.33	$0.0013 - 0.0608$	$0.88 - 1.56$	0.004	2.02
Pulmonalis Wrapped	Sample 2	$2.48e^{-14}$	0.5048	$2.34e^{-14}$	1.00	0.25	$0.0029 - 0.2226$	$0.99 - 1.21$	0.0157	3.48
Displacement-Controlled										
Aorta	Sample 2	0.0076	0.0299	0.219	1.57	0.31	$-0.00036 - 0.1499$	$0.98 - 1.64$	0.0038	3.22
Aorta Wrapped	Sample 1	0.0045	0.0101	0.5306	1.57	0.30	$-5.1512e^{-5} - 0.0833$	$0.96 - 1.76$	0.0025	6.45
Pulmonalis Wrapped	Sample 1	0.0053	0.6139	35.9413	1.57	0.28	$-0.0055 - 0.7831$	$0.97 - 1.29$	0.0188	1.91

Sheep BE57572-0434

Table D.4: Coefficients of constitutive modeling for sheep BE57572-0434

Sample Type	Sample No	C_{10} $[MPa]$	k_1 $[MPa]$	k_2 $[-]$	α $[rad]$	κ $[-]$	Range stress $[MPa]$	Range strain $[-]$	RMSE $[-]$	t $[mm]$
Force-Controlled										
Aorta	Sample 1	0.0053	0.0025	$2.23e^{-14}$	1.28	$1.56e^{-5}$	$0.0016 - 0.0233$	$0.96 - 1.31$	0.0013	4.28
	Sample 2	0.0081	0.0058	0.3012	0.97	$1.54e^{-7}$	$0.0026 - 0.096$	$0.98 - 1.55$	0.0023	2.97
Pulmonalis	Sample 1	$1.39e^{-13}$	0.0477	0.2801	1.57	0.32	$5.8450e^{-4} - 0.2970$	$0.87 - 1.93$	0.0313	1.98
Pulmonalis Wrapped	Sample 2	0.0237	0.0212	16.0687	0.48	$1.31e^{-8}$	$0.0042 - 0.0886$	$0.10 - 1.28$	0.003	2.37
Displacement-Controlled										
Aorta	Sample 3	0.005	0.0143	0.0699	1.57	0.32	$-6.0539e^{-4} - 0.0810$	$0.97 - 1.74$	0.0016	6.63
Aorta Wrapped	Sample 1	0.0057	0.0168	6.9938	0.95	0.25	$-1.1042e^{-4} - 0.1070$	$0.93 - 1.45$	0.0066	4.24
Pulmonalis Wrapped	Sample 1	0.0066	0.0752	8.0456	1.57	0.26	$-0.0014 - 0.1309$	$0.98 - 1.31$	0.0027	3.53

Sheep BE97572-0091

Table D.5: Coefficients of constitutive modeling for sheep BE97572-0091

Sample Type	Sample No	C_{10} $[MPa]$	k_1 $[MPa]$	k_2 $[-]$	α $[rad]$	κ $[-]$	Range stress $[MPa]$	Range strain $[-]$	RMSE $[-]$	t $[mm]$
Force-Controlled										
Aorta	Sample 1	0.015	0.0102	2.9972	$4.95e^{-7}$	0.33	$0.0030 - 0.2396$	$0.98 - 1.68$	0.0084	3.59
	Sample 2	0.003	0.0175	0.0572	0.94	$6.75e^{-8}$	$0.0043 - 0.2904$	$0.97 - 1.77$	0.0115	2.36
Pulmonalis	Sample 1	$1.61e^{-11}$	0.0267	0.8841	1.57	0.32	$3.7815e^{-4} - 0.2516$	$0.96 - 1.86$	0.029	2.76
Aorta Wrapped	Sample 1	0.0076	0.0071	5.8166	1.57	$8.21e^{-5}$	$0.0020 - 0.0322$	$0.99 - 1.18$	0.0012	5.63
Pulmonalis Wrapped	Sample 2	0.0047	0.014	1.6463	0.79	$1.92e^{-7}$	$0.0036 - 0.1624$	$0.98 - 1.37$	0.0077	2.88
Displacement-Controlled										
Aorta	Sample 3	0.0089	0.0213	0.1854	1.57	0.23	$4.0035e^{-4} - 0.1043$	$0.95 - 1.69$	0.0028	2.74
	Sample 4	0.0105	0.0172	0.1106	0.39	0.22	$-9.2396e^{-4} - 0.1628$	$0.96 - 1.73$	0.0033	2.60
Aorta Wrapped	Sample 2	0.0042	0.0146	2.3086	1.57	0.25	$-1.8690e^{-4} - 0.0565$	$0.98 - 1.46$	0.0026	4.23
Pulmonalis Wrapped	Sample 1	0.007	0.0652	5.3269	$5.44e^{-5}$	0.26	$-3.3634e^{-4} - 0.2201$	$0.98 - 1.36$	0.0054	3.02

Sheep BE47572-393

Table D.6: Coefficients of constitutive modeling for sheep BE47572-393

Sample Type	Sample No	C_{10} $[MPa]$	k_1 $[MPa]$	k_2 $[-]$	α $[rad]$	κ $[-]$	Range stress $[MPa]$	Range strain $[-]$	RMSE $[-]$	t $[mm]$
Force-Controlled										
Aorta	Sample 3	0.0068	0.0154	0.6312	1.57	0.29	$0.0025 - 0.1231$	$0.97 - 1.67$	0.0037	5.11
	Sample 4	0.0069	0.0099	$2.60e^{-14}$	0.96	$2.40e^{-9}$	$0.0019 - 0.0088$	$0.98 - 1.12$	0.0015	5.24
	Sample 6	0.0047	0.009	0.1764	0.94	0.09	$0.0021 - 0.1464$	$0.95 - 1.73$	0.0079	4.08
Pulmonalis	Sample 1	0.0078	0.0292	2.9407	$2.31e^{-7}$	0.30	$0.0015 - 0.2806$	$0.93 - 1.74$	0.0294	1.40
Aorta Wrapped	Sample 1	0.0053	0.0172	2.0446	1.04	$2.15e^{-10}$	$0.0034 - 0.1958$	$0.98 - 1.33$	0.003	3.40
Pulmonalis	Sample 1	0.087	0.0518	$2.22e^{-14}$	1.57	$1.77e^{-7}$	$0 - 0.0952$	$0.9848 - 1.114$	0.01	3.14
Wrapped	Sample2	0.1162	0.0545	$2.22e^{-14}$	1.57	$9.79e^{-11}$	$0.0006 - 0.1539$	$0.9903 - 1.138$	0.0158	3.14
Displacement-Controlled										
Aorta	Sample 2	0.0039	0.0073	0.5823	1.57	0.28	$5.0595e^{-5} - 0.0990$	$0.98 - 1.71$	0.0025	6.29
	Sample 5	0.0031	0.0065	0.2008	0.89	0.05	$-3.2811e^{-4} - 0.0989$	$0.903 - 1.7471$	0.0031	5.03
Aorta Wrapped	Sample 2	0.0049	0.0685	14.8436	$3.57e^{-4}$	0.32	$2.8299e^{-5} - 0.0845$	$0.97 - 1.34$	0.0032	6.25

Sheep BE07572-73

Table D.7: Coefficients of constitutive modeling for sheep BE07572-73

Sample Type	Sample No	C_{10} $[MPa]$	k_1 $[MPa]$	k_2 $[-]$	α $[rad]$	κ $[-]$	Range stress $[MPa]$	Range strain $[-]$	RMSE $[-]$	t $[mm]$
Force-Controlled										
Aorta	Sample 1	0.0221	0.0129	1.704	1.57	0.28	$0.0051 - 0.4517$	$0.98 - 1.84$	0.0112	2.13
	Sample 2	0.0137	0.0122	1.7152	1.57	0.32	$0.0028 - 0.1988$	$0.98 - 1.73$	0.0035	3.76
Pulmonalis	Sample 1	0.0027	0.039	1.7443	1.57	0.32	$8.3714e^{-4} - 0.1398$	$0.89 - 1.64$	0.0114	1.86
Pulmonalis Wrapped	Sample 2	$3.45e^{-10}$	0.076	3.2936	0.80	0.05	$0.0024 - 0.0890$	$0.10 - 1.20$	0.0013	4.30
Displacement-Controlled										
Aorta	Sample 3	0.0109	0.0211	0.4315	1.57	0.30	$-5.4167e^{-4} - 0.3005$	$0.95 - 1.83$	0.006	2.36
	Sample 4	0.0107	0.0308	0.1407	1.57	0.33	$-3.2480e^{-4} - 0.2147$	$0.96 - 1.80$	0.0064	2.49
	Sample 5	0.0163	0.0452	0.8307	1.57	0.31	$-0.0014 - 0.3391$	$0.96 - 1.67$	0.0081	1.68
Aorta Wrapped	Sample 1	0.0046	0.0149	11.176	0.0022	0.32	$-1.4317e^{-4} - 0.0265$	$0.98 - 1.34$	0.0012	6.31
Pulmonalis	Sample 1	0.0118	0.0351	8.3344	0.0017	0.27	$-0.0062 - 0.2408$	$0.97 - 1.45$	0.0091	2.04
Wrapped	Sample 3	0.0037	0.0815	2.3358	1.57	0.12	$-0.0035 - 0.7889$	$0.97 - 1.37$	0.0089	1.76

Sheep BE37572-385

Table D.8: Coefficients of constitutive modeling for sheep BE37572-385

Sample Type	Sample No	C_{10} $[MPa]$	k_1 $[MPa]$	k_2 $[-]$	α $[rad]$	κ $[-]$	Range stress $[MPa]$	Range strain $[-]$	RMSE $[-]$	t $[mm]$
Force-Controlled										
Aorta	Sample 1	0.0103	0.0057	15.0431	1.57	0.26	$0.0029 - 0.034$	$0.99 - 1.29$	0.0016	3.71
	Sample 2	0.005	0.0069	0.3234	1.01	0.10	$0.0025 - 0.0633$	$0.97 - 1.47$	0.002	4.36
	Sample 7	0.0082	0.0023	8.1791	1.56	0.21	$0.0023 - 0.0290$	$0.98 - 1.28$	0.0014	4.17
Pulmonalis	Sample 1	0.0019	0.0767	4.5411	$7.64e^{-7}$	0.31	$6.5141e^{-4} - 0.2638$	$0.99 - 1.60$	0.028	2.23
Aorta Wrapped	Sample 1	0.011	0.0201	22.2831	1.25	$8.65e^{-9}$	$0.0030 - 0.0449$	$0.10 - 1.17$	0.0018	3.74
Displacement-Controlled										
Aorta	Sample 3	0.0037	0.0122	0.5081	1.57	0.31	$-6.5095e^{-5} - 0.068$	$0.88 - 1.70$	0.002	5.52
	Sample 4	0.0059	0.0121	0.9559	1.57	0.30	$-7.6743e^{-5} - 0.0798$	$0.95 - 1.72$	0.0027	3.99
	Sample 8	0.0051	0.0046	3.573	1.57	0.18	$0 - 0.0262$	$0.98 - 1.31$	$9.78e^{-4}$	4.50
Aorta Wrapped	Sample 2	0.0042	0.1493	6.4378	1.57	0.29	$-0.0027 - 0.2022$	$0.98 - 1.32$	0.007	4.68
Pulmonalis Wrapped	Sample 1	0.002	0.1255	6.2898	1.57	0.24	$7.1256e^{-4} - 0.2208$	$0.98 - 1.28$	0.0048	2.88

Appendix E

Complementary Figures of Chapter 4

E.1 All samples plotted per tissue type

Aorta

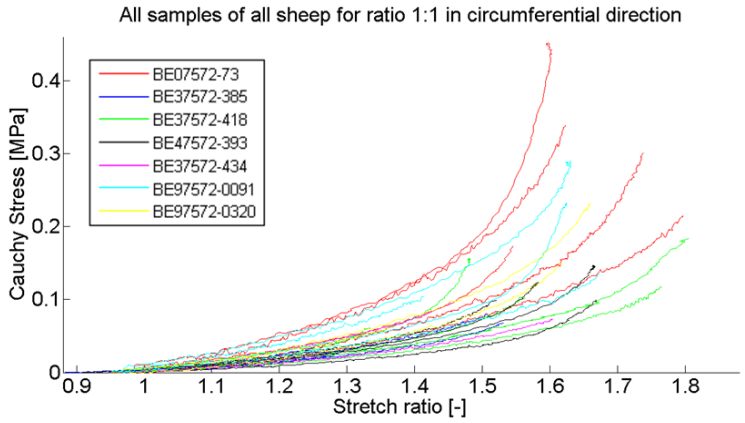

Figure E.1: Cauchy stresses in function of the stretch ratio for all the aorta samples in the circumferential direction for the test set with ratio 1:1

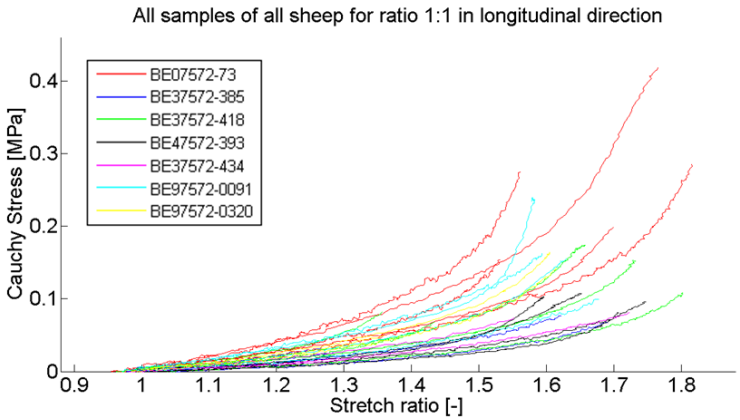

Figure E.2: Cauchy stresses in function of the stretch ratio for all the aorta samples in the longitudinal direction for the test set with ratio 1:1

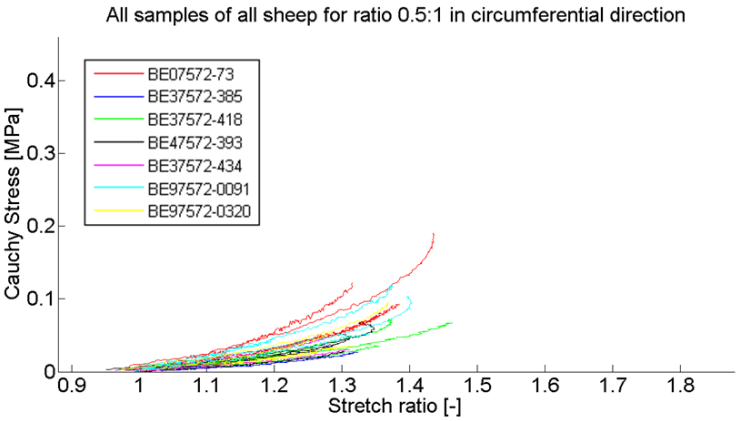

Figure E.3: Cauchy stresses in function of the stretch ratio for all the aorta samples in the circumferential direction for the test set with ratio 0,5:1

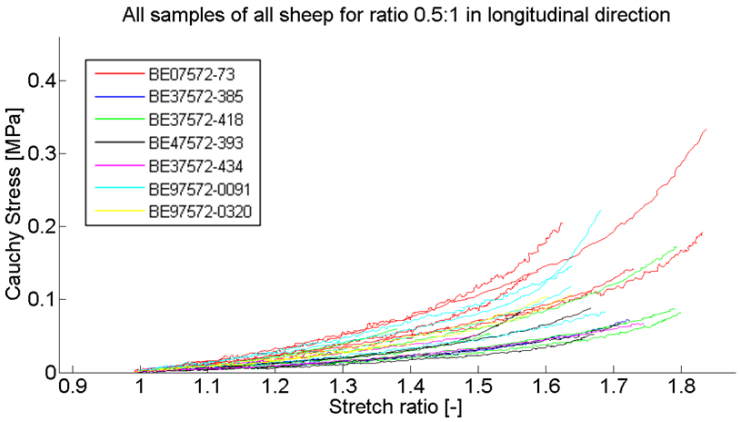

Figure E.4: Cauchy stresses in function of the stretch ratio for all the aorta samples in the longitudinal direction for the test set with ratio 0,5:1

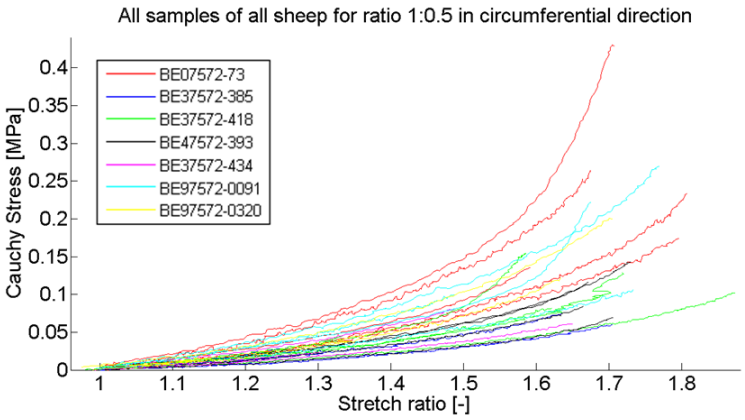

Figure E.5: Cauchy stresses in function of the stretch ratio for all the aorta samples in the circumferential direction for the test set with ratio 1:0,5

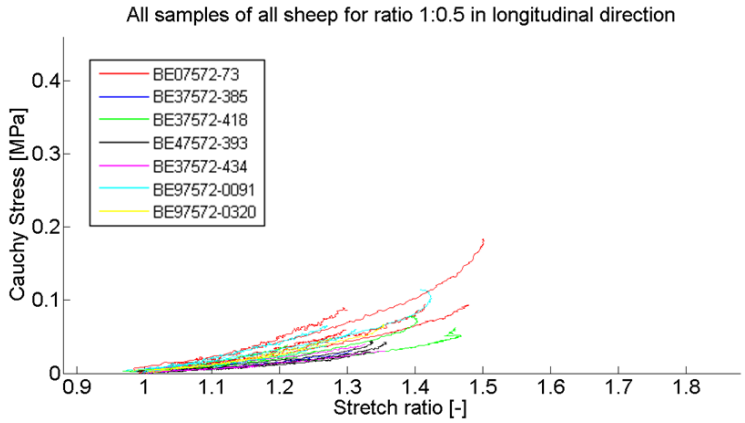

Figure E.6: Cauchy stresses in function of the stretch ratio for all the aorta samples in the longitudinal direction for the test set with ratio 1:0,5

Wrapped Aorta

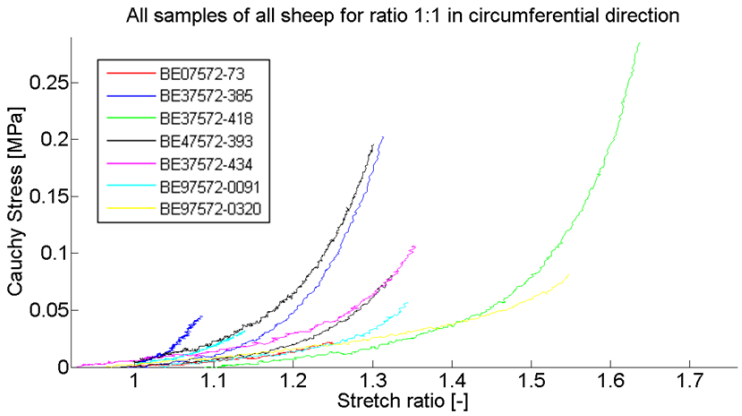

Figure E.7: Cauchy stresses in function of the stretch ratio for all the wrapped aorta samples in the circumferential direction for the test set with ratio 1:1

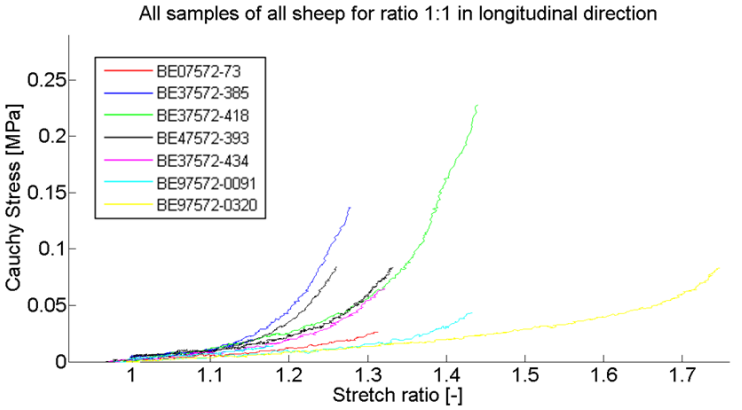

Figure E.8: Cauchy stresses in function of the stretch ratio for all the wrapped aorta samples in the longitudinal direction for the test set with ratio 1:1

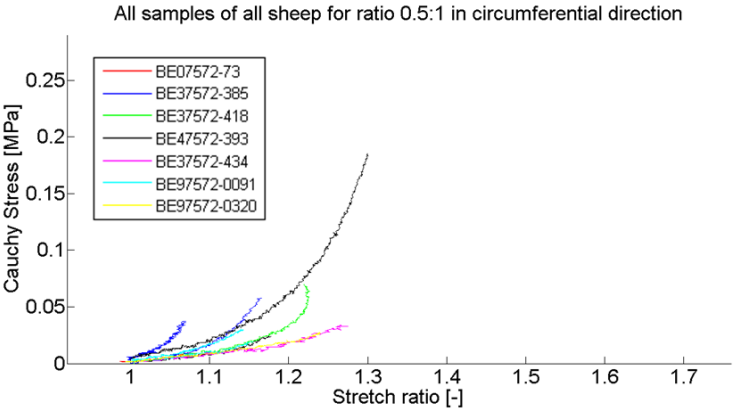

Figure E.9: Cauchy stresses in function of the stretch ratio for all the wrapped aorta samples in the circumferential direction for the test set with ratio 0,5:1

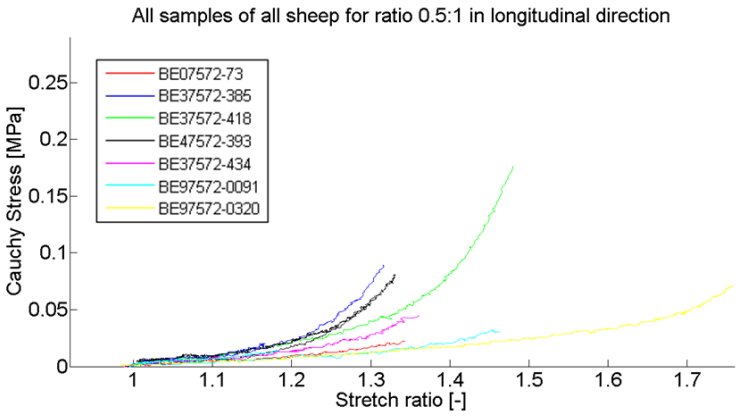

Figure E.10: Cauchy stresses in function of the stretch ratio for all the wrapped aorta samples in the longitudinal direction for the test set with ratio 0,5:1

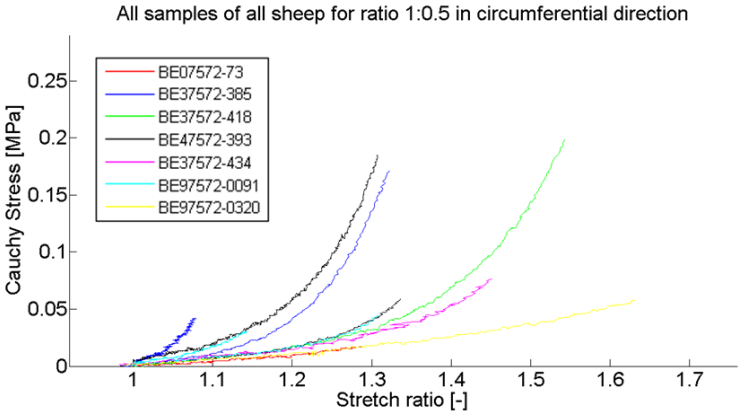

Figure E.11: Cauchy stresses in function of the stretch ratio for all the wrapped aorta samples in the circumferential direction for the test set with ratio 1:0,5

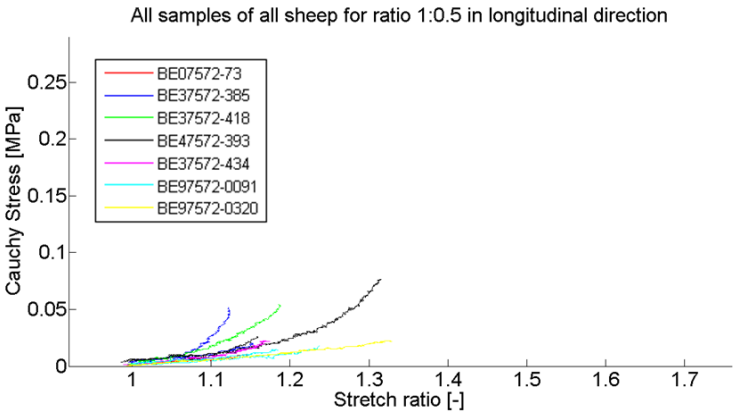

Figure E.12: Cauchy stresses in function of the stretch ratio for all the wrapped aorta samples in the longitudinal direction for the test set with ratio 1:0,5

Pulmonalis

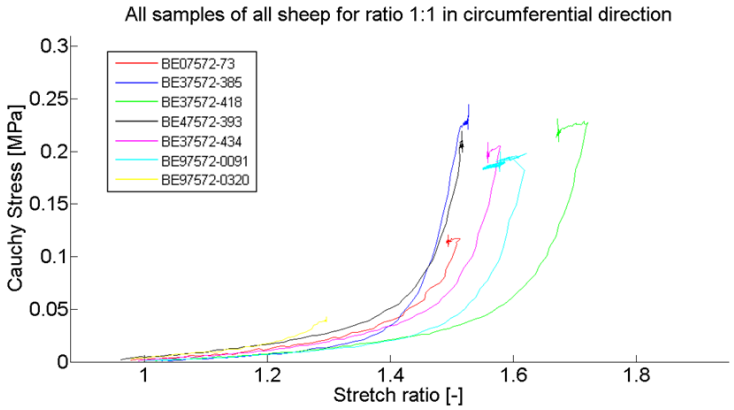

Figure E.13: Cauchy stresses in function of the stretch ratio for all the pulmonalis samples in the circumferential direction for the test set with ratio 1:1

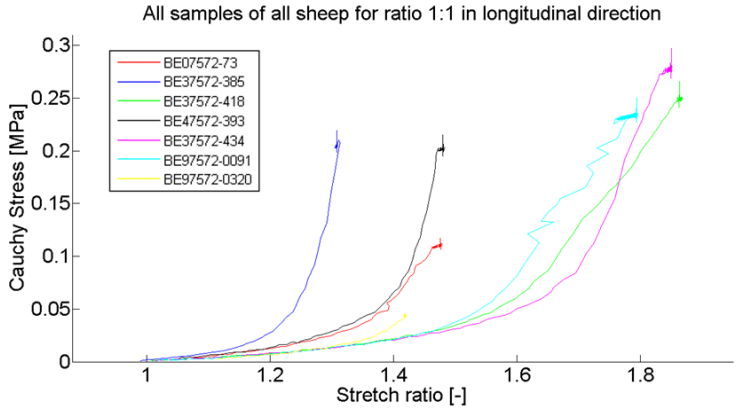

Figure E.14: Cauchy stresses in function of the stretch ratio for all the pulmonalis samples in the longitudinal direction for the test set with ratio 1:1

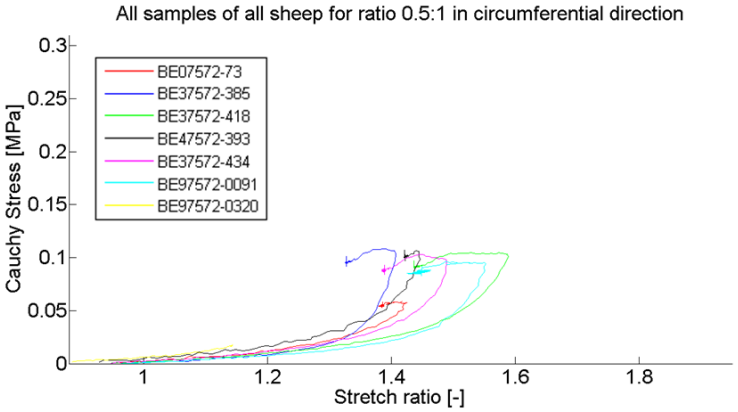

Figure E.15: Cauchy stresses in function of the stretch ratio for all the pulmonalis samples in the circumferential direction for the test set with ratio 0,5:1

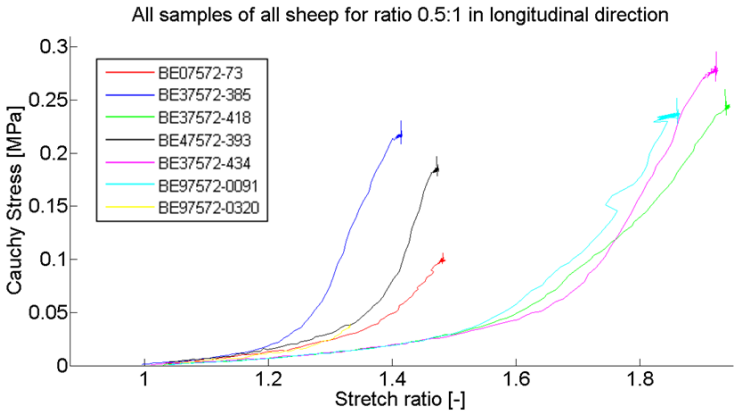

Figure E.16: Cauchy stresses in function of the stretch ratio for all the pulmonalis samples in the longitudinal direction for the test set with ratio 0,5:1

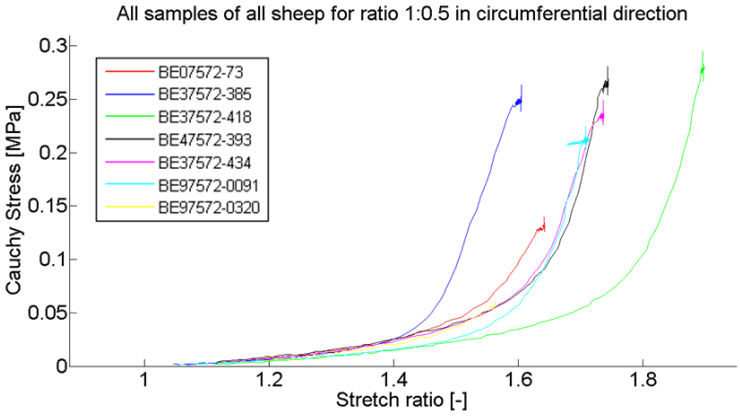

Figure E.17: Cauchy stresses in function of the stretch ratio for all the pulmonalis samples in the circumferential direction for the test set with ratio 1:0,5

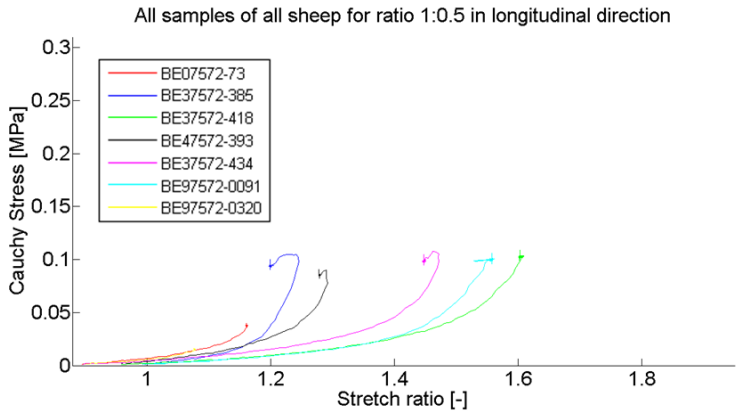

Figure E.18: Cauchy stresses in function of the stretch ratio for all the pulmonalis samples in the longitudinal direction for the test set with ratio 1:0,5

Wrapped Pulmonalis

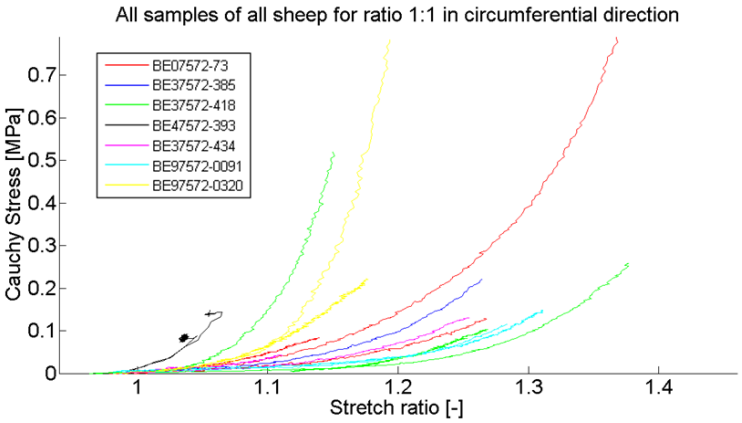

Figure E.19: Cauchy stresses in function of the stretch ratio for all the wrapped pulmonalis samples in the circumferential direction for the test set with ratio 1:1

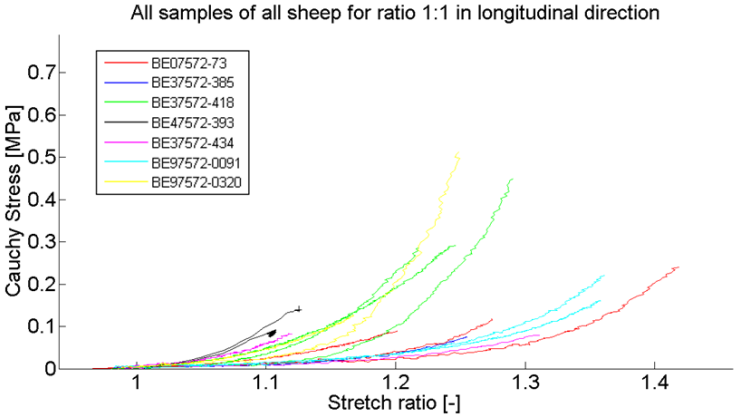

Figure E.20: Cauchy stresses in function of the stretch ratio for all the wrapped pulmonalis samples in the longitudinal direction for the test set with ratio 1:1

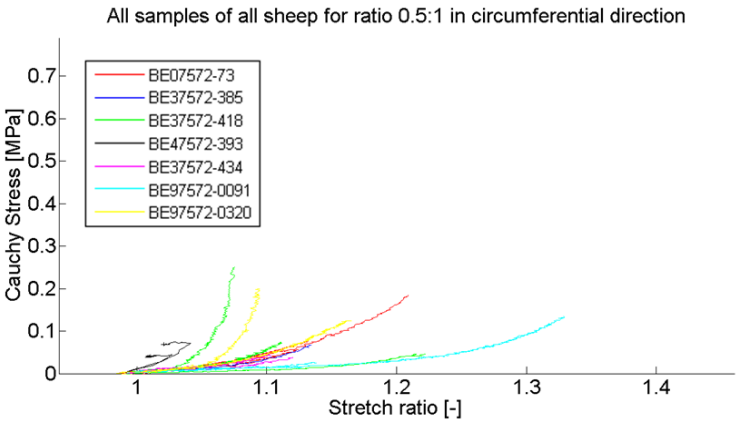

Figure E.21: Cauchy stresses in function of the stretch ratio for all the wrapped pulmonalis samples in the circumferential direction for the test set with ratio 0.5:1

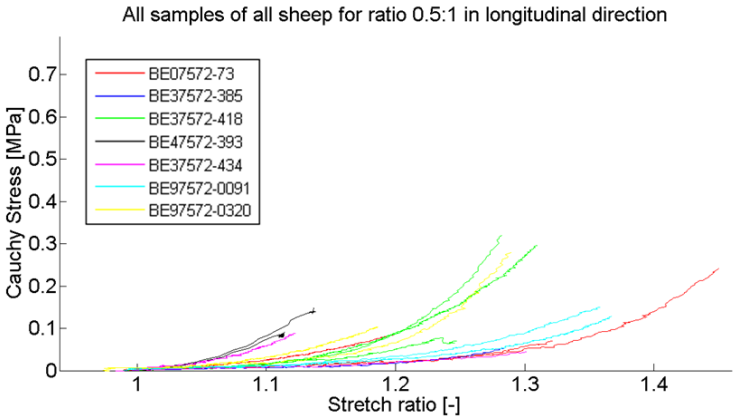

Figure E.22: Cauchy stresses in function of the stretch ratio for all the wrapped pulmonalis samples in the longitudinal direction for the test set with ratio 0.5:1

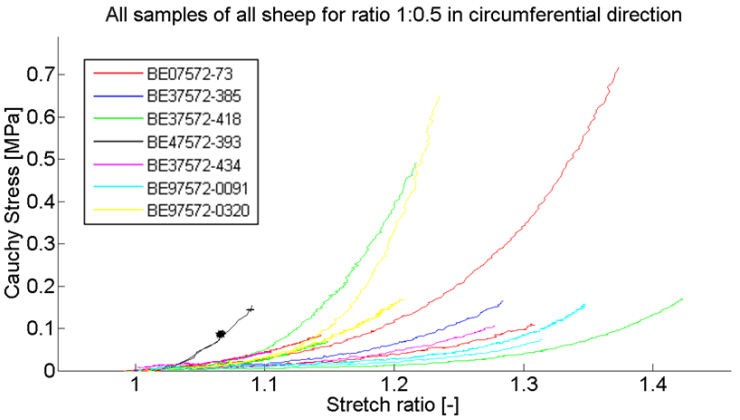

Figure E.23: Cauchy stresses in function of the stretch ratio for all the wrapped pulmonalis samples in the circumferential direction for the test set with ratio 1:0.5

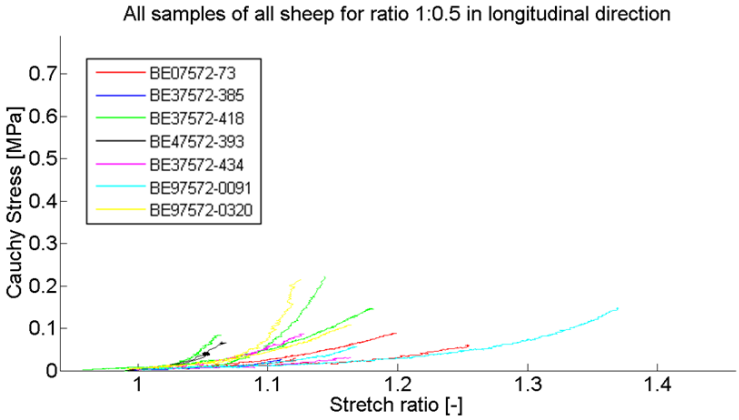

Figure E.24: Cauchy stresses in function of the stretch ratio for all the wrapped pulmonalis samples in the longitudinal direction for the test set with ratio 1:0.5

Appendix F

Construction of the Finite Element Model

This appendix will elaborate on the construction of the finite element model, used in this thesis. As previously stated, the model consists of several steps, which are *close*, *couple*, *moveback*, *axialprestretch*, *diastole* and *systole*. Each of these steps with corresponding boundary conditions will be elaborated on below.

F.1 Construction of the geometry

Before discussing the different steps of the model, there will be explained how the correct geometry is created in the sketch environment of Abaqus, shown in Figure F.1.

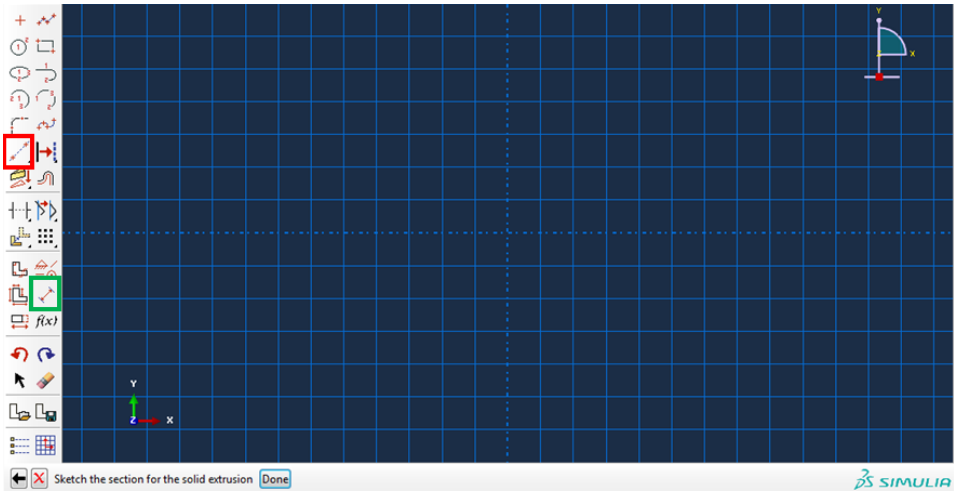

Figure F.1: Sketch Environment of Abaqus

The first step consists of drawing construction lines, using the button highlighted

in red in Figure F.1, following the x-axis and the y-axis. Subsequently, a third construction line is drawn, under an angle determined by the opening angle. In this case, the opening angle is taken as 120°. Since only half a cylinder will be used, the opening angle that needs to be drawn is 60°. The definition of the opening angle is given in Chapter 5. This third construction line is initially drawn with a random angle. The button, highlighted in green in Figure F.1 allows to measure the angle between the third construction line and the construction line on the y-axis. Moreover, the chance is given to choose a new value for the dimension, as can be seen in Figure F.2, while Figure F.3 visualizes the result after changing the angle. When entering a new dimension, the third construction line is moved, illustrated in Figure F.4. Using the highlighted button in this figure, the construction line can be moved to the origin.

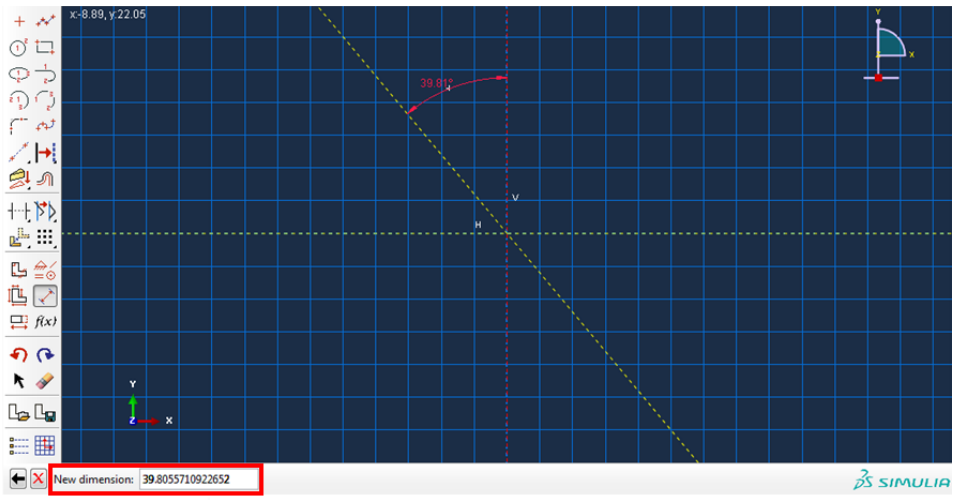

Figure F.2: Adding and changing the angle between the oblique construction line and the construction line on the y-axis

After drawing the construction lines, the first edge of the geometry, namely an arc, can be drawn using the highlighted button in Figure F.3. Care must be taken when drawing this arc, since it is essential that the origin of the arc corresponds to the origin of the sketch environment. The result is shown in Figure F.5, in which the radius of the arc is shown and readily changed to the correct value (which is 15 mm in this case), using the two highlighted buttons.

Thereafter, two lines delineating the thickness of the geometry are drawn, shown in Figure F.6, using the highlighted button. Moreover, the dimensions of these lines are changed to have the correct value 3,66 mm.

Drawing the second arc of which the origin corresponds to the origin of the sketch environment comprises the following step.

The result of sketching the geometry is shown in Figure F.7.

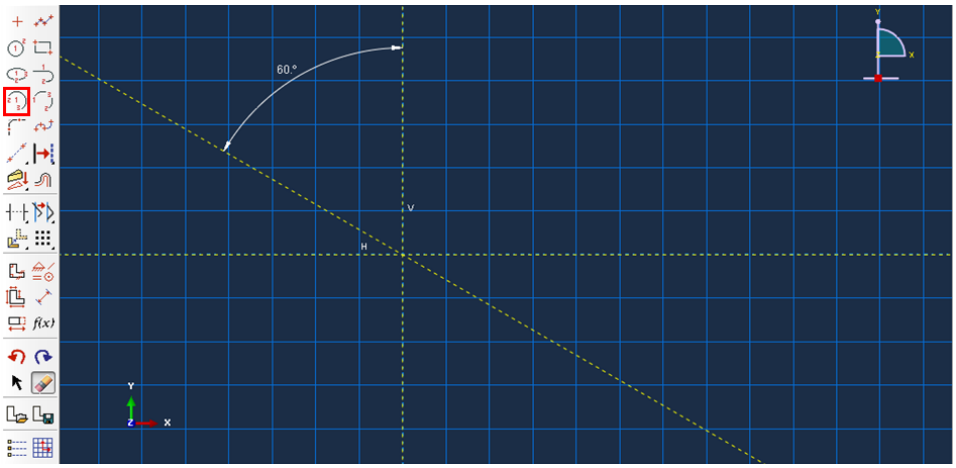

Figure F.3: Changed angle between the oblique construction line and the construction line on the y-axis

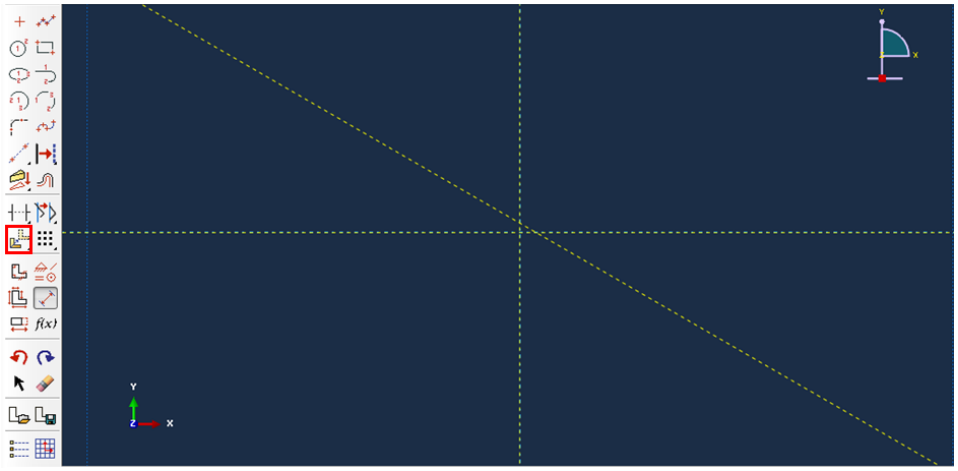

Figure F.4: Moved construction line

When finishing the sketch, there is asked to give an extrusion depth, which is taken as 20 mm.

F.2 Meshing and defining sets

The result of the previous step consists of a part with the right geometry. Subsequently, a few partitions need to be made in order to be able to assign different material parameters to certain sections. These partitions are based on the use of datum planes. These datum planes are created by using the option 'Create Datum Plane: Using Offset From Principal Plane'. The principal plane from which the offset is defined is the XY-plane, and the two datum planes have an offset of respectively 5 mm and 15 mm. The result of the partitioning step is shown in Figure F.8.

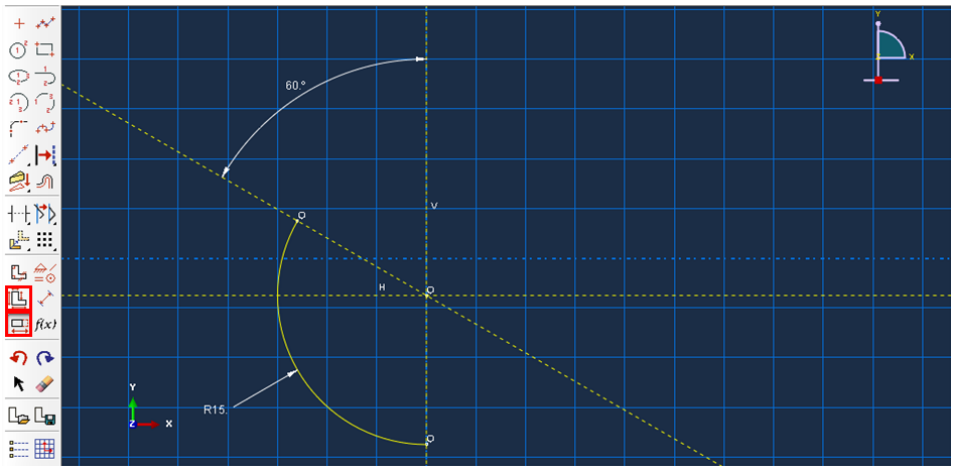

Figure F.5: Drawing of the first arc

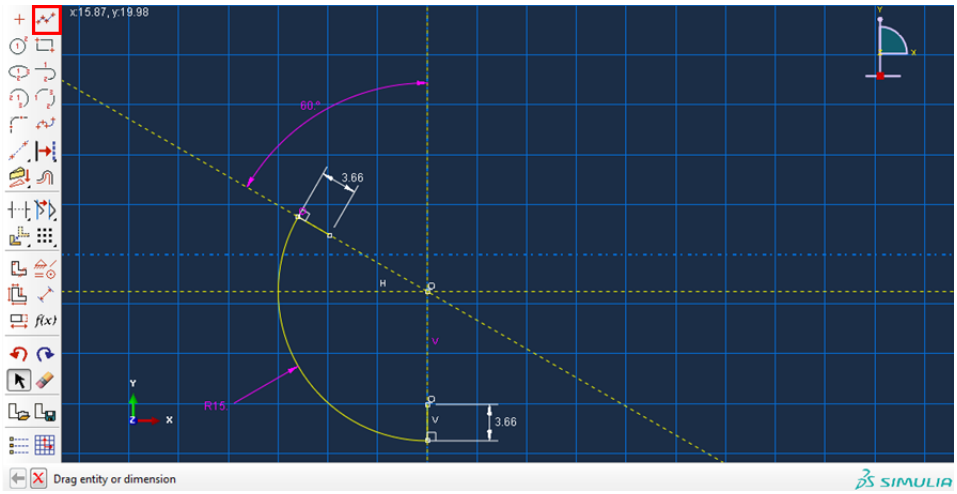

Figure F.6: Drawing of the two lines delineating the thickness of the geometry

After partitioning, the part can be meshed, which can be done in the Mesh module in Abaqus. The seed option allows to choose the element size of the mesh.
When the part is meshed the different sets, needed for the boundary conditions, can be defined. The following sets can be found in the model: ALL, AW, BOTTOM, BOTTOMLINE, EDGE, LOWEREDGE, MIDDLELINE, NODES_X, PW, TOP, TOUCHINGSURFACE, UPPEREDGE, of which the sets ALL, AW, and PW are geometry sets, while the rest of the sets are nodesets.
The set ALL comprises the whole model. The set PW defines the part of the geometry that is situated in the middle of the part, whereas the set AW entails the left and right section of the model. These geometry sets can be used to assign different material parameters to different sections of the part.
The set BOTTOM, as the name says, is the bottom surface of the part, whereas

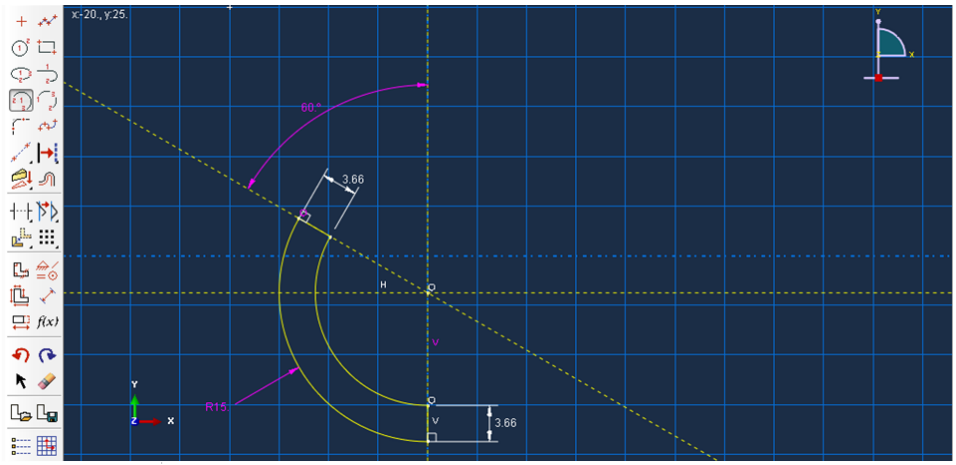

Figure F.7: Result of sketching the geometry

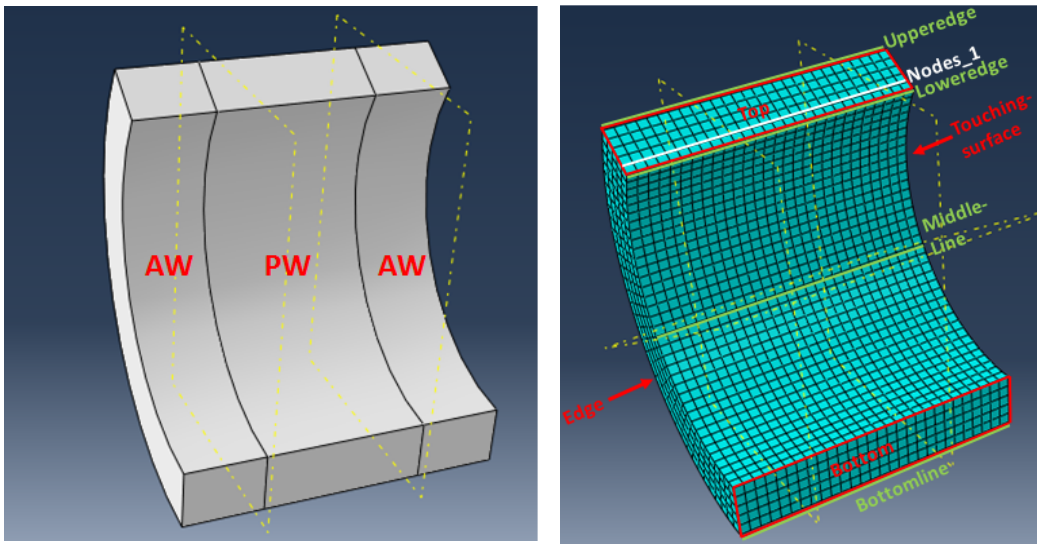

(a) Geometry Sets

(b) Node Sets

Figure F.8: The different sets of the model

the set TOP is the top surface. The sets EDGE and TOUCHINGSURFACE are respectively the right and left side of the part. The bottom line of the set BOTTOM can be found as the set BOTTOMLINE. The bottom edge and the lower edge of the TOP set can be found as the sets LOWEREDGE and UPPEREDGE. The set MIDDLELINE entails the middle row of nodes on the innersurface of the part. Finally, the nodesets NODES_X, where X can have different number, correspond to the X^{th} row of nodes of the TOP surface, starting from the LOWEREDGE nodeset. The different sets are visualized in Figure F.8.

F.3 Steps and corresponding boundary conditions, loads and interactions

Since the model consists of two parts, one with circumferential stresses and one part without circumferential stresses, a part without circumferential stresses is created. This is done by first simulating only the initial and closing step, and subsequently importing this deformed configuration, further referred to as wrap, into the model. Thereafter, the undeformed configuration, further referred to as aorta, is imported into the model, and the set-up of the model is complete and shown in Figure F.9.

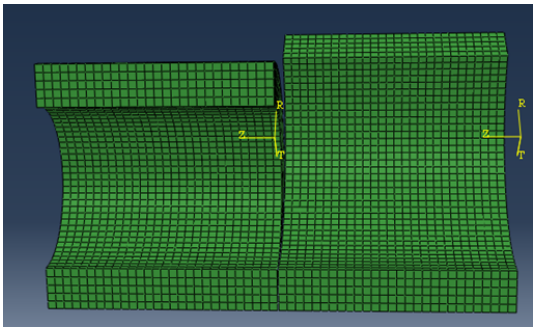

Figure F.9: The set-up of the model consisting of a part without circumferential stresses (deformed configuration) and a part with circumferential stresses (undeformed configuration)

In this section the different steps with their corresponding boundary conditions are discussed.

F.3.1 Initial

Initially three boundary conditions are defined. The first boundary condition fixes the bottomline of the aorta part in the y-direction, to restrict the part from translating. Secondly, the complete aorta is fixed in the z-direction, since in the next step no movement in the z-direction is expected. The third boundary condition fixes the bottom surface of the aorta in the x-direction.

F.3.2 Step: Close

The first step in this simulation is responsible for creating circumferential stresses in the aorta. By moving the nodesets LOWEREDGE, NODES_X, and UPPEREDGE to have an x-coordinate equal to zero, using boundary conditions, circumferential stresses will appear. The distances necessary to move the nodesets can be determined by finding the initial coordinates of these nodes and use the opposite of the x-coordinates as the distances over which the nodesets need to move.

F.3.3 Step: Couple

These step couples the wrap and aorta to each other. The boundary conditions, created in the previous step, are replaced by a boundary condition which fixes the top surface of the aorta in the current position in the x-direction. Moreover, the top and bottom nodesets of the wrap are fixed in the same direction. Furthermore, the wrap is fixed both in x- and y-direction, and the nodeset EDGE of the wrap is moved in the z-direction over a distance which is slightly larger than the distance between both parts, to ensure complete contact between both parts. The last boundary condition that is created, prevents the wrap part to translate by fixing its bottomline.
The interaction between the two parts is defined in this step. The touching surface of the wrap is the Master surface, whereas the touching surface of the aorta is the Slave surface in the interaction definition. Two specific interaction properties are applicable in this interaction. The first consists of the normal mechanical behaviour where 'Hard Contact' method is used for the Pressure-Overclosure option. The tangential mechanical behaviour interaction property defines a 'Rough' friction formulation. The interaction will be active in the rest in the simulation.

F.3.4 Step: MoveBack

In the previous step, the wrap part was moved slightly further than the distance between the two parts. This step will remove this extra distance.
The two boundary conditions that fix the bottomline of the wrap and the aorta are replaced by two boundary conditions that fix the middlelines of both parts. Furthermore, the boundary condition that fixes the aorta in the z-direction is made inactive and the aorta is fixed in the x- and y-direction in this step, while the boundary condition that fixes the wrap in the x- and y-direction is removed. Finally a boundary condition is created that will move the aorta in the z-direction to remove the extra distance.

F.3.5 Step: AxialPrestretch

Axial residual stresses are included in this model and are created in this step. Therefore, the right edge of the aorta is fixed in the z-direction and the aorta is allowed to move in x- and y-direction. The left side of the wrap is moved over a certain distance, 8 mm which corresponds to the 20% axial prestretch.

F.3.6 Step: Diastole

After creating the residual stresses in the model, the diastolic pressure is applied to the inner surfaces of the aorta and wrap. This condition is defined as a load rather than a boundary condition. The pressure however needs to be defined in megaPascal as opposed to mmHg.

F.3.7 Step: Systole

After applying the diastolic pressure, the systolic pressure acts on the inner surfaces of both parts. However, when modifying the previous load to correspond to the systolic pressure, Abaqus will commence by applying a pressure equal to zero and building up to the systolic pressure by the end of the step. Nevertheless, it is needed that the pressure starts from diastolic pressure in this step and builds up to systolic pressure. Creating an amplitude which starts not from zero but from the ratio equal to the ratio of diastolic pressure over systolic pressure and ending at 1, overcomes this problem.
An overview of the different boundary conditions can be found in Figure F.10.

Name	Initial	Close	Couple	MoveBack	AxialPreStret	Diastole	Systole
FixAortaBackEdge					Created	Propagated	Propagated
FixAortaBottomLineY	Created	Propagated	Propagated	Inactive	Inactive	Inactive	Inactive
FixAortaMiddleLine				Created	Propagated	Propagated	Propagated
FixAortaXY				Created	Inactive	Inactive	Inactive
FixAortaZ	Created	Propagated	Propagated	Inactive	Inactive	Inactive	Inactive
FixWrapBottomLineY			Created	Inactive	Inactive	Inactive	Inactive
FixWrapEdgeZ				Created	Inactive	Inactive	Inactive
FixWrapMiddleLine				Created	Propagated	Propagated	Propagated
FixWrapXY			Created	Inactive	Inactive	Inactive	Inactive
MoveAortaEdgeBack				Created	Inactive	Inactive	Inactive
MoveLowerEdge		Created	Inactive	Inactive	Inactive	Inactive	Inactive
MoveNodes1		Created	Inactive	Inactive	Inactive	Inactive	Inactive
MoveNodes2		Created	Inactive	Inactive	Inactive	Inactive	Inactive
MoveNodes3		Created	Inactive	Inactive	Inactive	Inactive	Inactive
MoveNodes4		Created	Inactive	Inactive	Inactive	Inactive	Inactive
MoveNodes5		Created	Inactive	Inactive	Inactive	Inactive	Inactive
MoveUpperEdge		Created	Inactive	Inactive	Inactive	Inactive	Inactive
MoveWrap					Created	Propagated	Propagated
MoveWrapEdge			Created	Inactive	Inactive	Inactive	Inactive
SymmAortaBottom	Created	Propagated	Propagated	Propagated	Propagated	Propagated	Propagated
SymmAortaTop			Created	Propagated	Propagated	Propagated	Propagated
SymmWrapBottom			Created	Propagated	Propagated	Propagated	Propagated
SymmWrapTop			Created	Propagated	Propagated	Propagated	Propagated

Figure F.10: Overview of boundary conditions of the finite element model

Appendix G

Complementary Figures of Chapter 5

Diastole

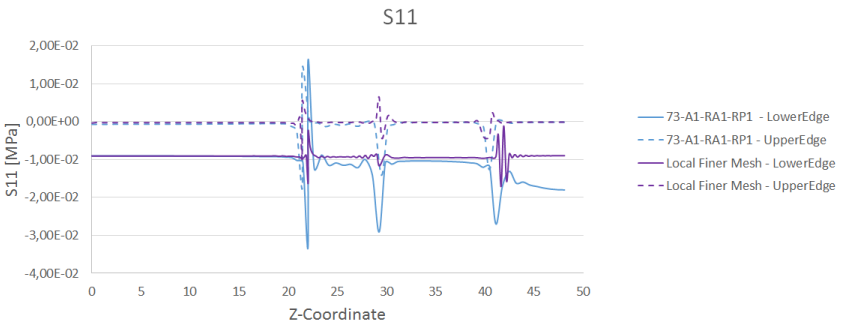

Figure G.1: The stresses in the x-direction both for upper- and loweredge in the original model and in the model where the sections between two parts with different material parameters, had a higher mesh density. The peaks present in the original model become attenuated.

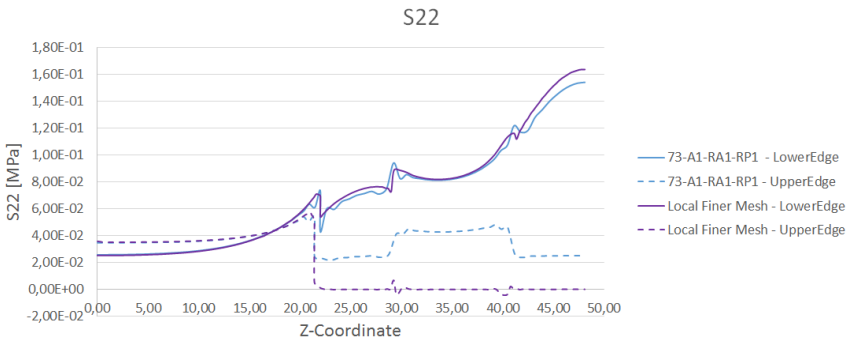

Figure G.2: The stresses in the y-direction both for upper- and loweredge in the original model and in the model where the sections between two parts with different material parameters, had a higher mesh density. The peaks present in the original model become attenuated.

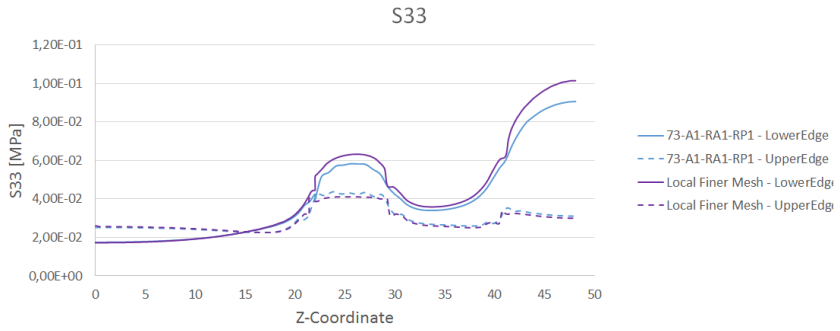

Figure G.3: The stresses in the z-direction both for upper- and loweredge in the original model and in the model where the sections between two parts with different material parameters, had a higher mesh density. The peaks present in the original model become attenuated.

Systole

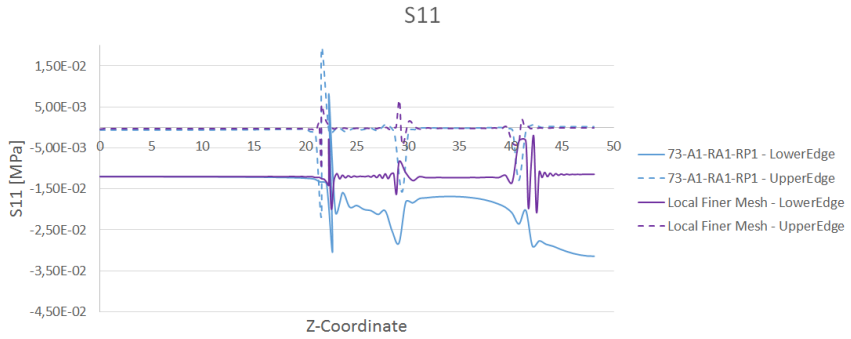

Figure G.4: The stresses in the x-direction both for upper- and loweredge in the original model and in the model where the sections between two parts with different material parameters, had a higher mesh density. The peaks present in the original model become attenuated.

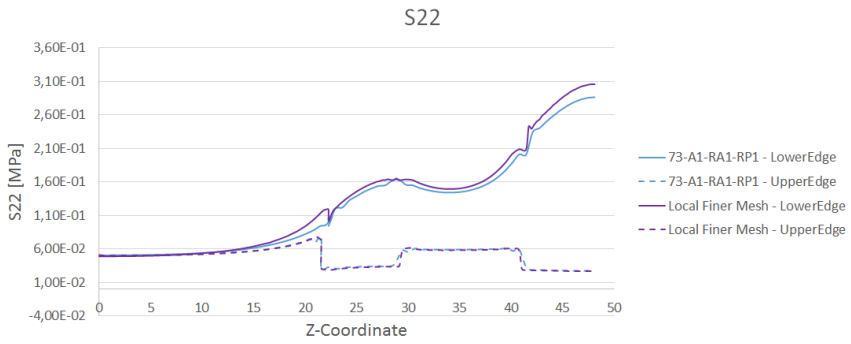

Figure G.5: The stresses in the y-direction both for upper- and loweredge in the original model and in the model where the sections between two parts with different material parameters, had a higher mesh density. The peaks present in the original model become attenuated.

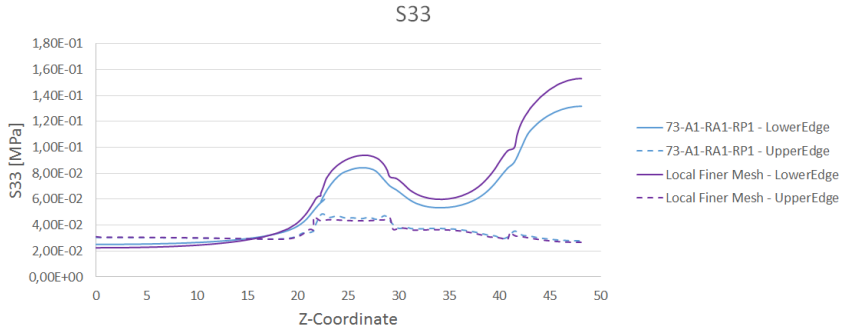

Figure G.6: The stresses in the z-direction both for upper- and loweredge in the original model and in the model where the sections between two parts with different material parameters, had a higher mesh density. The peaks present in the original model become attenuated.

Bibliography

[1] A. Avanzini, D. Battini, L. Bagozzi, and G. Bisleri. Biomechanical evaluation of ascending aortic aneurysms. *BioMed Research International*, 2014, 2014.

[2] A. N. Azadani, S. Chitsaz, P. B. Matthews, N. Jaussaud, J. Leung, A. Wisneski, L. Ge, and E. E. Tseng. Biomechanical comparison of human pulmonary and aortic roots. *European journal of cardio-thoracic surgery : official journal of the European Association for Cardio-thoracic Surgery*, 41(December 2011):1111–6, 2012.

[3] K. Benke, B. Ágg, B. Szilveszter, F. Tarr, and Z. B. Nagy. The role of transforming growth factor-beta in Marfan syndrome. *Cardiology Journal*, 20(3):227–234, 2013.

[4] D. Bia, R. L. Armentano, J. C. Grignola, D. Craiem, Y. a. Zócalo, F. F. Ginés, and J. Levenson. The vascular smooth muscle of great arteries: local control site of arterial buffering function? *Revista espanola de cardiologia*, 56(12):1202–1209, 2003.

[5] J. W. Brown, M. Ruzmetov, A. P. Shahriari, M. D. Rodefeld, Y. Mahomed, and M. W. Turrentine. Modification of the Ross aortic valve replacement to prevent late autograft dilatation. *European Journal of Cardio-thoracic Surgery*, 37(5):1002–1007, 2010.

[6] G. S. Carr-White, A. Afoke, E. J. Birks, S. Hughes, A. O'Halloran, S. Glennen, S. Edwards, M. Eastwood, and M. H. Yacoub. Aortic root characteristics of human pulmonary autografts. *Circulation*, 102:III15–I21, 2000.

[7] T. Carrel, M. Schwerzmann, F. Eckstein, T. Aymard, and A. Kadner. Preliminary results following reinforcement of the pulmonary autograft to prevent dilatation after the Ross procedure. *Journal of Thoracic and Cardiovascular Surgery*, 136(August):472–475, 2008.

[8] CellScale. BioTester Biaxial Test System - User Manual version 5.0, 2011.

[9] J. M. Clark and S. Glagov. Transmural organization of the arterial media. The lamellar unit revisited. *Arteriosclerosis (Dallas, Tex.)*, 5:19–34, 1985.

[10] Columbia University Medical Center. Aortic Surgery David Procedure. "http://www.columbiasurgery.org/aortic/david_procedure.html, 2013 (consulted on 18/01/2015).

[11] J. R. Cook and F. Ramirez. Clinical, Diagnostic, and Therapeutic Aspects of the Mardan Syndrome - Progress in Heritable Soft Connective Tissue Diseases. *Advances in Experimental Medicine and Biology*, 802:77–88, 2014.

[12] C. DiMario, J. Pepper, T. Golesworthy, and T. Treasure. External aortic root support for the Marfan aorta: anatomically normal coronary orifices imaged seven years after surgery. *Interactive cardiovascular and thoracic surgery*, 15(3):528–30, Sept. 2012.

[13] A. Farley, E. Mclafferty, and C. Hendry. The cardiovascular system. *Nursing Standard*, 27(9):35–40, 2012.

[14] Y. C. Fung and S. Q. Liu. Change of residual strains in arteries due to hypertrophy caused by aortic constriction. *Circulation research*, 65:1340–1349, 1989.

[15] T. C. Gasser, R. W. Ogden, and G. a. Holzapfel. Hyperelastic modelling of arterial layers with distributed collagen fibre orientations. *Journal of the Royal Society, Interface / the Royal Society*, 3(6):15–35, Feb. 2006.

[16] T. J. Golesworthy and M. U. Lamperth. Aortic root dissection treatment, 2012.

[17] M. Hasegawa and T. Azuma. Mechanical properties of synthetic arterial grafts. *Journal of biomechanics*, 12:509–517, 1979.

[18] D. Haskett, G. Johnson, A. Zhou, U. Utzinger, and J. Vande Geest. Microstructural and biomechanical alterations of the human aorta as a function of age and location. *Biomechanics and Modeling in Mechanobiology*, 9:725–736, 2010.

[19] H. Hoffman, S. Weinberg, and J. Park. High Strength Ligament Prosthesis, 1984.

[20] S. J. Hollister. BME 456: Biosolid Mechanics: Modeling and Applications.

[21] G. a. Holzapfel, T. C. Gasser, and R. W. Ogden. A new constitutive framework for arterial wall mechanics and a comperative study of material models. *J. Elasticity*, 61:1–48, 2000.

[22] L. Horny, T. Adamek, and M. Kulvajtova. Analysis of axial prestretch in the abdominal aorta with reference to post mortem interval and degree of atherosclerosis. *Journal of the Mechanical Behavior of Biomedical Materials*, 33:93–98, 2014.

[23] J. D. Humphrey. *Cardiovascular Solid Mechanics - Cells, Tissues, and Organs*. Springer-Verlag New York Inc, 2002.

[24] S. a. Jensen, I. B. Robertson, and P. a. Handford. Dissecting the fibrillin microfibril: Structural insights into organization and function. *Structure*, 20(2):215–225, 2012.

[25] J. Kim and S. Baek. Circumferential variations of mechanical behavior of the porcine thoracic aorta during the inflation test. *Journal of Biomechanics*, 44(10):1941–1947, 2011.

[26] J.-H. Kim, P. Badel, a. Duprey, J. P. Favre, and S. Avril. Characterisation of failure in human aortic tissue using digital image correlation. *Computer Methods in Biomechanics and Biomedical Engineering*, 14(January 2015):73–74, 2011.

[27] N. T. Kouchoukos, V. G. Davila-Roman, T. L. Spray, S. F. Murphy, and J. B. Perrillo. Replacement of the aortic root with a pulmonary autograft in children and young adults with aortic-valve disease. *The New England Journal of Medicine*, 330(1):1–6, 1994.

[28] P. Kurowski. Avoiding pitfalls in FEA. *Machine Design*, pages 78–86, 1994.

[29] C. Lally, a. J. Reid, and P. J. Prendergast. Elastic behavior of porcine coronary artery tissue under uniaxial and equibiaxial tension. *Annals of Biomedical Engineering*, 32(10):1355–1364, 2004.

[30] C. Martin, T. Pham, and W. Sun. Significant differences in the material properties between aged human and porcine aortic tissues. *European Journal of Cardio-thoracic Surgery*, 40(1):28–34, 2011.

[31] P. B. Matthews, A. N. Azadani, C. S. Jhun, L. Ge, T. S. Guy, J. M. Guccione, and E. E. Tseng. Comparison of Porcine Pulmonary and Aortic Root Material Properties. *Annals of Thoracic Surgery*, 89(6):1981–1988, 2010.

[32] R. W. Ogden. No Title. In G. Holzapfel and R. Ogden, editors, *Biomechanical Modelling at the Molecular, Cellular and Tissue Levels*, chapter Anisotropy, pages 179–254. Springer Vienna, 2009.

[33] R. J. Okamoto, J. E. Wagenseil, W. R. DeLong, S. J. Peterson, N. T. Kouchoukos, and T. M. Sundt. Mechanical properties of dilated human ascending aorta. *Annals of Biomedical Engineering*, 30(5):624–635, May 2002.

[34] J. Pepper, T. Golesworthy, M. Utley, J. Chan, S. Ganeshalingam, M. Lamperth, R. Mohiaddin, and T. Treasure. Manufacturing and placing a bespoke support for the Marfan aortic root: description of the method and technical results and status at one year for the first ten patients. *Interactive cardiovascular and thoracic surgery*, 10(3):360–5, Mar. 2010.

[35] J. Pepper, K. John Chan, J. Gavino, T. Golesworthy, R. Mohiaddin, and T. Treasure. External aortic root support for Marfan syndrome: early clinical results in the first 20 recipients with a bespoke implant. *Journal of the Royal Society of Medicine*, 103(9):370–5, Sept. 2010.

[36] J. Pepper, M. Petrou, F. Rega, U. Rosendahl, T. Golesworthy, and T. Treasure. Implantation of an individually computer-designed and manufactured external support for the Marfan aortic root. *Multimedia manual of cardiothoracic surgery : MMCTS / European Association for Cardio-Thoracic Surgery*, 2013(March):mmt004, Jan. 2013.

[37] J. Pepper, M. Petrou, F. Rega, U. Rosendahl, T. Golesworthy, and T. Treasure. Implantation of an individually computer-designed and manufactured external support for the Marfan aortic root. *Multimedia manual of cardiothoracic surgery : MMCTS / European Association for Cardio-Thoracic Surgery*, 2013(13):mmt004, Jan. 2013.

[38] O. H. Petersen, editor. *Human Physiology - Lecture notes*. Blackwell publishing, fifth edit edition, 2007.

[39] R. M. Radke and H. Baumgartner. Education in Heart Diagnosis and treatment of Marfan syndrome : an update. *Heart*, pages 1382–1391, 2014.

[40] P. H. Raven, G. B. Johnson, K. A. Mason, J. B. Losos, and S. R. Singer. *Biology*. McGraw-Hill Companies, ninth edit edition, 2011.

[41] D. Robertson and D. Cook. Unrealistic statistics : How average constitutive coef fi cients can produce non-physical results. 40:234–239, 2014.

[42] D. Roy, C. Kauffmann, S. Delorme, S. Lerouge, G. Cloutier, and G. Soulez. A literature review of the numerical analysis of abdominal aortic aneurysms treated with endovascular stent grafts. *Computational and Mathematical Methods in Medicine*, 2012, 2012.

[43] P. Segers and P. Verdonck. No Title. In M. Riethmuller and P. Corieri, editors, *Fluid dynamics of biological flows*, chapter Measuring, pages 1–27. Von Karman Institute for fluid dynamics, Sint-Genesius-Rode, 2010.

[44] P. Segers and P. Verdonck. Vascular Biomechanics and Hemodynamics. In M. Riethmuller and P. Corieri, editors, *Fluid dynamics of biological flows*, chapter Vascular B, pages 1–29. Von Karman Institute for fluid dynamics, Sint-Genesius-Rode, 2010.

[45] H. H. Sievers. Ross procedure. *HSR proceedings in intensive care & cardiovascular anesthesia*, 4:119–23, 2012.

[46] M. Smoljkic, P. Segers, J. Vander Sloten, and N. Famaey. Method for in vivo estimation of material properties of arterial tissue. In *13th National Day on Biomedical Engineering*, Brussels, 2014.

[47] P. Stelzer. The Ross procedure: state of the art 2011. *Seminars in thoracic and cardiovascular surgery*, 23(2):115–23, Jan. 2011.

[48] M. Thiriet. *Anatomy and Physiology of the Circulatory and Ventilatory Systems*, volume 6. 2014.

[49] T. Treasure, J. J. M. Takkenberg, T. Golesworthy, F. Rega, M. Petrou, U. Rosendahl, R. Mohiaddin, M. Rubens, W. Thornton, B. Lees, and J. Pepper. Personalised external aortic root support (PEARS) in Marfan syndrome: analysis of 1-9year outcomes by intention-to-treat in a cohort of the first 30 consecutive patients to receive a novel tissue and valve-conserving procedure, compared with the publishe. *Heart (British Cardiac Society)*, 100(12):969–75, June 2014.

[50] D. Tremblay, T. Zigras, R. Cartier, L. Leduc, J. Butany, R. Mongrain, and R. L. Leask. A comparison of mechanical properties of materials used in aortic arch reconstruction. *The Annals of thoracic surgery*, 88(5):1484–91, Nov. 2009.

[51] A. Tsamis, J. T. Krawiec, and D. a. Vorp. Elastin and collagen fibre microstructure of the human aorta in ageing and disease: a review. *Journal of the Royal Society Interface*, 10:1–22, 2013.

[52] R. M. Ungerleider, Y. Ootaki, I. Shen, and K. F. Welke. Modified ross procedure to prevent autograft dilatation. *Annals of Thoracic Surgery*, 90(3):1035–1037, 2010.

[53] D. Valdez-Jasso, M. a. Haider, H. T. Banks, D. B. Santana, Y. Z. Germán, R. L. Armentano, and M. S. Olufsen. Analysis of viscoelastic wall properties in ovine arteries. *IEEE Transactions on Biomedical Engineering*, 56(2):210–219, 2009.

[54] M. Van Den Abbeele. Characterisation of the biaxial mechanical properties of cardiovascular tissue. Master's thesis, Catholic University Leuven, 2014.

[55] P. Verbrugghe, E. Verbeken, J. Pepper, T. Treasure, B. Meyns, B. Meuris, P. Herijgers, and F. Rega. External aortic root support: A histological and mechanical study in sheep. *Interactive Cardiovascular and Thoracic Surgery*, 17(April):334–339, 2013.

[56] D. a. Vorp, B. J. Schiro, M. P. Ehrlich, T. S. Juvonen, M. A. Ergin, and B. P. Griffith. Effect of aneurysm on the tensile strength and biomechanical behavior of the ascending thoracic aorta. *Annals of Thoracic Surgery*, 75:1210–1214, 2003.

[57] J. H. C. Wang and B. P. Thampatty. An introductory review of cell mechanobiology. *Biomechanics and Modeling in Mechanobiology*, 5:1–16, 2006.

[58] WS Hampshire Inc. TYPICAL PROPERTIES of PTFE. pages 9–11, 2011.

[59] S.-m. Yuan and H. Jing. Marfan s syndrome : an overview Review article. 128(6), 2010.

[60] M. Zemánek, J. Burša, and M. Děták. Biaxial Tension Tests with Soft Tissues of Arterial Wall, 2009.

Master thesis filing card

Student: Julie Vastmans

Title: Biomechanical Evaluation of a Personalized External Aortic Root Support applied in the Ross procedure

UDC: 621.3

Abstract:
A treatment for patients suffering from aortic valve disease is the Ross procedure, where the surgeon replaces the diseased aortic root with a pulmonary root autograft. This autograft is subsequently exposed to systemic pressures possibly resulting in dilatation. [47] This study investigates the influence of adding a PEARS. A simplified version of the Ross procedure was performed on seven Lovenaar sheep: a part of the thoracic aorta descendens is replaced by part of the truncus pulmonalis and a wrapping is positioned around the pulmonary autograft. During this procedure pulmonary tissue was harvested. After six months, the sheep were sacrificed. Three types of tissue were harvested: aorta, reinforced aorta, and reinforced pulmonalis. The tissues underwent planar biaxial tests, and stress-strain curves for the four types of tissues were calculated from the obtained force-displacement curves. These curves served as input for the Gasser-Holzapfel-Ogden material model. [15] Subsequently, a finite element model (FEM) of the simplified procedure with and without reinforcement was constructed, as well as a FEM of solely the aorta or pulmonalis under physiological loading conditions. The following outputs were collected: the profile of the deformed shape after applying diastolic and systolic pressure, and the stresses in the three directions in diastolic and systolic conditions.
From the finite element analysis can be concluded that inserting a pulmonary section in the aorta position, alters the stress pattern. Adding a reinforcement changes the stress pattern compared to the unreinforced simulation and compared to the normal situation. Furthermore, the Ross procedure without reinforcement results in a larger diameter where the pulmonalis is positioned, while the wrapping appears to constrain the pulmonary section. The change in stress imposed on the pulmonalis in the aorta position with and without reinforcement, may have an influence on the long-term results of this procedure. However, improvements regarding the model can be made regarding the boundary conditions and material representation. Moreover, the influence of the circumferential and axial residual stresses needs to be investigated.

Thesis submitted for the degree of Master of Science in Biomedical Engineering

Thesis supervisors: Prof. dr. ir. Jos Vander Sloten
Prof. dr. Filip Rega,
Dr. ir. Nele Famaey

Assessors: Prof. dr. ir. Harry Van Lenthe
Dr. Peter Verbrugghe

Mentor: Ir. Heleen Fehervary